Modular Voltage Balancing Networks for Series Connected Battery Cells

by

Atrin Tavakoli

A thesis submitted in partial fulfillment of the requirements for the degree of

Doctor of Philosophy

in

Energy Systems

Department of Electrical and Computer Engineering
University of Alberta

Abstract

Battery cells are an emerging technology for storage in electrical vehicle, industrial and residential applications has become more popular. To meet the high voltage and power, battery cells are connected in series and parallel. Series connected battery cells share the same charge/discharge current. Therefore, in the case of characteristic mismatch between battery cells, a battery cell may be over-charged or overly-discharged. These conditions are two reasons that decrease the life-time and affect the performance of battery cells. All of these challenges can be tackled using battery voltage balancer circuits. These circuits can improve the performance, life-time of battery cells and reduce the maintenance and replacement cost of the battery cells.

Three battery voltage balancer circuits along with their control methods are described. The proposed methods are modular topologies where every two battery cells are connected to a single balancer circuit bridge/module. These bridges/modules are connected through inter-bridge/module windings. These circuits are based on various types of Buck-Boost and SEPIC converters and are modular, easy to implement, low-cost and, have low number of components. The first and second methods offer ZCS in turn ON. Moreover, the proposed methods are shown to be faster than the existing methods. The faster equalization speed is due to the ability of these circuits to exchange charge between all battery cells at the same time in each switching cycle.

The proposed distributed controllers require each bridge to monitor its own battery cell voltages and also those of the adjacent bridges. This reduces the number of feedback sensors. Detailed analysis is presented that quantifies the flow of charge between a number of series connected battery cells. Comprehensive design procedures based on circuit analysis are presented for all proposed circuits which guarantee a fixed switching frequency and zero current switching. Also, the proposed controllers limit the current in the system without using any current sensors. Analytical, simulation and experimental results are presented to verify the effectiveness of the proposed methods.

Dedicated to my lovely parents...

Acknowledgements

Throughout the writing of this dissertation I have received a great deal of support and assistance. I would first like to thank my supervisors, Professor S. Ali Khajehoddin and Professor John Salmon, whose expertise was invaluable in the formulating of the research topic and methodology in particular. I appreciate their immense knowledge and valuable suggestions that helped me learn something new every day. Their gentle personality and rigorous attitude toward research will benefit my career as well as my personal life. I am very lucky to have both professors as mentors during my time.

Second, I must express my very profound gratitude to my parents for providing me with unfailing support and continuous encouragement throughout my years of study and through the process of researching and writing this thesis. This accomplishment would not have been possible without them.

I am grateful to all of those with whom I have had the pleasure to work during this project. I am deeply indebted to Mohammad Ebrahimi for sharing his experience and providing intellectual input. I especially grateful to Masoud Shabestary an Shahed Mortazavian for all the time taken to show me the ropes and to ensure that I have the all I need to catch up in a new city. My heartfelt thanks also go to Moosa Moghimi, for his friendship an helping me get through the difficult times. As experimental work formed a significant part of this research program, special thanks go to Albert Terheide for helping me get started with lab equipment. I would also like to express my gratitude to my friend Ramiar Alaei, Ramin Rahmat Samii, Alireza Abbasian, Mohammad Daryayi, Nima Amouzegar, and Mohammad Shahabasi for their constructive comments and friendship during the last few years.

Finally, I would like to acknowledge the financial support provided by University of Alberta the course of this project.

Contents

List of Figures

List of Tables

Abbreviations

EV	**E**lectric **V**ehicle
ESS	**E**nergy **S**torage **S**ystem
DOD	**D**epth **O**f **D**ischarge
CBM	**C**ell **B**ypass **M**ethod
SOC	**S**tate **O**f **C**harge
ZCS	**Z**ero **C**urrent **S**witching
ZVS	**Z**ero **V**oltage **S**witching
DCM	**D**iscontinues **C**onduction **M**ode
TCCA	**T**ransformer **C**oupled **C**ascaded **A**ssymetrical-Bridge
TCSA	**T**ransformer **C**oupled **S**eries **A**ssymetrical-Bridge
TCPS	**T**ransformer **C**oupled **P**arallel **S**epic-module
SEPIC	**S**ingle-**E**nded **P**rimary-**I**nductor **C**onverter
PWM	**P**ulse **W**idth **M**odulation
PV	**P**hoto**V**oltaic
BMS	**B**attery **M**anagement **S**ystem
BM	**B**alancing **M**odule
BC	**B**alancing **C**ircuit
DSP	**D**igital **S**ignal **P**rocessor
GCU	**G**eneration **C**ontrol **U**nit

Symbols

L_f	added inductance in series with coupled inductor
V_{B_i}	Voltage of battery cell "i"
i_{w_i}	Current of winding "i"
Φ_c	core flux
$\mathcal{R}_c$	core reluctance
Φ_{li}	leakage flux of winding "i"
$\mathcal{R}_{li}$	leakage reluctance of winding "i"
N	Number of winding turns
L_m	magnetizing inductance of the coupled inductor
L_l	leakage inductance of the coupled inductor
v_{w_i}	voltage of winding "i"
i_{B_i}	Current of battery cell "i"
V_i	total voltage of battery cells in bridge "i"
Q_{B_i}	absorbed charge of battery cell "i"
f_s	switching frequency
$V_{D_{on}}$	forward voltage of diode
n	number of bridges/modules
i_{C_i}	current of capacitor "i"
i_{L_i}	current of inductor "i"
i_{Ls_i}	current of coupled inductor "i"

V_{C_i}	average voltage of capacitor "i"
D	duty cycle
ω_r	resonant angular frequency

CHAPTER 1

Introduction

The integration of energy storage technologies are important to improve the potential for flexible energy demand and to ensure that excess renewable energy can be stored for use at a later time. Energy storage technologies such as pumped hydro, compressed air energy storage, various types of batteries, flywheels, electrochemical capacitors, etc., are used in various applications: energy management, backup power, load leveling, frequency regulation, voltage support, and grid stabilization. Electrochemical batteries and flywheels are positioned around lower power and shorter discharge times, ranging from a few seconds to hours, and these technologies can generally be built without specific geographical features at the site. There are several different electrochemical battery technologies that are currently available for commercial applications. These technologies have been successfully deployed in both distributed and centralized applications in various power densities. The electrochemical rechargeable battery cells such as Lithium-ion are commonly used as energy storage units in EVs [4–6].

1.1 Battery Cells Types and Classifications

A brief review on the different kind of battery cells is provided to be able to choose the best battery cells for an specific application. A large portion of the electrochemical battery cells market size is taken by Electric Vehicle (EV) applications. Evs are vehicles that their driving force is electric instead of gasoline. They are usually driven by electric motors which are feed by battery cells in the car. Battery cells provide high specific energy, high power density, flat discharge profile, low resistance, negligible memory effect and good wide range of temperature performance. However, there are a lot of researchers focused on further improvement of battery cell performance and reduction of manufacturing cost. The battery cell technologies have various application based on their parameters such as energy density, cycle-life and efficiency. The important parameters are: Specific Energy, or gravimetric energy density, which is battery cell capacity in weight (Wh/kg); Energy Density, or volumetric energy density, reflects energy in liters (Wh/l); Specific Power which is amount of power in weight (W/kg); Efficiency of the batteries; Cycle life reflects the number of complete charging and discharging until the initial capacity decreases to its $60-80\%$. For example, 1000 times cycle life, does not mean that the battery cell should be replaced after using it 1000 times. This means that for a $1000Ah$ battery cell, the initial capacity drops to $800-600Ah$ after 1000 cycles of charging and discharging. The cycle life of battery cells can be increased by several-fold if they charge when their Depth-of-Discharge (DOD) is 80%. In other words, it is better to charge the battery cells when they are not discharge fully. A comprehensive comparison between several types of battery cells are provided in Table. 1.1 [7].

$Ni-Cd$ battery is useful in applications requiring high discharge current due to low internal resistance. It can provide high discharge current with no damage or

TABLE 1.1: Comparing different types of battery cells.

Spec / Type	Specific Energy (Wh/kg)	Energy Density (Wh/L)	Power Density (W/kg)	η	Cycle-life (@ %80 DOD)	Merits	Demerits
$Ni - Cd$	40-50	80-100	150-350	60-90	2000-3000	Low internal resistance, no degradation for deep charge/discharge	High cost cadmium toxicity, recycling issues
$Ni - MH$	50-70	100-140	150-300	50-80	500-3000	Low internal resistance, large temperature ranges, safety, long service life	High cost, high self-discharge, memory effect
$Na - S$	100	150	120	80	2500-4500	High efficiency, Long cycle life	Relatively expensive, High temperature effect, safety problem
$Zn - air$	230	269	105	60	300-600	High specific energy; technically feasible; the rate of reaction can be controlled by varying the flow of air; better life cycle; low materials cost	Difficult in design; necessary of Zinc anode replacement; short circuit problem
ZEBRA $Na/NiCl_2$	86	149	150	80	2500-3000	Less corrosive, intrinsically safer, good tolerance to overcharge and undercharge than Na/S, high cycle life, lowest cost than any other battery cells	Low specific power, need of thermal management, self-discharge problem
Li-polymer	155	200-250	315	70	> 1200	High energy density and specific energy, slim type; high voltage operation; high aspect-ratio form factor; no memory effect; tolerant to overcharged state without explosion; high energy efficiency; low self discharge; long life cycle	High cost, low conductivity and power density
$Li - ion$	120-140	240-280	200-300	70-85	1500-4500	High energy density and specific energy, high voltage operation; no memory effect; lighter and smaller; high energy efficiency; low self discharge; long life cycle	High cost, life shorten by deep discharges, affected by temperature, fragile, protection for overcharge and undercharge

loss of capacity. $Ni-Cd$ cells are used in portable electronics and toys to replace primary cells. However lower terminal voltage and smaller capacity may reduce performance of these kind of battery cells compared to primary cells.

$Ni-MH$ battery cells are mostly used in high current drain applications such as digital cameras where they show better performance compared to the battery cells which cannot be recharged. The main advantage of this kind of battery cells is low internal resistance therefore, they can provide almost constant voltage until they are almost completely discharged. However, they can be replaced in the devices where designed to operate with Alkaline battery cells since the charge indicator overstate the remaining charge in the system as the voltage drop is very small. Although, the applications of Ni based battery cells are limited due to environmental concerns and high cost. Among rechargeable battery technologies, $Ni-Cd$ rapidly lost market share to $Ni-MH$ and $Li-ion$ batteries. In $Ni-Cd$ and $Ni-MH$ battery cells, battery balancing is not necessary while they are charging regularly since the can dissipate the excessive charge without creating much heat in battery cells. However, if fast charging techniques are used, a battery management system or a ventilation system is necessary to keep them safe.

Sodium-sulfur ($Na-S$) and Sodium-metal Chloride ($Na/NiCl_2$, $Na/FeCl_2$ and $Na/Ni-FeCl_2$) battery cells have a good and feasible position in vehicular and energy storage applications. Due to the high operating temperature and corrosive nature of the sodium polysulfides, they need to be protected and isolated. The protection and isolation and the fact that these cells are more economical with increasing the size of them, make their applications limited to stationary energy storage. Although $Na-S$ battery cell has the problems of Na corrosion, high internal resistance, and high temperature; it needs maintenance for the molten electrodes; it is economy and secure. Although $Na-S$ battery cell has the problems of Na corrosion, high internal resistance, and high temperature; it needs maintenance for the molten electrodes; it is economy and secure.

The Sodium-metal chloride battery cells commonly known as ZEBRA battery cells are viable for high temperature EV applications due to high energy density, corrosion free, tolerance to over-discharge and over-charge conditions. These cells are often used in digital cameras and other high-drain devices, where over the duration of single-charge use they outperform non-rechargeable batteries. The ZEBRA battery cells are reliable and also economic in terms of design cost compared to $Ni - Cd$, Zn-halogen and $Na - S$ battery cells; nevertheless, they suffer for low specific power, high self-discharge and difficult thermal management. One of the advantages of these battery cell is that these battery cells can tolerate over charge and over discharge. This is due to the fact that the overcharge reaction requires a higher voltage than the normal charge reaction. Consequently, any further charge current would be stopped when the increased open circuit voltage equalizes the charger voltage. Moreover, in over-discharging, the reactions keeps current flow at a lower voltage.

The lithium battery cell technologies are promisingly advancing for EVs and accessories since lithium battery cells have high specific power, specific energy, energy density, small package in size and low weight. Nevertheless, lithium battery cells are costly; and they need the protection and charge management systems for enhancing the performance and cell life. Lithium battery cells can be used in low and high temperature operations but their performance is better in normal temperature application. Lithium-ion and Lithium-polymer battery cells are very attractive as EV energy storage systems as they can operate in ambient temperature of -20 to $60°C$. The lithium-polymer battery cells are very lucrative due to their high specific energy, high specific power, ruggedness, reliability and variety in shapes; however, they have low power density and poor electricity flow rate than those of lithium-ion battery cells. The Lithium-ion battery cells are specifically promising and growing battery cell technology for EV applications because of the highest energy density and the highest power density among all battery cells. Moreover, they do not have memory effect, rather negligible self-discharge, long life-cycle discharge cycles, smaller size, and high energy efficiency. The challenges of using Lithium-ion include the durability that is affected by the internal temperature and deep discharge and the need for overcharge and over-discharge protections with battery cell charge equalization controller. Moreover, the relation between SOC and Voltage in $Li-ion$ battery cells is linear. Therefore, it is possible to use voltage of battery cells to estimate its SOC, see Fig. 1.1.

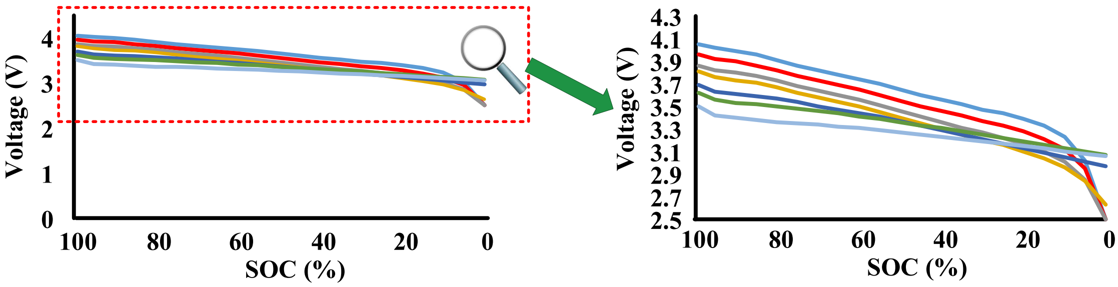

FIGURE 1.1: SOC vs. Voltage characteristic of $Li-ion$ NCR18650GA (Titan's Endurance Packs) [1]

High Voltage/Power Applications of Battery Cells

Battery cells play an important role in the performance of EVs and also the future development and reliability of EVs. The performance and sustainability of a battery cell are highly influenced by the battery cell charge. The terminal voltage of a single battery cell is usually low, for example, $2V$ in Lead-acid battery cells, $3.6V$ in Lithium-ion battery cells, and $3.3V$ in Lithium Iron Phosphate ($LiFePO_4$) battery cells [7, 8]. In many applications, it is necessary to generate high voltages or feed high power loads with the battery cells. Due to some technical difficulties, voltages and capacity of battery cells are limited. Therefore, to meet high voltage and power requirements, battery cells are connected in series and parallel. Since series connected battery cells are charged and discharged with the same current, cell voltage imbalance inevitably occurs. This is due to the mismatch cell properties, such as capacitance, internal impedance, and self-discharge rate. In addition to such nonuniform electrical properties, the temperature gradient in a module/battery cell that accelerates the nonuniform self-discharging of cells can also result in cell voltage imbalance. Series connected battery cells are charged and discharged with the same current, Therefore, characteristics mismatch leads to non-uniform State of charge in the battery cells in a string. The latter in extreme case scenarios leads to over-charged and over-discharged in some battery cells. Since overcharging and over-discharging the cells causes irreversible deterioration, each individual cell voltage should be maintained within a specified safety voltage range. However, as long as the cells are charged (discharged) in series, the charging (discharging) process should be limited by the cell with the highest (lowest) voltage so that no cell is overcharged (over-discharged). With such limitations, the cells cannot be fully charged (discharged), and hence, series connected cells exhibit poor energy utilization. Therefore, cell voltage imbalances should be minimized to prolong the life of the cells and maximize their available energies [9–11]. A lot of researches have been working on the Battery cell balancing systems for the rechargeable battery cell to enhance the life-cycle, efficiency and safety [12–14]. Battery cell balancing systems protect storage cell from damaging and to enhance cell performance and life-cycle as well [14, 15].

1.2 Battery Cell Balancing Systems

Battery cell charge or voltage balancing system can be categorized into three major groups, see Fig. 1.2. These three groups are discussed and their advantages and disadvantages are addressed briefly.

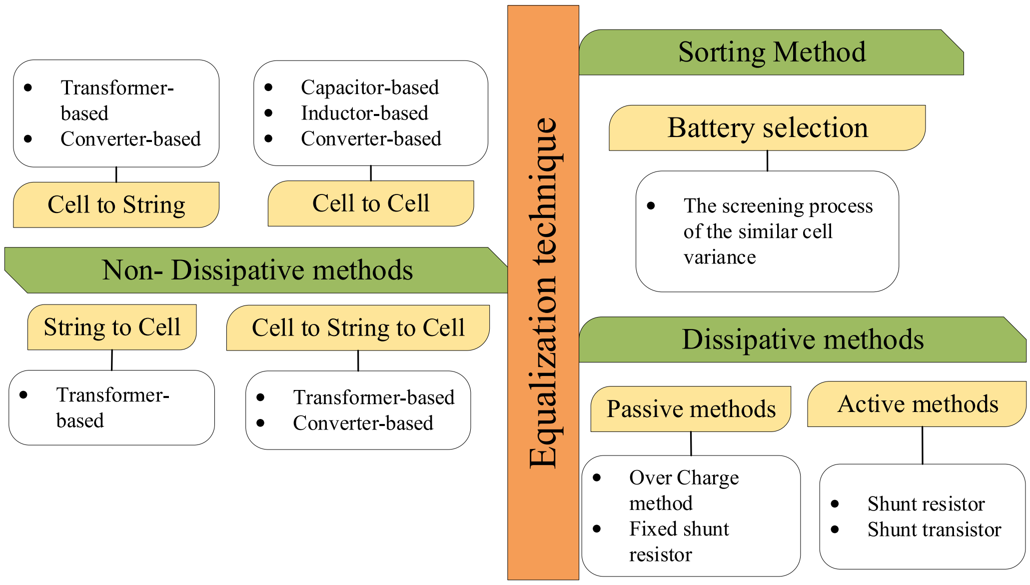

FIGURE 1.2: Battery equalization techniques categorization.

1.2.1 Sorting Method

The main idea of this off-line method is to find the battery cells with the similar characteristics and use them to form a string. In this way, all the battery cells which are used to from the string are similar and will be charged and discharged with the same rate. Two different processes, capacity and resistance sorting, are used to find the similar battery cells. Although the characteristics of similar battery cells may vary differently during usage. Therefore, this method can be used to complement a balancing system [16–18].

1.2.2 Dissipative Methods

The idea behind dissipative equalization or Cell Bypass Method (CBM), is to connect a shunt dissipative component to dissipate or drain excessive charge from the higher charged battery cells. The passive equalization methods consist of two groups: no control, or controlled group. In the first group, no control or active component is used such as overcharge method and the shunting resistor method. In the overcharge method [19–23], when cells are fully charged, the excessive energy is converted into heat. It is only effective on a small number of cells since repeating this action for many times eventually degrades the performance and life of the battery cells. These methods are useful for Lead-acid and Nickel-based battery cells as Li-ion battery cells should not be overcharged. The shunting resistor method [24, 25] uses a resistor in parallel with each battery cell and the current is always partially or totally bypassed from the cells to limit the cells voltages. The problem with this method is that the resistor is always in the charging and discharging path and causes loss and heat in the circuit. This technique can be used for Li-ion battery cells and they are simple and inexpensive. However, these methods dissipate the excessive charge in the battery cells in order to balance the charge of battery cells. Therefore, the efficiency of this technique is low.

In active methods, an active components such as a transistor is used. This group can be categorized into shunt resistor [26–28] and shunt transistor method [29]. Controlled shunt resistor methods have better performance compared to the no controlled shunt resistor but they still cause loss and heat in the circuit and their efficiency is not good. The second group, shunt transistor, bypasses the charging current from the battery cell which has the higher charge. This method is has better efficiency compared to shunt resistor since they do not lead to heat and loss in the circuit. However, adding a transistor in the charging path causes loss in the circuit and also, they are not useful in discharging process.

1.2.3 Non-dissipative Methods

In non-dissipative methods, the excessive charge of battery cells with higher charge is transferred to battery cells with lower charge using capacitors, inductors, transformers or DC/DC converters. Charge transfer is used to categorize methods in this group. Charge can be transferred between cells and/or the string. The possible direction of charge flow are shown in Fig. 1.3(a)-(d). Therefore, these methods can be categorized into four main groups:

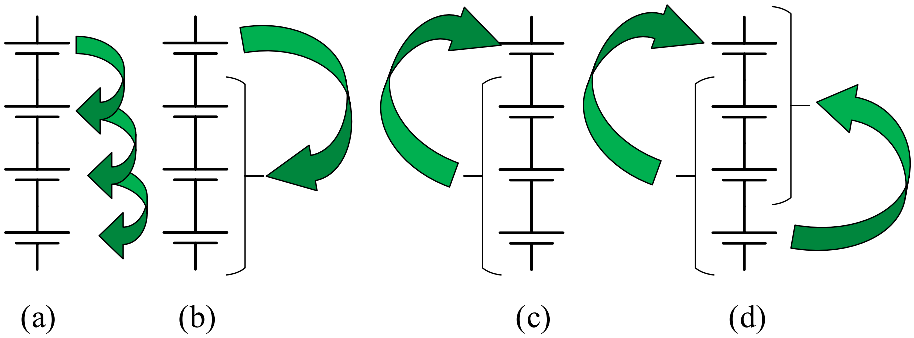

Figure 1.3: Charge transfer methods (a) Cell to Cell methods (b) Cell to String methods (c) String to Cell methods (d) Cell to String to Cell methods.

a) Cell to Cell Transfer Methods:

The idea of these methods is to transfer charge only between the neighbors battery cells or the highest and lowest charge battery cell in a cycle, see Fig. 1.3(a). These methods can be categorized into three groups:

Capacitor-based Cell to Cell Transfer Methods: In these methods a capacitor is the mediator component between higher charged cells and lower charge cell. In other words, higher voltage cells transfer charge to the capacitors and in the stored charge in the capacitors is transferred to the lower charged cells. This group is categorized as follows:

- **Switched Cap:** a capacitor is placed across every two adjacent battery cells and the current path is controlled by the complementary switches. The equalization procedure is as follows: the switches toggles the battery cell which is connected in parallel to the capacitor. First, it is connected to the battery cell with higher charge to store charge and then it will be connected to the lower charge battery cell. Since these two states constantly switching, the charge exchange between any two adjacent cells is achieved, see Fig. 1.4(a), [30, 31]. This topology is improved in [32–34], see Fig. 1.4(b), to decrease the cost of the system, achieve ZVS and decrease the stress on the switches. It is proposed that this method can be used in high power applications. Although the down side is that it decreases the speed of equalization since charge transfer occurs between only two cells in a cycle. The main advantages of this method include high neighbor to neighbor charge transfer efficiency, low complexity and the possibility of low and high power applications but the disadvantage are low far away charge transfer efficiency and low speed of equalization.

- **Double-tiered Switched Cap:** The problem with the previous method is that when the battery cells with highest and lowest charge are far away, the speed of equalization is low. To overcome this problem, another solution is presented in [35, 36], see Fig. 1.4(c). In this method the string is divided into two sections with the equal number of battery cells. For example in Fig. 1.4(c) , B_1 and B_2 in one group and B_3 and B_4 in another group , and the switched capacitor equalization method is performed in these two section. Finally these two sections are treated as two battery cells and switched cap. method is performed on these two section, S_2 and S_4 are used two connect a capacitor across these two groups. The same thing can be repeated to have strings with lower number of battery cells. The advantage over the Switched Capacitor is the lower equalization time and its disadvantages are higher cost and low power density.

Inductor-based Cell to Cell Transfer Methods: In this method, an inductor is used as the mediator to store the charge of the higher charged cells and transfer it to lower charged cells. This group is categorized as follows:

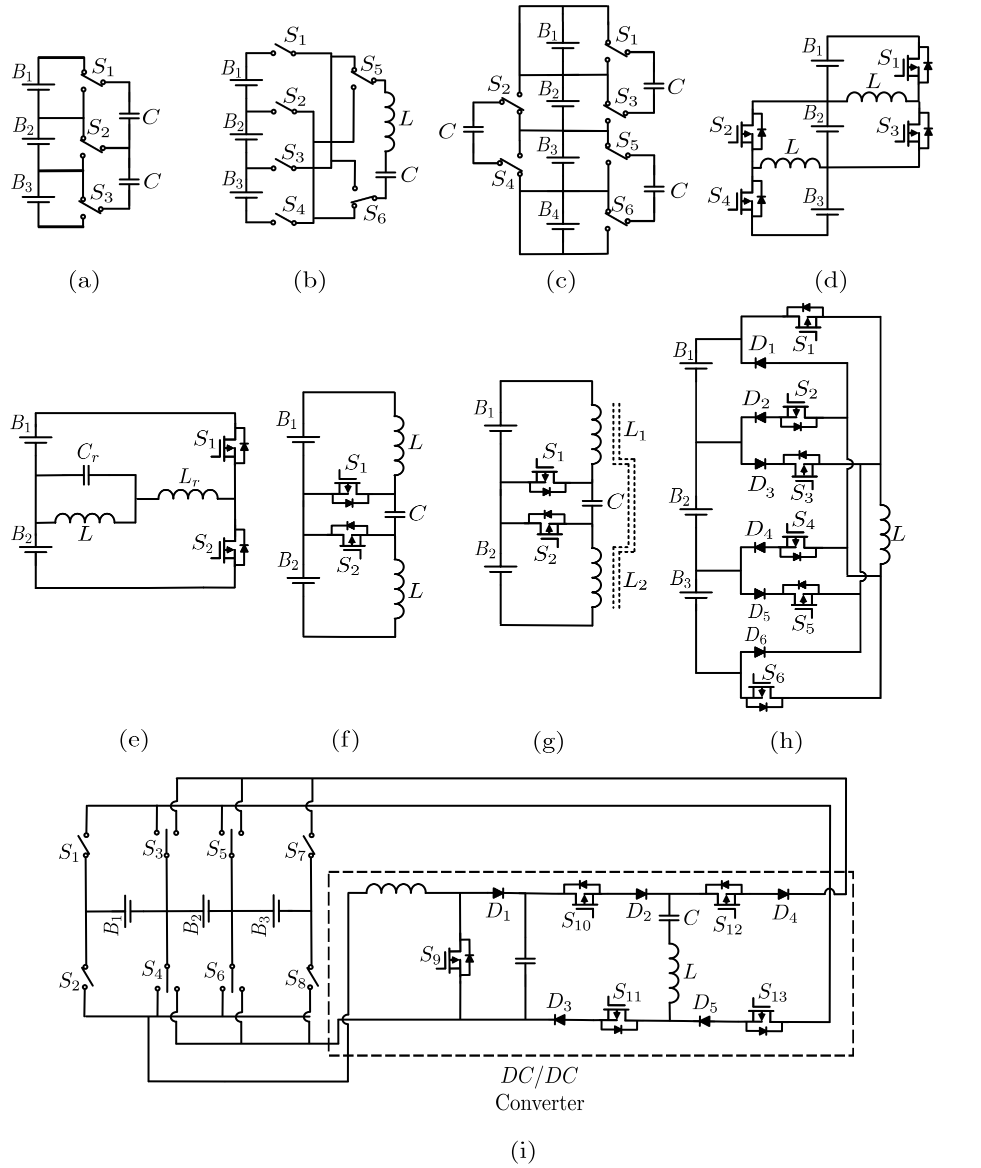

Figure 1.4: Cell to Cell Transfer basic topologies (a) Switched Capacitor (b) Single Switched Cap(c) Double-Tiered (d) Bidirectional Buck-Boost converter (e) Quasi-resonant (f) Cûk Converter (g) Modified Cûk Converter (h) Switched Inductor (i) DC/DC converter based.

- **Bidirectional Buck-Boost Converter:** The simplest topology to transfer charge between two neighbor battery cells uses Bidirectional Buck-Boost converter [37–40], see Fig. 1.4(d). For example, assume $V_{B1} > V_{B2}$ in Fig. 1.4(d), the switch of the battery cell with the higher voltage, S_1, is turned ON and B_1 charges the inductor, when S_1 is turned OFF, S_2 is turned ON and the stored charge in the inductor is transferred to B_2. This strategy applies to all the switches. This topology is easy to implement and cheap. However, due to the hard switching, the voltage stress on the switches are high and if the higher and lower charged cells are far away, the speed of equalization is low. This is due to the fact that charge is exchanged between neighbor cells.

- **Quasi-resonant Converter:** The problem with the previous method is hard switching and stress on the battery cells, therefore, [41, 42] uses a Quasi-resonant converter instead of the boost converter, see Fig. 1.4(e). using Quasi-resonant converter, ZVS can be achieved at the cost of increasing components count. The charge transfer and control procedure is similar to the previous approach. This method is proposed for high power applications but still exchanges charge only between neighbor cells therefore, the speed of equalization is low.

- **Cûk Converter:** Another solution to overcome hard switching in Bidirectional Buck-Boost converters is presented in [43, 44], by using Cûk converter, see Fig. 1.4(f). The charge transfer procedure is similar to the Bidirectional Buck-Boost converter and ZVS can be achieved at the cost of increasing components count. The main advantage is ZVS but the disadvantage is the complexity of the system. Also, the advantage over the previous method is that, all inductors are similar.

- **Modified Cûk Converter:** The advantage of this method over Cûk converter is that the currents of the battery cells is ripple free. To prevent the ripple in battery cells current, it is possible to couple the inductors as it is proposed in [45, 46], see Fig. 1.4(g). The advantage of this method include ZVS and ripple free currents and the disadvantage is that, the charge is exchanged only between neighbor cells therefore, the speed of equalization is low.

- **Flying Inductor:** This method focuses on decreasing the cost of the system by decreasing the number of inductors in Bidirectional Buck-Boost converters [47, 48], see Fig. 1.4(h). The principal of operation of this method is similar to the Switched Cap. method: the switch of the battery cell with the highest voltage is turned ON and charge is stored in the inductor. When the switch is turned OFF switch of the battery cell with the lowest voltage is turned ON and the stored charge is transferred to the lowest voltage battery cell. This method is simple but it needs a central controller.

Converter-based Cell to Cell Transfer Methods: This group uses a converter as the mediator to exchange charge between battery cells. The focus of this method is on ZCS, reducing power loss and, ripple free current of the battery cells. For example, the proposed method in [49, 50] is a combination of Quasi-resonant Converter and Flying Inductor topology. A Quasi-resonant Converter is connected to the battery cells through two separate switch modules, see Fig. 1.4(i). The battery cell with the highest voltage and the battery cell with the lowest voltage are chosen and they will be connected to the converter through those switch modules. The DC/DC converter absorbs charge of the higher charged cells and transfers it to lower charge cell. For example in Fig. 1.4(i), the DC/DC converter is chosen as Quasi-resonant converter since the ZVS and ZCS can be guaranteed and the stress on the switches and switching loss are minimized. Due to ZVS and ZCS, this method is proposed for high power applications but its control is complex.

In Cell to Cell methods, charge is only exchanged between two battery cells or neighbor cells in a cycle. Therefore, the speed of equalization is low specially when the highest and lowest charged cells are far away in the string of battery cells. In addition, in the methods which exchange charge between neighbor cells, charge has to go through all the battery cells and equalizer modules to go from the first battery cells to the last battery cell in the string of battery cells. This results in higher losses and decrease of the efficiency. The outstanding advantages of this system are the modular design, the extremely low voltage stress, and its simple control.

b) Cell to String Transfer Methods

To improve the speed of equalization of previous method, this category is introduced. The principal of operation of this method is as follows: Charge goes from the highest charge battery cell to the string of battery cells, see Fig. 1.3(b). Therefore, the charge transportation is fast. These techniques can be categorized into:

Transformer-based Cell to String Transfer Methods: This group uses a transformer as the mediator to exchange charge between the battery cells and the string of battery cells. In other words, the excessive charge of the highest voltage battery cells is transferred to the string of battery cells through a transformer. This group is categorized as follows:

- **Multiple Transformers:** This method uses several transformers to connect battery cells to the string of battery cells. A transformer is used for each battery cell, see Fig. 1.5(a), [51]. By using the switches, the higher charged battery cell is connected to the transformer and the excessive charge is transferred to all the battery cells. The major parts of this circuit are transformers, these transformers must be designed based on the number of battery cells in the string and their nominal voltage. This method is recommended for high power applications due to soft switching but the disadvantages are cost, low power density and, control complexity.

- **Switched Transformer:** To decrease the cost of the system in the previous method, a single transformer is connected to the all the battery cells through a network of switches as it is shown in Fig. 1.5(b), [52, 53]. The principal of operation is similar as previous method: the switches of the highest charged cells are turned on to transfer excessive charge to the transformer and when switches are turned off, the stored charge goes to the string of battery cells. The transformer should be designed based on the nominal voltage and number of battery cells in the string. It is recommended that this method can be utilized in high power applications, but it is expensive, power density is low, and the control circuit is complex.

- **Multi-secondary Transformer:** To decrease the number of cores in the first method, another method is proposed in [54–56]. In this method a multi-winding transformer is used to connect to all the battery cells to the string of battery cells. Therefore, only one magnetic core is used in this method. Also, compared to the second method, the number of switches is reduced and the control is simpler. The main disadvantage of this method is size of the transformer when the number of battery cells is high.

Converter-based Cell to String Transfer Methods: In this group, a converter is the mediator between a battery cell and the string of battery cells. The charge transfer procedure is the similar to the transformer-based method, the only difference is that the transformer of the previous method is replaced with a converter. This group is categorized as follows:

- **Interleaved Converter:** The principal of operation of the interleaved converter is based on Flyback converter, see Fig. 1.5(d), [57, 58]. The switches in legs are controlled by complimentary schemes. The good point about this converter is

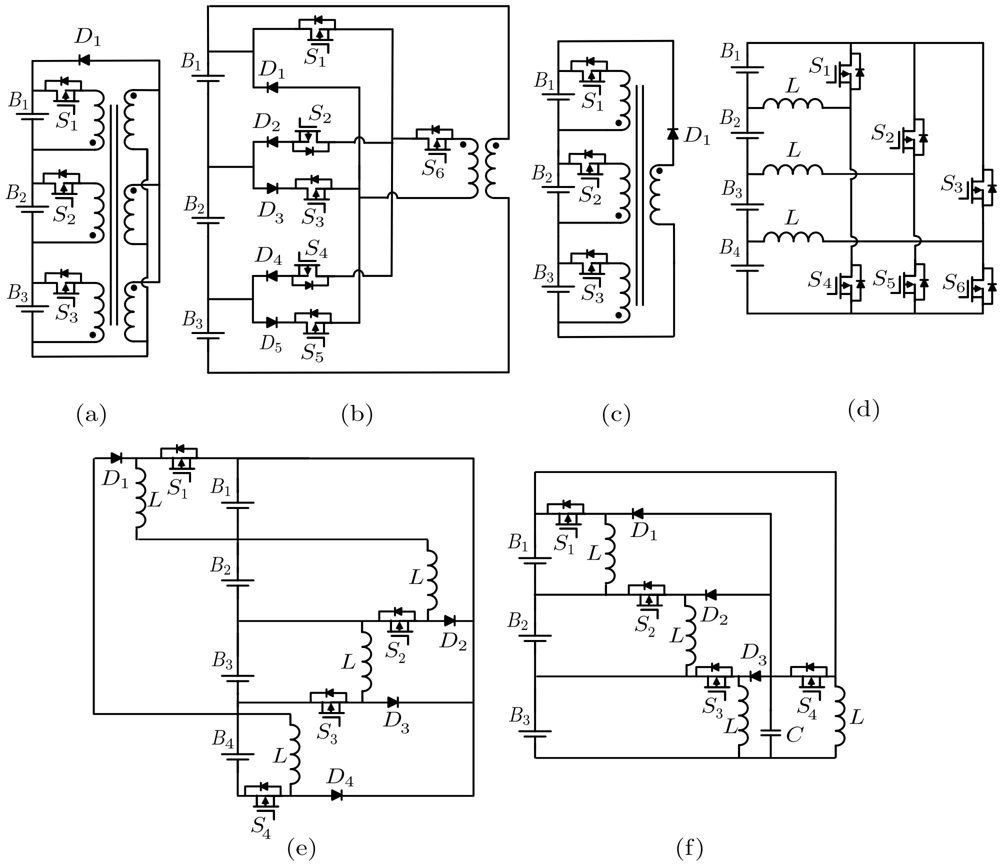

Figure 1.5: Cell to String Transfer basic topologies (a) Multiple Transformers (b) Switched Transformer (c) Multi-secondary Windings Transformer (d) Interleaved Converter (e) Boost DC/DC converter (f) Modified Boost DC/DC converter.

that the design of the switching scheme should be done off-line and there would be no need for any complicated control system. The control of this method is simple and the topology is based on natural cell balancing but the main disadvantage of this method is direct dependency of the inductor size to maximum current and switching frequency.

- **Boost DC/DC Converter:** In this method, the excessive energy is stored in parallel inductor and then transfers the energy to other cells by controlling the MOSFET switch, Fig. 1.5(e), [59]. This method is an improved version of Cell to Cell Boost converter. The speed of equalization is improved since the excessive charge of highest charged battery cell transfers to all the battery cells instead of the neighbor cells. The advantage is that the control is simple but the method is not good for high power applications since power density is low.

- **Modified Boost DC/DC Converter:** The problem with the previous technique is hard switching and switching loss of the converter. To overcome this issue, another method is proposed in [60, 61], Fig. 1.5(f). The idea is to use resonant theorem to make the current zero before turning the switches off. Moreover, the energy can be retrieved by the parallel path with a capacitor, as shown in Fig. 1.5(f), to distribute the energy efficiently with a short equitation time. The advantage is ZVS and disadvantage is the low power density of the circuit in high voltage applications.

This solution would be the best choice in cases when a battery cell is charged more than the other battery cells although, in the cases when a battery cell is charged less than the other battery cells these methods show very poor performance. The reason is that if one battery cell is charged less than the others, all the other battery cells should transfer their extra charge to the battery pack and therefore, it takes lots of time for the battery cells charge to be equalized.

c) String to Cell Transfer Methods

In contrast to the previous methods, in these methods, the charge is transferred from the string to the least charged cell in the battery cell string, see Fig. 1.3(c). Therefore, the problem of the previous method can be solved. There is only one category in this method which is transformer based method.

Transformer-based String to Cell Transfer Methods: This group similar to the Transformer based Cell to String methods, uses a transformer as the mediator to exchange charge between the string of battery cells and lowest charged battery cell. This group is categorized as follows:

- **Multiple Transformer:** a 2-winding transformer is connected to each battery cell and the secondary side of the transformers are connected together, see Fig. 1.6(a), [62]. When the switch is ON, the least charged cells absorbs the charge from the battery cell string. Similar to the similar methods, the transformer should be designed based on the number of battery cells and their voltage level. The design can be manipulated to be able to cover a large number of battery cells, however, power density is low and the cost is expensive. Moreover, this method has magnetizing losses due to the use of multiple transformers.

- **Multi-secondary Transformer:** To decrease the number of cores in the system, this method is proposed in [63], see Fig. 1.6(b). This method is similar to the previous method, the only difference is that reduces the number of cores to the cost of having a large core with multiple secondary windings. This method is not good for high power application due to low power density of the multi-winding transformer.

- **Switched Transformer:** To decrease the number of windings compared to the previous method, The Switched Transformer is introduced in [64], see Fig. 1.6(c). The cost of the system may increase due to the switch module which is needed to connect the transformer to all the battery cells. This method is effective for low number of battery cells but it is expensive, power density is low and control is complex.

String to Cell methods can solve the problem of Cell to String methods in the

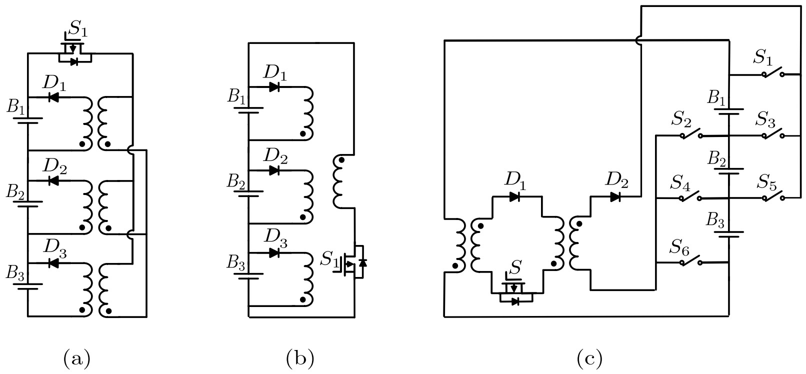

FIGURE 1.6: String to Cell Transfer basic topologies (a) Multiple Transformers (b) Multi-secondary Transformer (c) Switched Windings Transformer (d) Voltage Multiplier.

cases when one battery cell is charged less than the other. The speed of equalization in those cases are improved compared to the previous method. However, if a battery cell is charged more than the other this method would not be a good choice and it would be better to choose Cell to String method.

d) Cell to String to Cell Transfer Methods

Based on the previous sections, the weakness of Cell to String methods is strength of String to Cell methods and vice versa. Therefore, another method is presented to combine the strength of Cell to String and String to Cell methods and provide the best performance in all conditions. Cell to String to Cell methods allow the Cell to String equalization in case a battery cell has a higher voltage than the others in the battery string, and the String to Cell equalization in case a cell has a lower voltage than the others, see Fig. 1.3(d). Therefore, the weakness of the previous methods can be solved while their advantages are kept. These methods fall into 2 major groups.

Transformer-based Cell to String to Cell Transfer Methods: In this group, a transformer is the mediator component between highest charge and lowest charged battery cells. Therefore, the transformer absorbs charge from higher charged cell and transfer it to the lower charged cells. This group is categorized as follows:

- **Multiple Transformer Ramp Converter:** Ramp Converter is the improved version of multi-windings transformer. It is composed of a multi-winding transformer as shown in Fig. 1.7(a) where two adjacent battery cells as a pair are connected to a secondary winding of the transformer [65]. The operation of the Ramp converter is in a way that the odd numbered cells are considered to supply the current for capacitor charging in the first half cycle and in the second half of the cycle the even numbered cells are allowed to be recharged by capacitor or vice versa depending on the direction of current in the primary side of the transformer. This is a more cost-effective solution due to the lower number of windings, although, the design is quite complex.

- **Multi-secondary Transformer:** Another method is presented in [66] which is less complex than the ramp converter and has fewer diodes, see Fig. 1.7(b). It is also possible to achieve the ZVS and decrease the voltage stress on the switches using this method. This method is recommended for high power applications but still this method is not good for high number of battery cells due to the huge size of the transformer.

Converter-based Cell to String to Cell Transfer Methods: In this group, converters distribute charge between all the battery cells. To be more clear, the converters absorb charge from the higher charged battery cells and then transfer it the lower charged battery cells. This group is categorized as follows:

- **Voltage Multiplier Converter:** This topology uses only one switch and

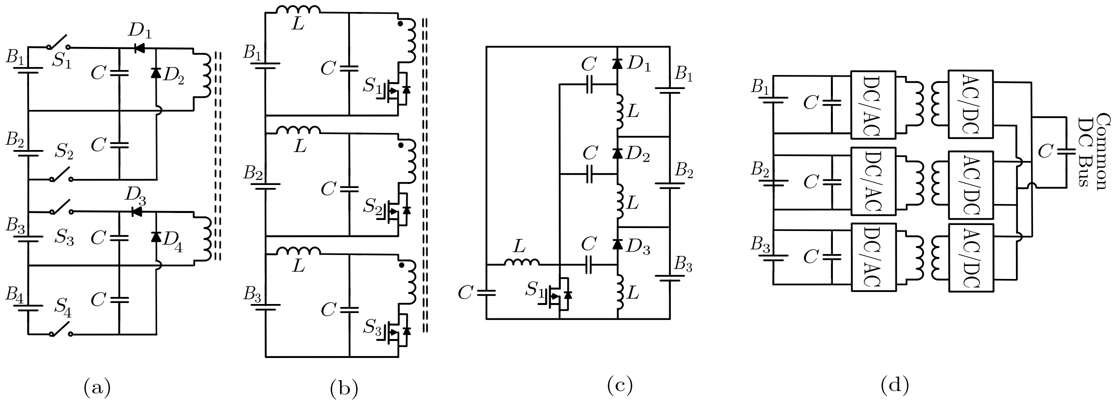

FIGURE 1.7: Cell to String to Cell Transfer basic topologies (a) Multiple Transformers (b) Multi-windings Transformer (c) Voltage Multiplier (d) DC/DC Converter based.

multi-stacked buck-boost converters, see Fig. 1.7(c), [67]. Since this method operate with a single switch, the circuit is cheap and control is simple. In addition, feedback control is not required when operating in discontinuous conduction mode. This would be good for low power application since the switch should tolerate a high voltage. However, as the number of battery cells increases the voltage and current rating of the inductors, capacitors and the switch should be increased which is not desirable.

- **DC/DC converter:** This is the most popular solution for battery charge balancing. Two DC/DC converters are connected back to back for each battery cell and they are controlled based on the battery cell charge, [68], see Fig. 1.7(d). The battery cells exchange charge with the common DC link based on their charge, i.e, lower charged cells absorb charge and higher charged cells transfer charge. This method has a high efficiency and speed of equalization but it is expensive and power density is low.

Cell to String to Cell methods are the best method in terms of speed of equalization and efficiency. Their cost and power density can be compromised by their modularity and efficiency. Therefore, the main focus is to minimize the cost and power density of the converters and transformers which are using in these methods. Many methods are introduced to improve the power density and cost of the circuit. One of the promising solutions is presented in [2] although, this method sacrifices the speed of equalization.

1.2.4 Comparison

The aforementioned methods can be compared to highlight their advantages and disadvantages. The features which are studied are modularity, ability to transfer charge between non-neighbor cells, number of batteries supported due to the limited number of controller input, amount of exchanged charge between different cells in one cycle, number of switches, diodes and, sensors, controller and its complexity. Some of the introduced methods are compared in Table. 1.2.

TABLE 1.2: Comparing different methods for a system with $2n$ battery cells.

Method / Feature	Cap. & Inductor-based						Trans. based	Conv.-based	
	[30]	[43]	[67]	[65]	[59]	[57]	[64]	[68]	[2]
Modularity	y*	y	n*	n	y	y	y	y	y
Non-neighbor Cell Charge Transfer	n	n	y	y	y	y	y	y	y
Supports Unlimited Number of Batteries	y	y	n	n	y	y	n	y	y
Simultaneous Charge Transfer Between All Cell in a Cycle	n	n	y	y	n	n	n	y	y
Number of Switches	$4n$	$2n$	1	$2n$	$2n$	$4n$	$8n+1$	$16n$	$2n$
Number of Diodes	0	0	$2n$	$2n$	$2n$	0	2	0	$2n$
Number of Sensors	0	$2n$	0	0	$2n$	$2n$	$2n$	$2n$	n
Central/Distributed Controller	Dist	Dist	Dist	Cent	Cent	Cent	Cent	Dist	Dist
Complexity	S**	S	S	C**	C	C	C	C	S

* y for Yes and n for No
** S for Simple and C for Complex

1.3 Control Variables

The controller decision making is based on input signals. The are several control variables introduced in literature as controller variables of battery cell equalizers. Advantages and disadvantages of these variables are listed in Table. 1.3. The first three control variables have a defective relation to the cell energies and effects like the variances of internal resistances and total charge capacities are not considered; these effects increase over time. For example, two 3.8V battery cells and SOCs of 50% differ in their cell energies, when they have different energy capacity. On the other hand, control variables with model-based estimation suffer from estimation, measurements and model errors [69].

TABLE 1.3: Comparing different control variable for battery balancing systems.

Control Variable	Advantages	Disadvantages
Cell Voltage	➢no state estimation/complex calculation required ➢no error influence by state estimation	➢error by internal resistance variance ➢error by total charge capacity variance ➢no balancing in flat OCV area
Open-circuit Voltage	➢compensation of internal resistance variance	➢error by internal resistance variance ➢influence of state estimation error ➢error by total charge capacity variance ➢no balancing in flat OCV area
State of Charge	➢compensation of internal resistance variance ➢balancing in flat OCV area ➢consideration of temperature influence	➢error by internal resistance variance ➢influence of state estimation error ➢error by total charge capacity variance
Charge capacity	➢compensation of internal resistance variance ➢balancing in flat OCV area ➢consideration of temperature influence ➢balanced cell energies	➢multiple error influences e.g. SOC estimation, measurements

1.4 Motivation

The review of the existing battery charge equalization methods reveals that the best strategies, from the speed of equalization and efficiency point of view, are Cell to String to Cell methods. However, based on Table. 1.2, it can be concluded that there are features, which can be improved to achieve better performance. There are important feature such as scalability, power density, cost, controller complexity and, controller system which can be improved to achieve better performance. Scalability or modularity are important features since they provide the possibility of using the batteries in a large number of applications and voltage ranges. High number of components increases the cost of the system which is not desirable. A central controller, due to its limited number of inputs and extensive wiring limits the number of battery cells that can be supported. Therefore, the main goal of the topologies examined is to keep the advantages of the Cell to String to Cell methods and to strengthen the weaknesses of the previously published methods.

1.5 Objectives & Outline

The main objective of this research was to design and implement a compact, modular and efficient battery voltage balancing systems along with their controllers. To accomplish this goal, three topologies and their control systems are proposed. The analysis of the circuits and comprehensive design procedure for each one of them is presented. Concisely, the research objectives are as follows:

- The circuits and controllers are scalable and modular. This means that the controller should be distributed and its inputs should be local data. The local data can only come from its neighbor bridges/modules that the bridge/module has connection with.

- The number of switches and diodes are minimized to decrease the cost and complexity of the system. Lower number of switches not only decreases cost of switches but also decreases hidden cost of gate driver systems.

- The number of sensors are minimized to decrease the cost. This would decrease the component cost as well as hidden cost of signal isolation, conditioning and/or digitization circuitry.

- The circuits are able to transfer charge between all battery cells in every switching cycle, and the charge goes from the higher voltage battery cells to lower voltage battery cells. Since battery cells are magnetically or electrically coupled, it is possible to exchange charge between battery cells even when they are not neighbor.

- The system is compatible for different kind of battery cells with different voltage levels. Therefore, a comprehensive and flexible design procedure is required to design circuits with different power ranges.

- These modules do not operate or consume power unless voltage of a battery cells drifts. Then, all the modules start operating to equalize voltage of battery cells. In some cases, it is important to know how much time it takes to equalize the voltage of battery cells when voltage of one of them drifts. So, the calculation and estimation of the equalization time is one of the objective of this reach.

- To avoid centralized or master/slave controller, distributed controllers are proposed. The first converter that detects the unbalanced voltage, generates the synchronization signal and sends it to all the controllers. Therefore, there is no master-slave controller which could make a problem in case of the master controller failure.

- The circuits should operate with a fixed switching frequency and to decrease the losses in the circuits Zero Current switching (ZCS) operation is guaranteed.

1.6 Proposed Circuits

Three battery voltage equalization methods are described and schematics of the proposed methods along with their controllers are shown in Fig. 1.8. The proposed methods are modular, low-cost, low component count and small compared to the methods in this category. A comparison between the proposed methods and methods in this category is presented in comparison chapter.

From a topology perspective, each bridge/module is connected between two neighboring battery cells of the string in a way that neither of modules share a battery cell. Also, the basic topology in the first and second methods is asymmetrical bridges and in the third method is a Sepic module. Neighboring modules are connected using transformer coupled inductor shown in Fig. 1.8. Three types of bridge/modules connections are used to connect the inter-bridge/module windings: “Cascaded”, “Series” and “Parallel” Connection, see Fig. 1.8.

In the first method, see Fig. 1.8(a), asymmetrical bridges are connected as Daisy chain, that is the reason this method is called “Transformer Coupled Cascaded-Connected Asymmetrical Bridges” (TCCAB) or in the short form “Cascaded method”. The inter-bridge windings of each asymmetrical bridge is connected to its neighbor and the first and last bridge windings are also connected together, therefore, coupled inductors make a chain connection in which all windings are connected together through each other. In the second method, “Transformer Coupled Series Connected Asymmetrical Bridges” (TCSAB) or in the short form

"Series method", Fig. 1.8(b), asymmetrical bridges are connected in series using their inter-bridge winding. Finally, in the third method, "Transformer Coupled Parallel Connected Sepic Module" (TCPSP), or in the short form "Parallel method" Fig. 1.8(c), Sepic modules are connected in parallel using inter-module windings. The inter-module windings share a bus and connected in parallel. Consequently, these methods are scalable and can be extended to cover more battery cells by connecting more modules to the string of battery cells. Each bridge/module has a distributed controller and that uses local data to generate switching pattern of the bridge/module. These method do not require a central controller. The distributed controller approach has many advantages over a central controller. For example, there is no limit on the number of battery cells which can be supported. The central controller can support limited number of battery cells due to their limited number of inputs. Moreover, the use of local data makes the wiring and controller implementation simpler.

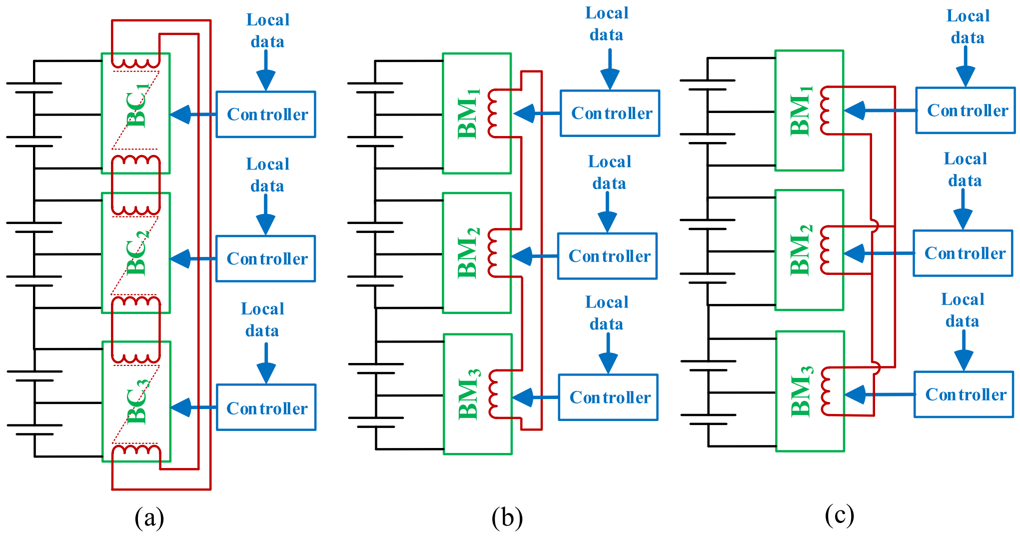

FIGURE 1.8: Schematics of the proposed methods (a) First method (Cascaded) (b) Second method (series) (c) Third method (Parallel).

The controller feedbacks in the proposed circuits use only the voltage of battery cells. To compare the voltage feedback and SOC estimation advantages and disadvantages refer to Table. 1.3. To make it more clear, when the voltages of battery cells are equal, it does not mean their SOCs are necessarily equal. Although the SOC estimation has advantages over voltage measurements, SOC estimation requires more complicated control and calculations and it needs a higher number of feedback signals; current and voltage of each battery cell. The SOC estimation procedure is complex and there may be some state estimation errors. Moreover, the SOC estimation method should be completely modified when the battery cell types are changed while this is not necessary in the voltage balancing methods. On the other hand, the voltage feedback is simple, not expensive and there is no estimation error. Moreover, in the proposed methods, controllers use the total voltage of battery cells in a bridge/modules as their inputs. Therefore, only one voltage sensor per two battery cells are used which makes the system cost lower. Furthermore, due to the fact that $Li-ion$ battery cells have a linear SOC vs. voltage characteristic, see Fig. 1.1, voltage of battery cells can be used as control variable in systems with $Li-ion$ battery cells.

Three battery voltage balancing topologies and control systems in this research are described briefly as follows:

In Transformer Coupled Cascaded-Connected Asymmetrical Bridge, Cascaded method, [70–72], a modular two-switch flyback battery cell voltage balancing circuit is presented. This method falls into Cell to String to Cell which shows a better performance among all the methods. The topology is modular with a low switch count per battery cell, see Fig. 1.8(a). Charge transfer to and from battery cell pairs in adjacent bridge cells is decided locally within each bridge by monitoring the DC voltages of the battery cells connected to adjacent bridges. Therefore, the system requires only one voltage sensor per battery cell pair. This “Distributed" controller is based on local data without requiring a central controller. Cascaded method operates in Discontinues Conduction Mode (DCM), therefore, it can maintain a fixed switching frequency and guarantees ZCS. Faster voltage balancing is achieved at a high efficiency using no current sensors and fewer voltage sensors when compared to conventional methods. The distributed controller improves upon previously published controllers using similar topology [2]. The controller has a much faster battery cell charge equalization than was obtained in [2]. The control is demonstrated to transfer charge between neighboring bridge cells in one switching cycle, but can also transfer charge between all bridges. The converter is analyzed and a design methodology is proposed. A prototype is built based on the designed values and experimental results are presented. simulations and experimental results are presented to validate the analysis and design procedure.

Transformer Coupled Series-Connected Asymmetrical Bridges, Series method, similar to Cascaded method, is a modular and can be categorized into Cell to String to Cell group that has their advantages such as transferring charge between all the cells in a cycle, see Fig. 1.8(b). This method does not need a central controller, all the controllers input are local data, and there is no limitation on the number of battery cells similar to Cascaded method. Moreover, this method requires only one per a battery cell and one voltage sensor per two battery cells similar to cascaded method. Also, this method guarantees the fixed switching frequency and ZCS. Although, in this method, the number of connections and coupled inductor windings is lower compared to Cascaded method, ergo and the total cost of the system will be decreased. This decrease in the cost of the system is achieved by scarifying the voltage stress on the components. In addition, circuit analysis and the design procedure are simpler than Cascaded method. In this approach, it is possible to predict currents and voltage waveforms. Also, there is an option to set the equalization time as one of the design constraints which cannot easily achieved in Cascaded method. Analysis of the circuit is presented to be used to present design procedure, based on which, a prototype circuit is built. To validate the method, experimental results are compared with analytical calculations and simulations.

Transformer Coupled Parallel-Connected Sepic Module, Parallel method, is modular similar to Cascaded and Series methods but has fewer number of switches. This method similar to Cascaded and Series methods is able to transfer charge between all battery cells in a cycle, therefore, it is categorized into Cell to String to Cell methods. This circuit maintains a fixed switching frequency but it cannot guarantees ZCS. Moreover, the controller limits the current in the circuit without using any feedback control signals. Therefore, Parallel method is a modular, low-cost and fast method. Every two battery cells are connected to a module and modules are connected through transformers secondary windings. The connection causes all modules to have the similar effect on each other and make the operation and analysis more predictable. The distributed controller is easy to implement and requires only one voltage sensor per two battery cells. A comprehensive analysis and design procedure are presented, and a prototype circuit is designed and implemented. To validate the method, experimental results are compared with analytical calculations and simulations.

CHAPTER 2

Transformer Coupled Cascaded Connected Asymmetrical Bridge

The proposed distributed control method improves upon previously published controllers using similar topology [2], . The controller has a much faster battery cell charge equalization than was obtained in [2]. The control method is demonstrated to transfer charge between neighboring bridge cells in one switching cycle while, can also transfer charge between all bridges. Also, the circuit offers ZCS in turn ON which decrease the loss in the circuit. The structure and operation of the modular bridge cell is examined to derive a new simplified system circuit model that containing a series of $2n$ connected battery cells with n bridge cells. This simplified model uses per-unit design parameters to provide a detailed charge flow analysis, select appropriate circuit inductance and to place limits placed on the controller switching periods. A maximum battery cell voltage deviation is assumed in the design procedures together with the following design guidelines: (a) a maximum component peak current; (b) a maximum switching frequency where all circuit currents reach zero at the end of each switching cycle; (c) the controller maximizes the charge transfer rate. Finally, it is compared to previously published work.

2.1 Structure and Operation

A single Bridge Cell, or in the shorter form bridge or BC, consists of asymmetric half-bridge, two series connected battery cells, and a toroidal transformer with 4 windings, see Fig. 2.1(a): w_1, $w_{1'}$, w_2 and $w_{2'}$. The magnetizing inductance associated with the transformer windings w_1 and w_2 places a limit on the peak current that is common to both windings during the switch on time. Conversely, L_f, controls the difference between the winding currents which can also produce large peak winding currents: L_f is necessary due to the very low leakage inductance of the transformer windings (typical $< 0.1\%$.). The transformer windings $w_{1'}$ and $w_{2'}$ are used to couple one bridge with its neighboring bridges, making the topology modular: see Fig. 2.1(b) for a multi bridge system. The topology needs an even number of battery cells, although it is possible to use the system with an odd number of battery cells. There are two options to use the system with an odd number of battery cells: 1) It is possible to add a capacitor in series with the string of battery cells and treat that capacitor as a battery cell in the string. 2) It is possible to use the circuit shown in Fig. 2.2. The only difference between these two solutions is that the analysis would be a bit different. Since the analysis would be different, the analysis and design procedure are presented for the first option. The analysis and design procedure can be modified to use the second option.

2.1.1 Equivalent Circuit

An equivalent circuit is introduced to make it easier to analyze the circuit and calculate current of battery cells and windings. To achieve the equivalent circuit

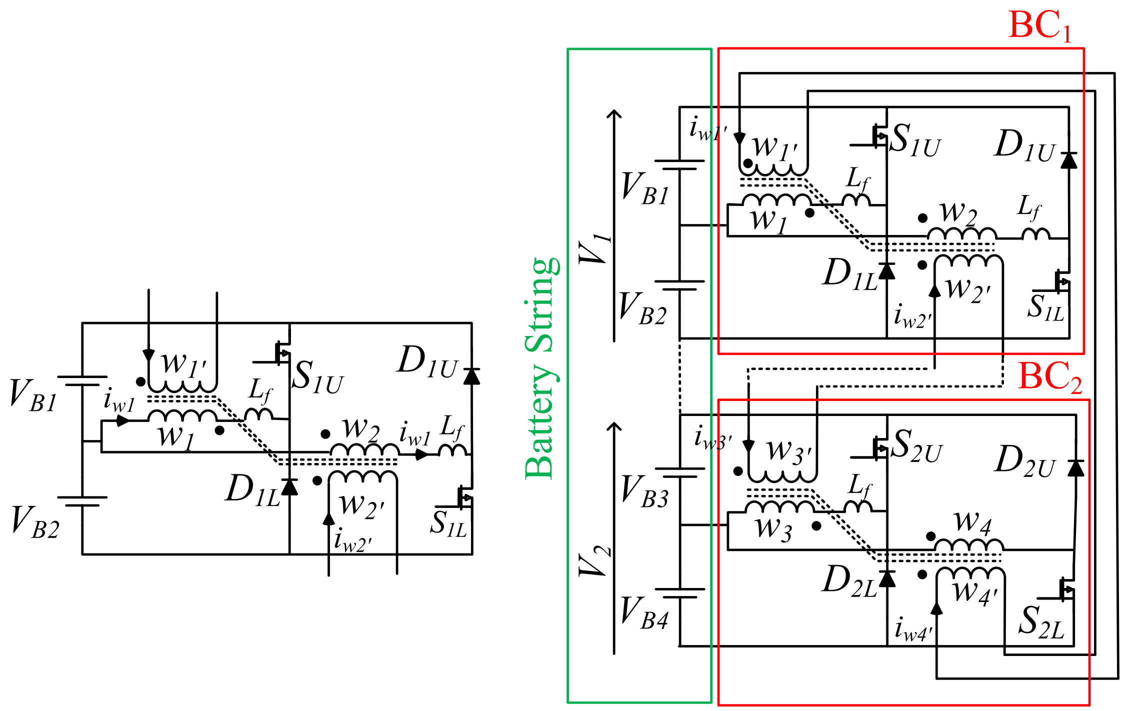

(a) (b)

FIGURE 2.1: Schematic of the proposed circuit (a) a bridge (b) multi bridge connection.

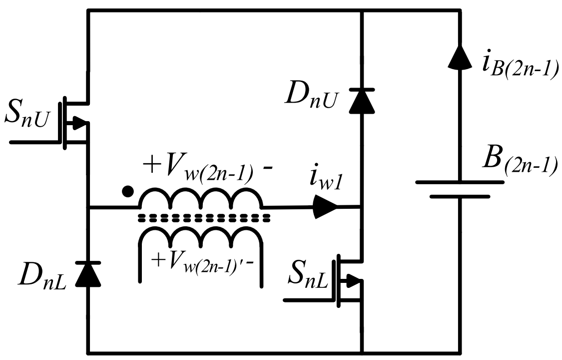

FIGURE 2.2: A solution to use Cascaded method with an odd number of battery cells.

of the system, first an equivalent circuit of a bridge should be presented. The resulting equivalent circuit of the coupled inductors in bridges is shown in Fig. 2.4. To prove this, assume all the windings are similar, number of turn is N and ϕ_c and ϕ_{li} are core and leakage flux in the circuit, see Fig. 2.3(a). These flux can be calculated as follows:

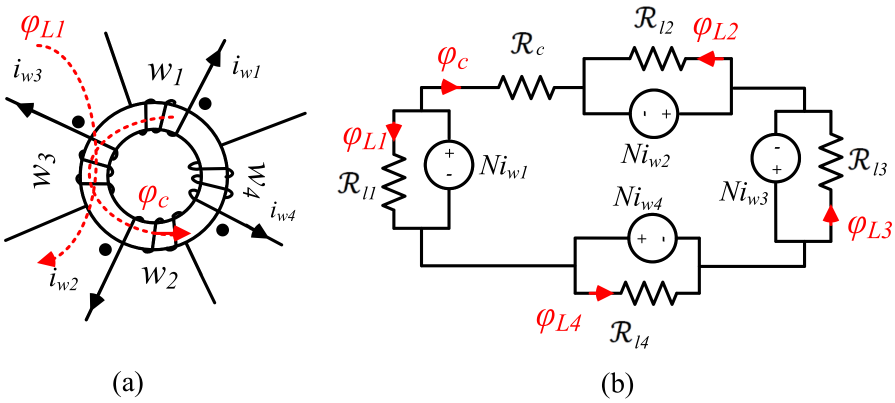

FIGURE 2.3: Coupled inductor (a) real model (b) equivalent model.

$$\begin{cases} \Phi_c = \dfrac{N(i_{w1} + i_{w2} + i_{w3} + i_{w4})}{\mathcal{R}_c} \\ \Phi_{li} = \dfrac{Ni_{wi}}{\mathcal{R}_{li}} \end{cases} \tag{2.1}$$

$$\lambda_{wi} = N(\Phi_c + \Phi_{li}) = \frac{N^2 \sum_{k=1}^{4} i_{wi}}{\mathcal{R}_c} + \frac{N^2 i_{wi}}{\mathcal{R}_{li}} \tag{2.2}$$

Therefore, voltage of each winding is as follows:

$$v_{wi} = \frac{d\lambda_{wi}}{dt} = N\frac{d(\Phi_c + \Phi_{li})}{dt} = \frac{N^2 \sum_{k=1}^{4} \frac{di_{wi}}{dt}}{\mathcal{R}_c} + \frac{N^2 \frac{di_{wi}}{dt}}{\mathcal{R}_{li}} \tag{2.3}$$

The above equation can be simplified as:

$$v_{wi} = L_{mi}\frac{d}{dt}\left(\sum_{k=1}^{4} i_{wi}\right) + L_{li}\frac{di_{wi}}{dt} \tag{2.4}$$

Since all the coupled inductor are identical, it is assumed that L_m and L_l for all of them are equal. Therefore, it can be concluded that the equivalent circuit of Fig. 2.4(a) is shown in Fig. 2.4(b).

Now, the switching action should be studied to achieve the equivalent model in

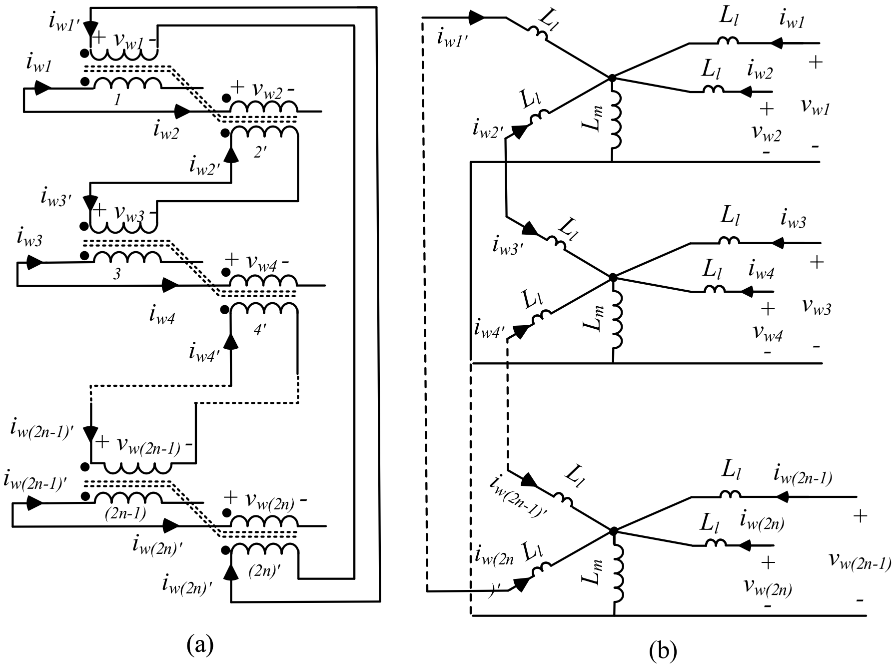

FIGURE 2.4: Windings connection of three Bridge Cells (a) real model (b) equivalent model.

different switching states. The effect of switching actions in the equivalent circuit is shown in Fig. 2.5. There is a connection between windings of a coupled inductor in the centre tap of the battery cells which is removed in the equivalent circuit. That connection is removed since there is no current through that connection.

To show the switching action and equivalent circuit better see Fig. 2.6.

It is assumed that $L_l << L_f$ and $L_l << L_m$, therefore, it is possible to neglect L_l when it is connected in series with L_f. Thus, voltage of all windings in a coupled inductor would be equal. For example, voltage of windings in the coupled inductor in bridge 1 can be calculated as follows:

$$v_{w_1} = v_{w_2} = v_{w_3} = v_{w_4} = L_m \frac{d}{dt}\left(i_{w_1} + i_{w_1'} + i_{w_2} + i_{w_2'}\right) \tag{2.5}$$

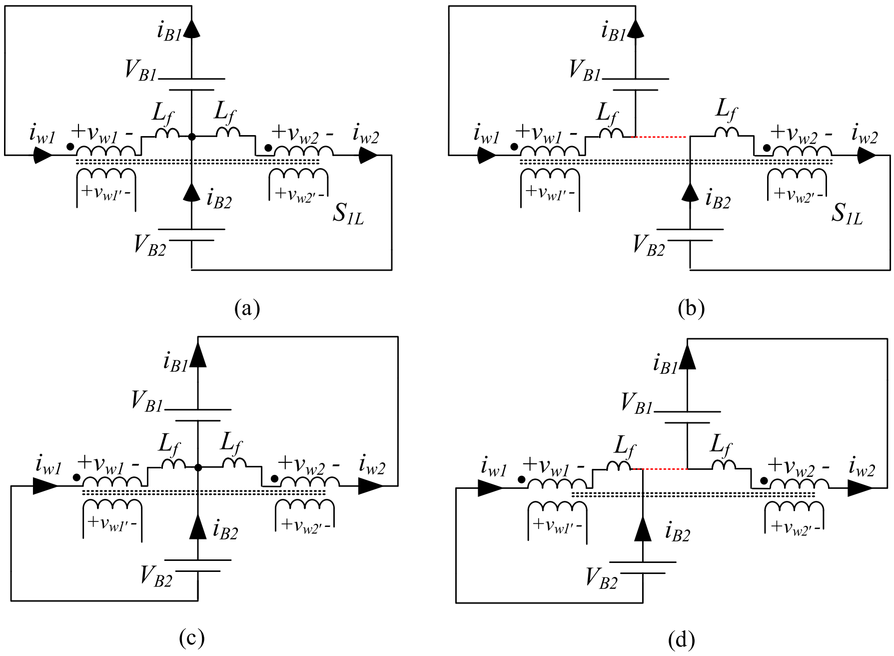

FIGURE 2.5: Schematic of the circuit (a) when switches are ON (b) equivalent circuit when switches are ON (c) when diodes are ON (d) equivalent circuit when diodes are ON

Therefore, the final equivalent circuit for a BC can be drawn as it is shown in Fig. 2.7.

The general equivalent circuit for a *BC* in Fig. 2.7(b), can be extended to a system containing "n" BCs and "$2n$" battery cells, as shown in Fig. 2.8.

The main goal is to calculate the current in the windings of the system. To be able to calculate the winding currents it is necessary to calculate the voltages, V_{w_i} in Fig. 2.8. All the coupled inductors are assumed to be identical and the circuit is symmetrical therefore, matrix representation of KCL on Fig. 2.8, is shown in Eq. (2.6).

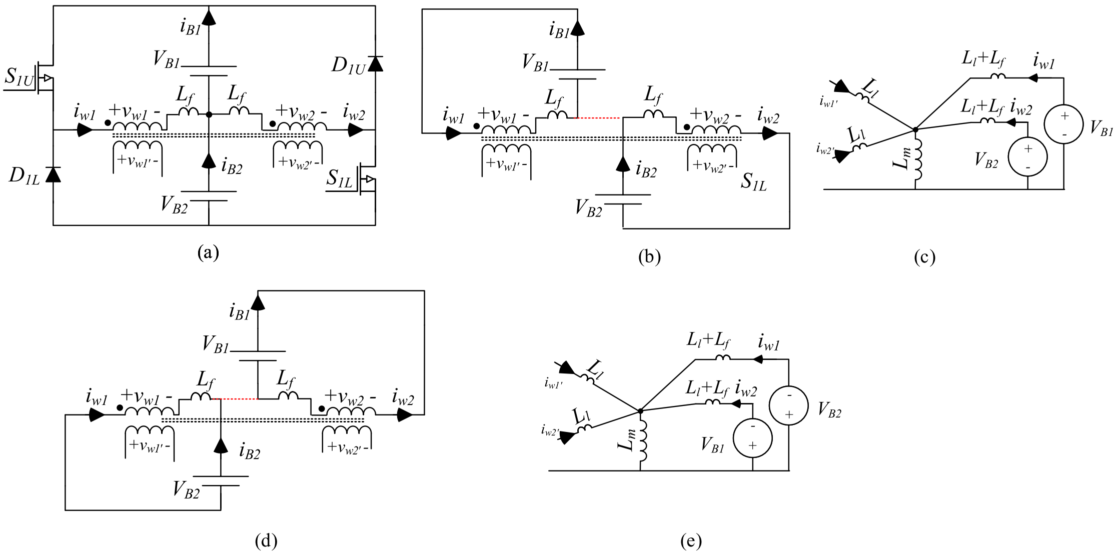

FIGURE 2.6: Schematic of the circuit (a) with switches and diodes (b) when switches are ON (c) equivalent circuit when switches are ON (d) when diodes are ON (e) equivalent circuit when diodes are ON

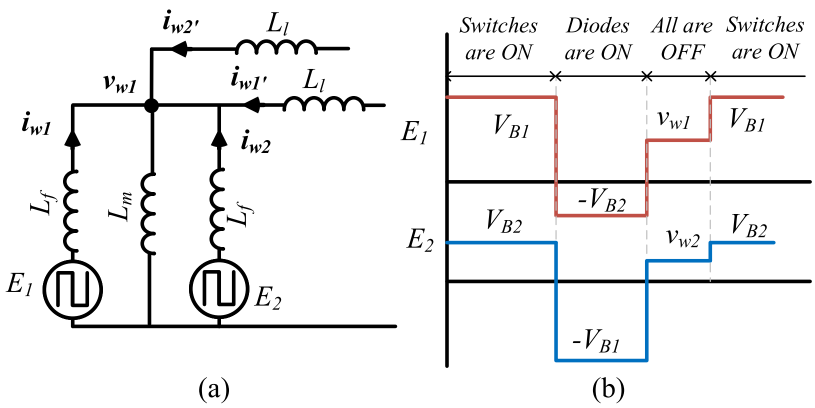

FIGURE 2.7: BC equivalent circuit of 1 bridge: (a) general equivalent circuit (b) voltage waveform of E_1 and E_2 (L_m: magnetizing inductance for two windings, L_l: leakage inductance for two windings, L_f added series inductance)

$$
\begin{bmatrix}
Y_s & \frac{-1}{2L_l} & 0 & 0 & \dots & \frac{-1}{2L_l} \\
\frac{-1}{2L_l} & Y_s & 0 & \dots & 0\dots & \frac{-1}{2L_l} \\
0 & \frac{-1}{2L_l} & Y_s & \dots & 0 & 0 \\
0 & 0 & \frac{-1}{2L_l} & Y_s & \dots & 0 \\
\vdots & \vdots & \vdots & \vdots & \ddots & \vdots \\
\frac{-1}{2L_l} & 0 & 0 & \dots & \frac{-1}{2L_l} & Y_s
\end{bmatrix}
\times
\begin{bmatrix}
v_{w1} \\ v_{w3} \\ v_{w5} \\ v_{w7} \\ \vdots \\ v_{w(2n-1)}
\end{bmatrix}
=
\begin{bmatrix}
\frac{E_1+E_2}{L_f} \\ \frac{E_3+E_4}{L_f} \\ \frac{E_5+E_6}{L_f} \\ \frac{E_7+E_8}{L_f} \\ \vdots \\ \frac{E_{(2n-1)}+E_{(2n)}}{L_f}
\end{bmatrix}
$$

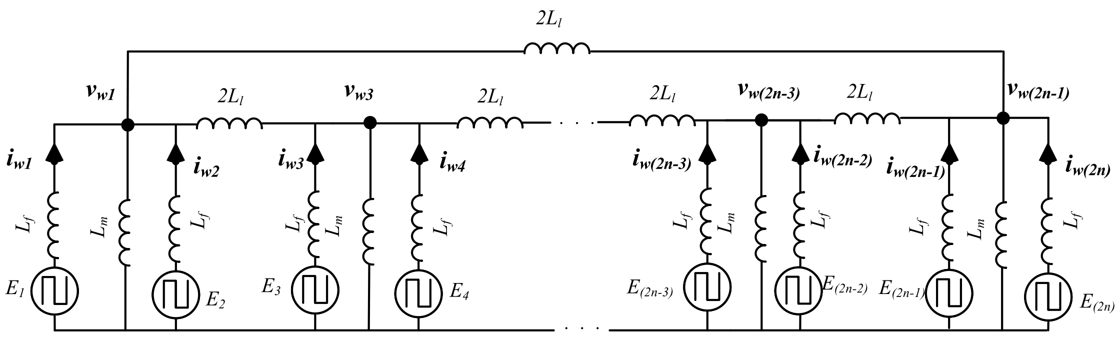

FIGURE 2.8: The equivalent circuit of a system with "n" bridges and "$2n$" battery cells.

where:

$$Y_s = \frac{L_m L_l}{L_m + L_l} + \frac{1}{L_f} \tag{2.7}$$

Assume all voltage sources are open circuit except for E_1, using Eq. (2.6) and Fig. 2.9(a), v_{w_1}. By calculating i_{w_1} based on v_{w_1} and E_1, the formula for calculating E_1 as a function of i_{w_1} can be calculated as follows:

$$\begin{bmatrix} Y_1 & \frac{-1}{2L_l} & 0 & 0 & \dots & \frac{-1}{2L_l} \\ \frac{-1}{2L_l} & Y_2 & 0 & \dots & 0\dots & \frac{-1}{2L_l} \\ 0 & \frac{-1}{2L_l} & Y_2 & \dots & 0 & 0 \\ 0 & 0 & \frac{-1}{2L_l} & Y_2 & \dots & 0 \\ \vdots & \vdots & \vdots & \vdots & \ddots & \vdots \\ \frac{-1}{2L_l} & 0 & 0 & \dots & \frac{-1}{2L_l} & Y_2 \end{bmatrix} \times \begin{bmatrix} v_{w1} \\ v_{w3} \\ v_{w5} \\ v_{w7} \\ \vdots \\ v_{w(2n-1)} \end{bmatrix} = \begin{bmatrix} \frac{E_1}{L_f} \\ 0 \\ 0 \\ 0 \\ \vdots \\ 0 \end{bmatrix} \tag{2.8}$$

$$where \begin{cases} Y_1 = \frac{1}{L_m} + \frac{1}{L_f} + \frac{1}{L_l} \\ Y_2 = \frac{1}{L_m} + \frac{1}{L_l} \end{cases}$$

$$\begin{bmatrix} v_{w1} \\ v_{w3} \\ v_{w5} \\ v_{w7} \\ \vdots \\ v_{w(2n-1)} \end{bmatrix} = \begin{bmatrix} \frac{E_1}{L_f} \\ 0 \\ 0 \\ 0 \\ \vdots \\ 0 \end{bmatrix} \times \begin{bmatrix} Y_1 & \frac{-1}{2L_l} & 0 & 0 & \dots & \frac{-1}{2L_l} \\ \frac{-1}{2L_l} & Y_2 & 0 & \dots & 0\dots & \frac{-1}{2L_l} \\ 0 & \frac{-1}{2L_l} & Y_2 & \dots & 0 & 0 \\ 0 & 0 & \frac{-1}{2L_l} & Y_2 & \dots & 0 \\ \vdots & \vdots & \vdots & \vdots & \ddots & \vdots \\ \frac{-1}{2L_l} & 0 & 0 & \dots & \frac{-1}{2L_l} & Y_2 \end{bmatrix}^{-1} \tag{2.9}$$

The similar procedure can be done to calculate the effect of $E_{(2n)}$ on i_{w_1}, see Fig. 2.9(b). Note that L_l is negligible when it is connected in series with L_f. Thus,

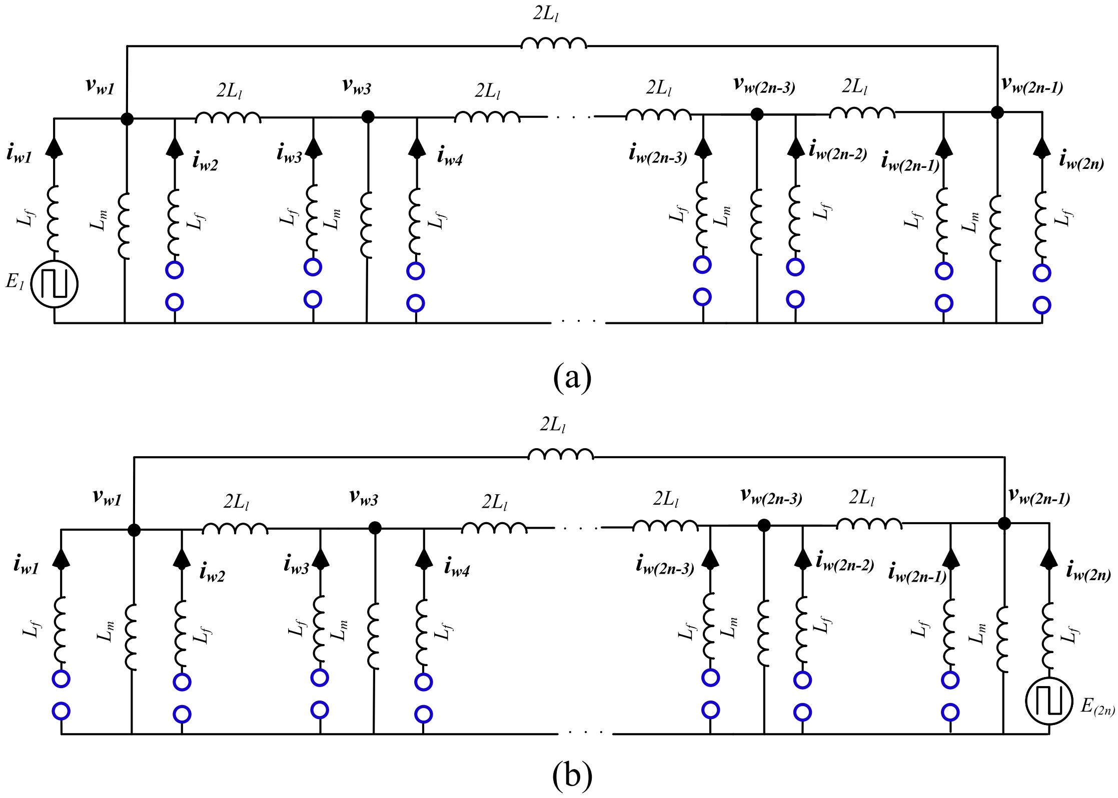

FIGURE 2.9: Effect of a voltage source on windings voltage (a) when only E_1 is connected (b) when only E_{2n} is connected.

voltage of windings in a module are equal, for example $v_{w_1} = v_{w_2}$. Finally, the following equation can be achieved:

$$\begin{bmatrix} L_{se} & L_{se} & L_{mu}(j) & L_{mu}(j) & \dots & L_{mu}(j) \\ L_{se} & L_{se} & L_{mu}(j) & L_{mu}(j) & \dots & L_{2,2n} \\ L_{mu}(j) & L_{mu}(j) & L_{se} & L_{se} & \dots & L_{mu}(j) \\ L_{mu}(j) & L_{mu}(j) & L_{se} & L_{se} & \dots & L_{mu}(j) \\ \vdots & \vdots & \vdots & \vdots & \ddots & \vdots \\ L_{mu}(j) & L_{mu}(j) & L_{mu}(j) & L_{mu}(j) & \dots & L_{se} \end{bmatrix}^{-1} \times \begin{bmatrix} E_1 \\ E_2 \\ \cdots \\ \cdots \\ \cdots \\ E_{(2n)} \end{bmatrix} = \frac{d}{dt} \begin{bmatrix} i_{w1} \\ i_{w2} \\ \cdots \\ \cdots \\ \cdots \\ i_{w(2n)} \end{bmatrix}$$

$$\rightarrow \begin{cases} [L_{pq}]^{-1} \times [v_{w,p}] = [a_{pq}] \times [v_{w,p}] \\ [a_{pq}] \times [v_{w,p}] = \dfrac{d}{dt}[i_{w,p}] \,, 1 < p, q < 2n \end{cases} \tag{2.10}$$

where:

$$\begin{cases} L_{se} = \dfrac{L_f}{\dfrac{-Y^{-1}(1,1)}{L_f} + 1} = \dfrac{{L_f}^2}{-Y^{-1}(1,1) + L_f} \\ L_{mu}(j) = L_{se} \dfrac{Y^{-1}(j,1)}{L_f} = \dfrac{L_f \times Y^{-1}(j,1)}{-Y^{-1}(1,1) + L_f} \end{cases} \tag{2.11}$$

L_{ii} can be defined as self-inductance; L_{ij} can be defined as mutual inductance between winding i and j; V_w and i_{w_i} are voltage and current of the i^{th} winding. Matrix "a" is the inverse of "L" matrix. Since all inductors are identical, self-inductance of all windings are equal and mutual inductance between inductors are equal, $L_{ij} = L_{ji}$.

Using the above equation, the voltage of nodes in Fig. 2.8 can be calculated and consequently, the windings current can be calculated which will be used in the design section.

As it can be concluded, the analysis of the following circuit is a bit complicated since bridges are connected together through windings are of other bridges. The

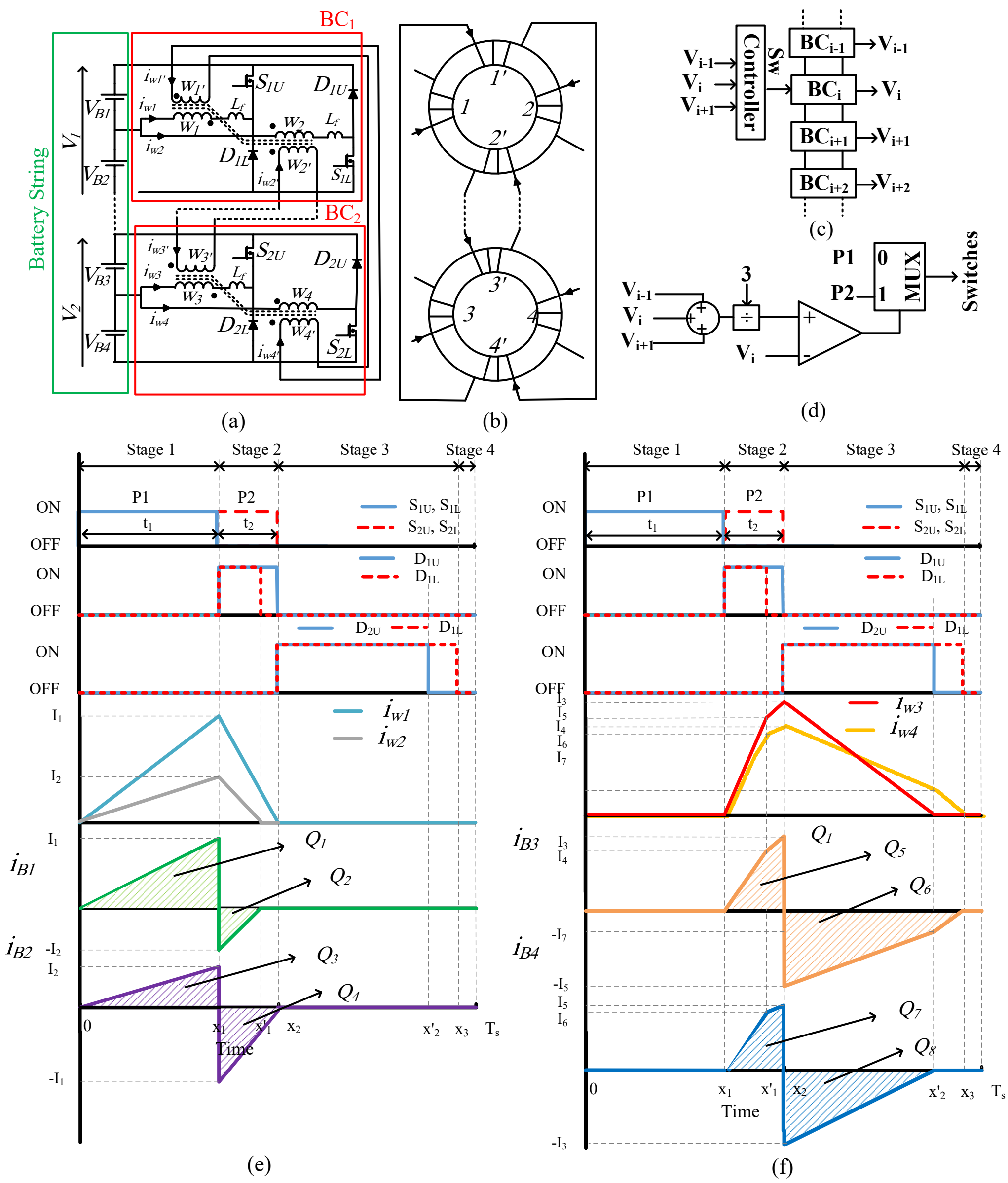

FIGURE 2.10: Connection of two Bridge Cells to 4 battery cells: (a) circuit and (b) transformer connections; (c) controller connections (d) controller decision making (e) BC_1 currents (f) BC_2 currents.

analysis of the TCS and TCP circuit are more straightforward since bridges are connected directly together.

2.1.2 Principal of Operation and Control: 2-Switch Flyback

The main goal is to distribute charge between battery cells based on their voltage. In other words, if voltage of a battery cell is greater than the voltage of its neighbor, the battery cells transfers charge or if its voltage is lower than its neighbor, the battery cell absorbs charge. Therefore, the idea is to identify the higher voltage battery cells locally and transfer charge from them to the lower voltage cells.

The controller which is responsible to distribute charge is a distributed controller since it has several advantages over a central controller. For example, the number of battery cells which can be supported by a central controller is limited due to the limited number of controller inputs. While, in a distributed controller, the number of battery cells is not limited by number of controller inputs. Furthermore, distributed controller keeps the system modular. The distributed controller chooses the switching pattern of each bridge by monitoring the dc battery cell voltages in adjacent bridges, see Fig. 2.10(c)-(d). The dc voltage V_i of BC_i (sum of its 2 battery cell voltages) is compared to the average of the adjacent bridge voltages and its own: $\frac{(V_{i-1} + V_i + V_{i+1})}{3}$. If V_i is the largest voltage, BC_i chooses the switching pattern "P1". If BC_i does not have the largest, it chooses the switching pattern "P2", see Fig. 2.10(e)-(f) for "P1" and "P2".

Assume, the battery cells voltage are as follow $V_{B1} > V_{B2} > V_{B3} > V_{B4}$. Therefore, BC_1 has the higher voltage ($V_1 > V_2$) and chooses the switching pattern $P1$, and BC_2 has a lower voltage and chooses $P2$, see Fig. 2.10.

In the first state, see Fig. 2.11, the switches in BC_1 are turned. Since $V_{B1} > V_{B2}$, i_{w1} increases more rapidly and reaches a higher value ($I_1 > I_2$), therefore, more energy is stored in w_1, see Fig. 2.10. This can be proved easily using the equivalent

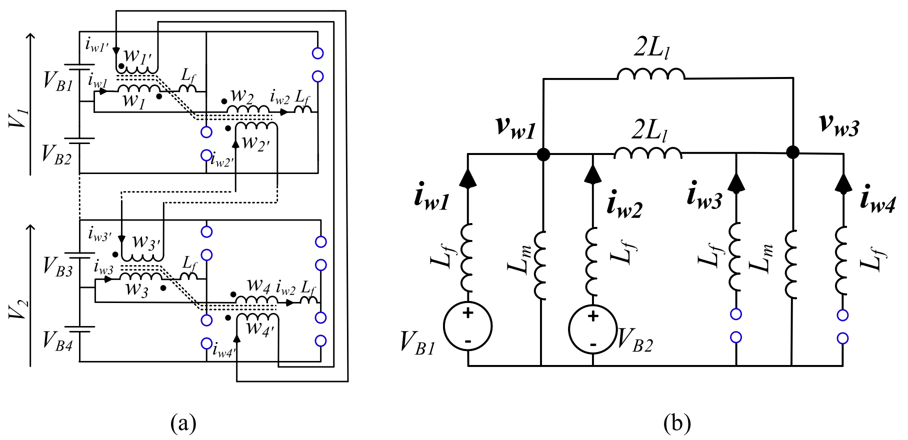

FIGURE 2.11: The proposed circuit in the first state (a) circuit with switches and diodes (b) the equivalent model.

circuit in Fig. 2.11(b). Slopes of i_{w_1} and i_{w_2} can be calculated as follows:

$$\begin{bmatrix} \dfrac{1}{L_m}+\dfrac{1}{L_f}+\dfrac{1}{L_l} & \dfrac{-1}{L_l} \\ \dfrac{-1}{L_l} & \dfrac{1}{L_m}+\dfrac{1}{L_l} \end{bmatrix} \times \begin{bmatrix} v_{w_1} \\ v_{w_3} \end{bmatrix} = \begin{bmatrix} \dfrac{V_{B_1}+V_{B_2}}{L_f} \\ 0 \end{bmatrix} \tag{2.12}$$

$$v_{w_1} = \frac{V_{B_1}+V_{B_2}}{L_f} \times \frac{L_f L_m (L_l + L_m)}{L_f L_l + 2L_f L_m + L_l L_m + {L_m}^2} \tag{2.13}$$

Since $V_{B_1} > V_{B_2}$ It can be concluded that $I_1 > I_2$:

$$\frac{V_{B_1}-V_{w_1}}{L_f} > \frac{V_{B_2}-V_{w_1}}{L_f} \Rightarrow \frac{di_{w_1}}{dt} > \frac{di_{w_2}}{dt} \tag{2.14}$$

$$\frac{di_{w_1}}{dt} \times x_1 > \frac{di_{w_2}}{dt} \times x_1 \Rightarrow I_1 > I_2 \tag{2.15}$$

Finally, peak of currents can be calculated as follows:

$$
\begin{cases}
I_1 = \dfrac{V_{B_1} - \dfrac{V_{B_1}+V_{B_2}}{L_f} \times \dfrac{L_f L_m (L_l + L_m)}{L_f L_l + 2L_f L_m + L_l L_m + {L_m}^2}}{L_f} \times x_1 \\
I_2 = \dfrac{V_{B_1} - \dfrac{V_{B_2}+V_{B_2}}{L_f} \times \dfrac{L_f L_m (L_l + L_m)}{L_f L_l + 2L_f L_m + L_l L_m + {L_m}^2}}{L_f} \times x_1
\end{cases}
\tag{2.16}
$$

In the second state, see Fig. 2.12, switches in BC_1 are turned off, thus diodes in BC_1 turn on. Therefore, the winding which has the higher current, w_1, is connected to lower voltage battery cell, B_2. Consequently, charge goes from higher voltage cell to lower voltage cell, this procedure is called intra-bridge charge transfer, see Fig. 2.13. This can be proved using Fig. 2.12(b) and these equations:

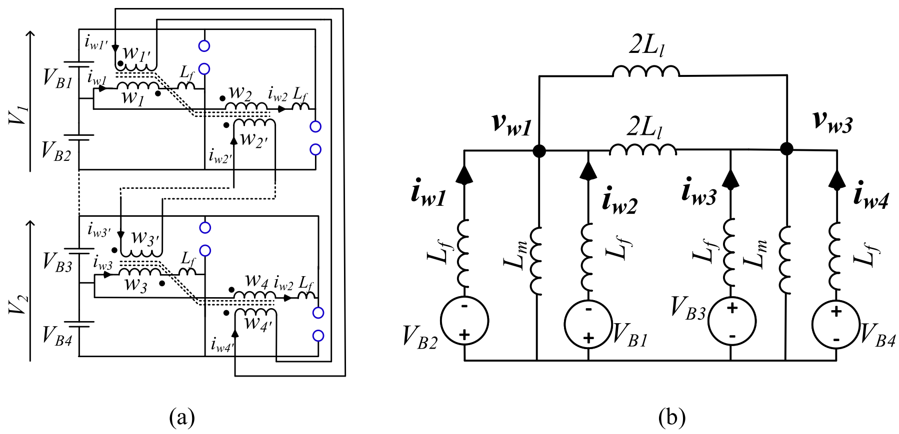

FIGURE 2.12: The proposed circuit in the second state (a) circuit with switches and diodes (b) the equivalent model.

$$
\begin{bmatrix}
\dfrac{1}{L_m} + \dfrac{1}{L_f} + \dfrac{1}{L_l} & \dfrac{-1}{L_l} \\
\dfrac{-1}{L_l} & \dfrac{1}{L_m} + \dfrac{1}{L_f} + \dfrac{1}{L_l}
\end{bmatrix}
\times
\begin{bmatrix} v_{w_1} \\ v_{w_3} \end{bmatrix}
=
\begin{bmatrix}
\dfrac{-V_{B_1} - V_{B_2}}{L_f} \\
\dfrac{V_{B_3} + V_{B_4}}{L_f}
\end{bmatrix}
\tag{2.17}
$$

$$\frac{-V_{B_2} - v_{w_1}}{L_f} < \frac{-V_{B_1} - v_{w_1}}{L_f} \Rightarrow \frac{di_{w_1}}{dt} < \frac{di_{w_2}}{dt} \tag{2.18}$$

Since $I_1 > I_2$ and $\frac{di_{w_1}}{dt} < \frac{di_{w_2}}{dt}$, it can be concluded that, i_{w_2} reaches zero first, $x_2 > x_1'$ in Fig. 2.10(e). Therefore, using Fig. 2.10(e) the exchanged charge of battery cell1 and 2 can be calculated as follows:

$$\begin{cases} Q_{B_1} = Q_1 - Q_2 = \dfrac{I_1 \times x_1 - I_2 \times x_1'}{2} \\ Q_{B_2} = Q_3 - Q_4 = \dfrac{I_2 \times x_1 - I_1 \times x_2}{2} \end{cases} \Rightarrow Q_{B_1} > Q_{B_2} \tag{2.19}$$

This means that B_1 transfers more charge than B_2.

Also, the switches in BC_2 are turned on in the second state. Therefore, some of the stored energy in the magnetic core of w_1 and w_2 is transferred to magnetic core of w_3 and w_4. This procedure is called inter-bridge charge transfer, see Fig. 2.13. This charge exchange can be seen more clear in Fig. 2.13, where different polarity of B_3 and B_4 cause L_{m_1} to discharge faster consequently, less charge goes back to B_1 and B_2.

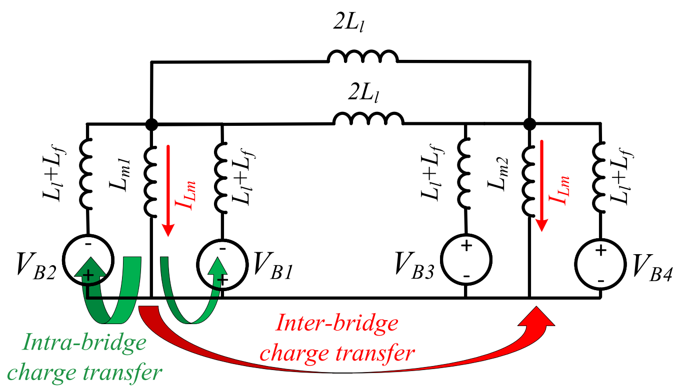

FIGURE 2.13: Intra and inter-bridge charge transfer.

In the third state all switches are off and the stored charge in L_{m_2} is transferred to B_3 and B_4. Again, in this state, the battery cell with lower voltage absorbs more charge, intra-bridge charge transfer.

Finally, in state 4, all switches and diodes are off until the next state starts. This switching state is added to guarantee the ZCS in turn ON and fixed switching frequency operation. Therefore, it is necessary to make sure that this state always exists.

In Fig. 2.10(e)-(f), the areas under the current waveforms represent the exchange charge. Examination of i_{B1}, i_{B2} for example, represent exchanged charge of battery cells in BC_1. For example, the exchanged charge of battery cell 2 in Fig. 2.10(e)-(f) equals to:

$$Q_{B2} = \int_0^{T_s} i_{B_2}(t)dt = \int_0^{t_1} i_{w_2}(t)dt - \int_{t_1}^{t_2} i_{w_1}(t)dt = \frac{I_2 \times t_1}{2} - \frac{I_1 \times (t_2 - t_1)}{2} = Q_3 - Q_4 \tag{2.20}$$

Comparing $Q_{B1} = Q_1 - Q_2$ and Q_{B2} in Fig. 2.10(e)-(f) it can be concluded that $Q_{B1} > Q_{B2}$, thus, battery cell 1 transfers more charges compared to battery cell 2. Similarly, it can be seen that battery cell 3 and battery cell 4 absorb charge.

2.2 Design Procedure

The main goal is to present a solution to choose components of the circuit and setting of the controller. In other words, a design procedure is presented which gets some inputs and the outputs would be design parameters. Input parameters, which are called system constraints, are number of bridges (n, equals to $2n$ battery cells), maximum and minimum voltage of battery cells (V_{max} and V_{min}) maximum allowable current (I_{max}) and, fixed switching switching frequency (f_s). The design parameters are duty cycles of the $P1$ and $P2$ (t_1 and t_2), inductance of the inductors, L_m and L_f, and components rating.

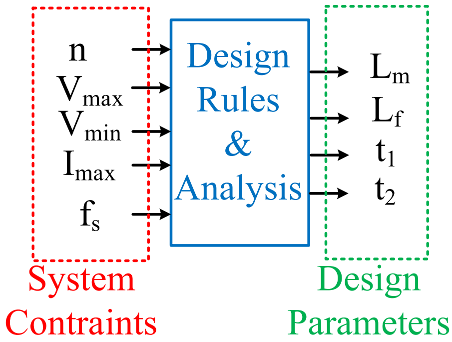

FIGURE 2.14: Design plan.

Therefore, circuit analysis is presented for a system containing a series of $2n$ connected battery cells with n bridge cells. The analysis uses the equivalent circuit, see Fig. 2.8, to calculate the inductors current waveforms and switching period as functions of the design parameters where the currents and voltages are maximum; worst cases. The predefined system constraints and designed rules are then used to calculate the design parameters. Given that the system is designed for a maximum allowable battery cell voltage deviation, this analysis also assumes the following design rules: (a) the controller is maximizing the charge transfer rate, (b) prevent charge back-flow. These two rules are applied by studying the effect of inductance variation.

2.2.1 Justification for Worst Case Design Scenarios

Circuit constraints i.e., I_{max} and f_s, are calculated as functions of the design parameters, L_m, L_f, t_1 and t_2. By applying the circuit constraints and design rules on the resultant functions, all design parameters can be calculated. In the beginning, the worst case scenarios are clarified then, the worst case scenarios are analyzed and I_{max}, V_{max} and, f_s are calculated as functions of design parameters.

The analysis are done for the worst case scenarios since no current sensor is used in the circuit, hence, it is necessary to make sure that the currents of inductors and switches never beat their maximum limit and the circuit operates in DCM mode. Worst case scenarios for the currents and switching period occur when currents reach their maximum and, the switching period is the longest. To make sure all the system constraints are met in all the conditions, two extreme-case scenarios are considered:

Case 1: Battery cell 1 has the highest possible voltage and the others have the lowest possible voltage.

Case 2: Battery cell 1 has the lowest possible voltage and the others have the highest possible voltage.

Case 1 and 2 are the extreme cases for currents and switching period. To clarify the extreme case scenarios, assume Fig. 2.8, maximum current occurs when (a) case 1: only battery cell 1 has the highest voltage and, bridge 1 switches are on and all the other bridges are off. In this case, all the magnetizing inductance are cascaded the equivalent inductance would be very small. Also, the fact that all other bridges are on in state 2 and their current should reach zero before end of the cycle makes a worst case scenario for switching period too. (b) case 2: all battery cells have the highest voltage except battery cell 1 which has the lowest voltage. In this case, switches of all bridges are on except switches of bridge 1. Since in the second state the voltage polarity of bridges are different it can make a high current in bridge 1. Therefore, it is necessary to analyze these two cases and make sure all the system constraints are met in these two cases.

2.2.2 Worst Case Scenarios Analysis

The maximum current and, switching period in worst case scenarios should be calculated based on the design parameters. Then, based on the predefined system constraints and design rules all design parameters can be found. The analysis of case 1 is as follows:

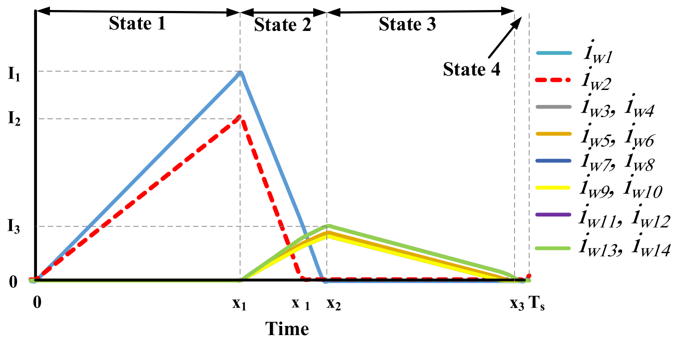

FIGURE 2.15: Current waveforms of a 7 bridges system under case1.

Case Scenario 1: This case results in bridge 1 choosing switching pattern $P1$ and rest choose $P2$, see Fig. 2.10, 2.15. During the first switching state, the switches BC_1 are turned on and i_{w1} and i_{w2} increase. Since battery cell 1 has the highest voltage, i_{w1} reaches a higher value, I_1, compared to i_{w2}, I_2. I_1 can be calculated as follows:

$$I_1 = [+V_{\max}a_{11} + V_{\min}a_{12} + V_{\min}\sum_{j=3}^{2n} a_{1j}] \times t_1,\ t_1 = x_1 \tag{2.21}$$

V_{min} and V_{max} - the minimum and maximum voltage of battery cells, t_1 is the duration of the first state and, $a = L^{-1}$.

The voltage variation considered around the nominal is $\pm 0.5V$ for a $4V$ battery cell. Therefore, it is not possible that the Diodes D_{2U} and D_{2L} conduct since the voltage drop of diodes and the drop on the series added inductance would be more than $1V$. Therefore, the allowable battery voltage swing of $4 \pm 0.5V$ means that the MOSFET body diodes never get forward biased so as to conduct. The system inductance also contributes to prevent the diodes from conduction significant current.

The next state should be long enough to make the currents of the inductors in the first bridge reach zero. Therefore, the duration of the second state, t_2, can be calculated as follow:

$$t_2 = \frac{-I_1}{-V_{\min}a_{11} - V_{\max}a_{12} + V_{\min}\sum_{j=3}^{2n} a_{2j}}, \quad x_2 = t_1 + t_2 \tag{2.22}$$

During the second state, the currents in bridges 2 to 7 ramp positively with the currents in bridges 2 and 7 reaching a higher value as they are situation closer to the bridge 1 in the circuit. Therefore, the maximum current in this state in winding 3 is:

$$I_3 = [-V_{\min}a_{31} - V_{\max}a_{32} + V_{\min}\sum_{j=3}^{2n} a_{3j}] \times t_2 \tag{2.23}$$

The third state should be long enough to make sure all currents reach zero. Therefore, duration of this state can be calculated based on the time that takes for i_{w3} to reach zero.

$$t_3 = \frac{-I_3}{-a_{3,1}V_{\min} - a_{3,2}V_{\min} - V_{\min}\sum_{j=3}^{2n} a_{3,j}}, \quad x_3 = t_1 + t_2 + t_3 \tag{2.24}$$

To satisfy the design constraints which are f_s and I_{max}:

$$\begin{cases} T_s = T_{s,desired} \\ I_{\max} = \mathrm{I}_{max,desired} \end{cases} \Rightarrow \begin{cases} T_{s,desired} = t_1 + t_2 + t_3 \\ \mathrm{I}_{\max,desired} = I_1 \end{cases} \tag{2.25}$$

After some equation simplifications, the system design constraints can be defined as:

$$A = \sum_{j=1}^{2n} a_{1j} \rightarrow \begin{cases} T_{s,desired} = t_1 + \dfrac{-(3V_{\min} + V_{\max})a_{13} \times [\Delta V a_{11} + V_{\min}A] \times t_1}{-V_{\min}A \times [-2V_{\min}a_{11} - (V_{\min} + V_{\max})a_{12} + V_{\min}A]} \\ \mathrm{I}_{max,desired} = \Delta V a_{11} + V_{\min}A \times t_1 \end{cases} \tag{2.26}$$

The unknown variables in Equation 2.26 are t_1 and matrix "a" elements, these can be calculated using the magnetizing inductance of the coupled inductor and the added series inductance. It is assumed that the leakage inductance is $= 1\%$ of magnetizing inductance since the coupled inductors used normally have very low leakage inductance. As there are two equations and three unknown variables, t_1, L_m and L_f, the series added inductance is assumed to be sized relative to the magnetizing inductance.

The design constraints for I_{max} and f_s are discussed in equations. 2.25 and 2.26. The third constraint, maximizing the charge transfer, is satisfied by setting the duration of switching state 2 so that the first bridge currents reach zero at the end of the state. As a result, the transferred charge by other bridges and the absorbed charge by the first bridge are minimized. Since the first bridge has the highest voltage and it should be transferring charge as much as possible, the duration of state 1 is long enough so that the currents of first bridge reaches the maximum allowable current. This means that for state 1, the charge transfers of bridge 1 is maximized. During state 2, the other bridges are transferring charge while bridge 1 absorbs charge. The duration of state 2 is therefore minimized to limit the absorbed charge by bridge 1.

Case Scenario 1: Battery cell 1 has the lowest voltage, while the other battery cells have the highest voltage. Consequently, BC_1 chose the P_2 switching pattern while the rest choose P_2, see Fig. 2.16. The maximum bridge current in switching state 1 is:

$$I_3 = [a_{31}V_{min} + a_{32}V_{\max} + V_{max}\sum_{j=3}^{2n} a_{3j}] \times t_1,\ x_1 = t_1 \tag{2.27}$$

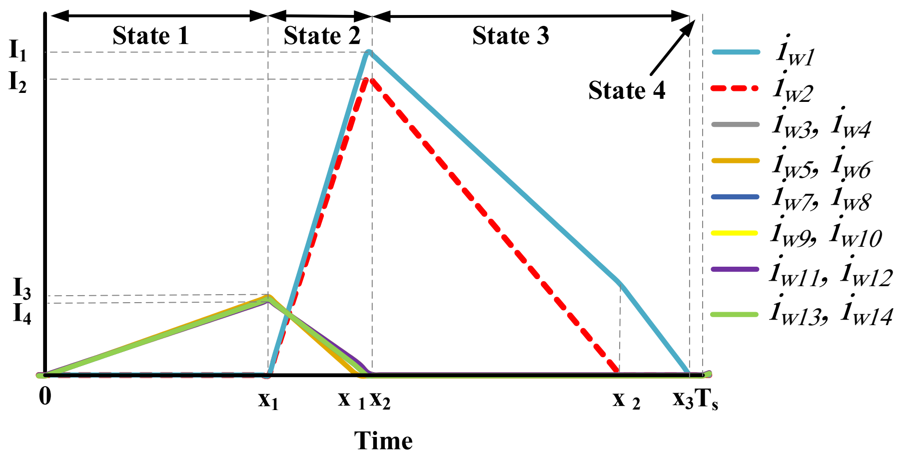

FIGURE 2.16: current waveforms of a 7 bridges system under case2.

Similar to the previous case, switching state 2 should be long enough to make sure all the currents in bridges 2 to 7 reach zero. Therefore, the lowest ramping rate of the currents should be considered, associated with the middle bridges as they tare least affected by bridge 1. If there are odd number of bridges, the middle bridge would be the $(n-1)/2+1^{th}$ and $(n-1)/2+2^{th}$ bridges and if the number is even, the middle bridge is the $(n-1)/2+1^{th}$ bridge: bridge 4 in a 7 bridge system. The duration of the second state is:

$$t_2 = \frac{-I_4}{a_{m,1}V_{\min} + a_{m,2}V_{\max} - V_{\max}\sum_{j=3}^{2n} a_{m,j}}\ ,\ x_2 = t_1 + t_2 \tag{2.28}$$

where the "m" subscript refers to the middle bridge. The maximum current occurs in the second inductor of the first bridge since $V_{B1} < V_{B2}$.

$$I_1 = [+V_{\min}a_{21} + V_{\max}a_{22} - V_{\max}\sum_{j=3}^{2n} a_{1j}] \times t_2 \tag{2.29}$$

To calculate the duration of state 3, the ramping rate of i_{w1} should be used as it has the highest current at the end of switching state 2. The third state duration should be long enough to make sure that i_{w1} returns to zero at the end of this state:

$$t_3 = \frac{-I_1}{-V_{\min}a_{21} - V_{\max}a_{22} - V_{\min}\sum_{j=3}^{2n} a_{2j}},\ x_3 = t_1 + t_2 + t_3 \tag{2.30}$$

Similar to the previous case, to get the optimum design:

$$\begin{cases} T_s = T_{s,desired} \\ I_{\max} = \mathrm{I}_{max,desired} \end{cases} \Rightarrow \begin{cases} T_{s,desired} = t_1 + t_2 + t_3 \\ \mathrm{I}_{max,desired} = I_1 \end{cases} \tag{2.31}$$

After simplification:

$$\begin{cases} T_s = t_1 + \dfrac{[a_{11}(-\Delta V + V_{\min} + 3V_{\max}) - (V_{\min} + V_{\max})A] \times [-2a_{13}\Delta V + V_{max}A] \times t_1}{[-\Delta V a_{11} - V_{\min}A] \times [a_{1,m}(V_{\min} + 3V_{\max}) - V_{\max}A]} \\ \mathrm{I}_{max,desired} = +V_{\min}a_{21} + V_{\max}a_{22} - V_{\max}\sum_{j=3}^{2n} a_{1j} \times t_2 \end{cases} \tag{2.32}$$

Similar to case 1, the unknown variables in 2.32 are t_1 and matrix "a" elements. With the similar assumption, $L_l = 0.01 \times L_m$ and L_f equal to the amount picked in the previous case, t_1 and L_m for the second case can be found. After calculating all the unknown variables for the both cases, the smallest t_1, smallest t_2 and the biggest magnetizing inductance are the best design. For example, if t_1 in case 2 is bigger than t_1 in case 1, the smaller t_1 should be chosen to make sure the current does not exceed the maximum allowable value. Similarly, the magnetizing inductance is set so that current does not exceed the maximum allowable value, therefore, the bigger magnetizing inductance should be chosen.

2.2.3 Design Rules

The design rules are as follows: (a) Maximize the charge transfer and (b) prevent charge back-flow. To apply these two rules, The effects of the leakage inductance variation on the transferred charge and charge back-flow phenomenon are described.

Charge Transfer

Using the best design, the transferred charge in each cycle can be calculated based on the per-unit values as below:

$$\begin{aligned} Q_{Bj,pu} &= \frac{1}{Q_{base}} \int_0^{T_s} i_{Bj}(t)dt = \int_0^{T_s} \frac{i_{Bj}(t)}{I_{base} \times T_{bases}} dt = \\ &\int_0^{T_s} \frac{i_{Bj}(t)}{I_{base}} \times \frac{dt}{T_{bases}} = \int_0^1 i_{Bj,pu}(t_{pu}) \times dt_{pu} \end{aligned} \tag{2.33}$$

where V_{base} and I_{base} and T_{base} are the main base values, $Q_{base} = I_{base} \times T_{base}$ and $L_{base} = V_{base} \times T_{base}/I_{base}$. For example, transferred charge by battery cell 1 in a cycle in Fig. 2.16 is:

$$
\begin{aligned}
Q_{B1,pu} &= \frac{1}{Q_{base}} \int_0^{T_s} i_{Bj}(t)dt = \frac{1}{Q_{base}} \left(\int_{x_1}^{x_2} i_{w1}(t)dt - \int_{x_2}^{x_2'} i_{w2}(t)dt \right) \\
&= \frac{1}{I_{base} \times T_{base}} \left(\frac{I_1 \times (x_2 - x_1)}{2} - \frac{I_2 \times (x_2' - x_2)}{2} \right) \\
&= \frac{I_{1,pu} \times (x_{2,pu} - x_{1,pu})}{2} - \frac{I_{2,pu} \times (x_{2,pu}' - x_{2,pu})}{2} \\
&= \frac{I_{1,pu} \times (t_{2,pu})}{2} - \frac{I_{2,pu} \times (t_{2,pu}')}{2} \Rightarrow Q_{transferred} = Q_1 + Q_2
\end{aligned}
\tag{2.34}
$$

The charge transferred by battery cell 1 as a function of added inductance L_f in case 1 is illustrated in Fig. 2.17 when the leakage is 1% and 5% for a 7-bridge system with $I_{base} = 1.5A$, $V_{base} = 4.5V$, $f_{s,base} = 100kHz$, $L_m = 10\mu H$. The graph is normalized based on the transferred charge when there is no added inductance and leakage is 1%. As it can be observed from Fig. 2.17, when the value of L_f is low, the difference between transferred charge between using L_l at 1% and 5%, becomes significant but as the value of L_f increases, ΔQ is negligible, in other words, the effect of the leakage uncertainties becomes negligible as L_f dominates. The difference between charge transfer is significant, which leads to longer equalization time and more losses as the converter should operate for a longer time. As it is shown, when the series added inductance is bigger than $0.4 \times L_m$, ΔQ is negligible. Therefore, the effect of uncertainty in the leakage inductance can be mitigated by choosing the series added inductance larger than $0.4 \times L_m$. Moreover, L_f should not be chosen too high since it will slow down the transfer rate. Thus a reasonable value is around $0.4 \times L_m$ to $0.6 \times L_m$ which should be used in the design procedure.

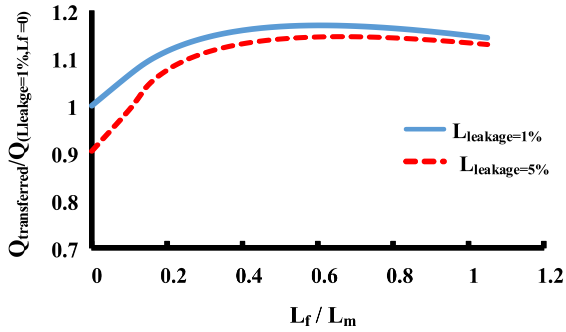

FIGURE 2.17: The effect of series inductance on the transferred charge of a 7 bridges system ΔV=5 % .

Charge Back-flow

When the added inductance increases from 0 to $0.5 \times L_m$ the transferred charge increases, see Fig. 2.17. This is the effect of charge back-flow. Charge back flow is a phenomenon in the third state that transfers charge from lower voltage bridges to higher voltage bridges. Although the lower series inductance is more preferable since the lower series inductance leads to lower current transfer region, shorter state 2, consequently less charge goes back to higher voltage bridges and more charge goes to lower voltage bridges, it may cause charge back flow, see Fig. 2.18. The shaded area in Fig. 2.18, is the amount of charge which transfers back to the higher voltage bridge.

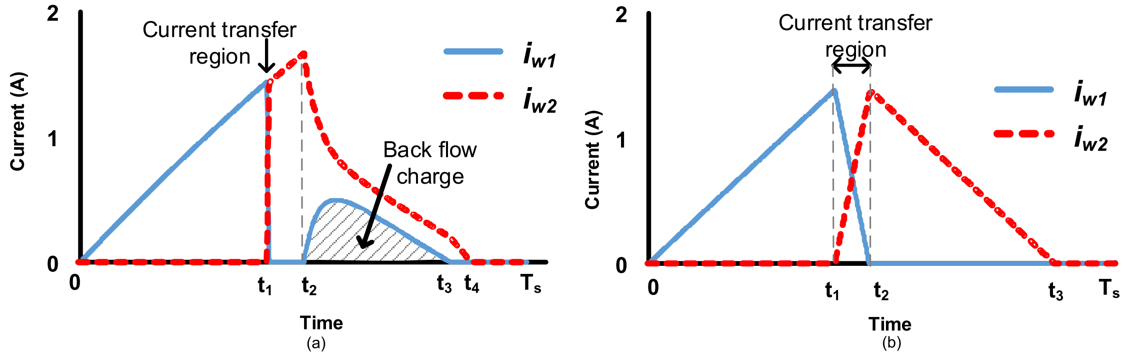

FIGURE 2.18: The 2-switch flyback for a two-bridge system: (a) low leakage (b) high leakage.

The model of a two-bridge system in the third state is shown in Fig. 2.19, where $V_{B1} + V_{B2} > V_{B3} + V_{B4}$. The voltage of inductor 1 and 2 in the first bridge are:

$$\begin{aligned} V_{w1} &= V_{w2} = \frac{V_{w3} + V_{w4}}{L_{33} + L_{34}} \times L_{31} \\ V_{w3} &= V_{B4} + R_7 \times i_{w3} + V_{Don} \\ V_{w4} &= V_{B3} + R_6 \times i_{w4} + V_{Don} \end{aligned} \tag{2.35}$$

To check whether this phenomenon happens or not check the below constraints.

$$if \begin{cases} V_{w2} > V_{B1} + V_{DU1} \\ or \\ V_{w1} > V_{B2} + V_{DL1} \end{cases} \tag{2.36}$$

The diode in bridge 1 turns ON, consequently, the current flows to charge the battery cells in bridge 1 and decrease the transferred charge to bridge 2. This problem can be prevented by increasing the series inductance, leakage or series added inductance. It is better to increase the series added inductance since increasing the leakage inductance decreases the coupling factor between bridges. For example, in a system with $V_{max} = 4.5V$ and $I_{max} = 1.5A$, the series inductance, which is enough to prevent this phenomenon, can be calculated based on:

$$\begin{gathered} \min(V_{B1}, V_{B2}) + V_{Don} > \frac{V_{B4} + V_{B3} + 2 \times V_{Don} + (R_7 \times i_{w3}) + (R_6 \times i_{w4})}{L_{33} + L_{34}} \times L_{31} \Rightarrow \\ \frac{\min(V_{B1}, V_{B2}) + V_{Don}}{V_{B4} + V_{B3} + 2 \times V_{Don} + (R_7 \times i_{\max}) + (R_6 \times i_{\max})} > \frac{L_{31}}{L_{33} + L_{34}} \Rightarrow \\ \frac{4.5 + 0.7}{9 + 2 \times 0.7 + (R_7 \times 1.5) + (R_6 \times 1.5)} = \frac{5.2}{10.4 + 1.5(R_6 + R_7)} > \frac{L_{31}}{L_{33} + L_{34}} \end{gathered} \tag{2.37}$$

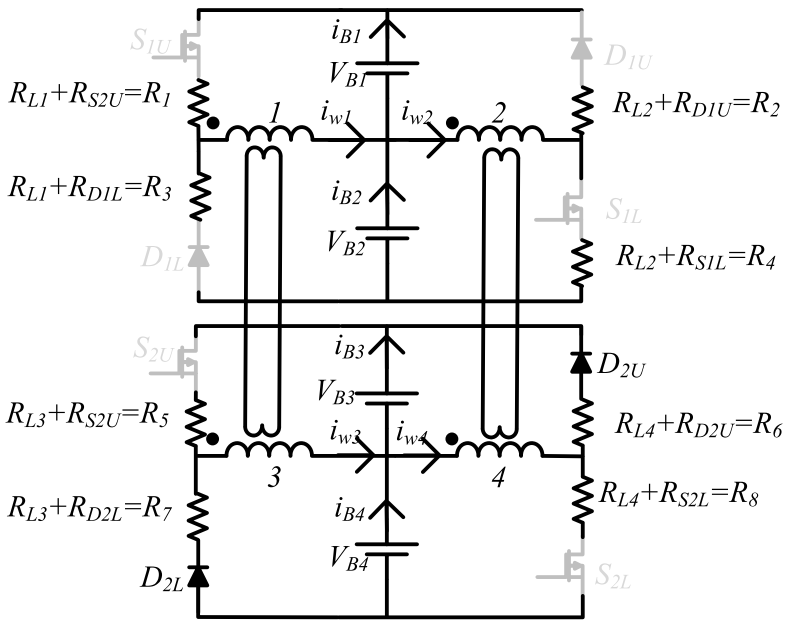

FIGURE 2.19: The equivalent circuit of a two bridge systems when diodes of the lower voltage bridge are ON.

Design Example

The design procedure for a 7 bridge system assumes: $V_{max} = 4.5V$, $\Delta V = 15\%$, $I_{max} = 1.5A$,and $f_s = 100kHz$ is as follows:

1. Choosing L_f between $0.4 \times L_m$ and $0.6 \times L_m$.
2. Solve Eqs. (2.26) and (2.32) to obtain values for L_m and t_1: all variables can be calculated for both scenarios.
3. Choose the minimum t_1 and maximum L_m from step 2.
4. Calculate t_2 based on t_1 and L_m: t_2 can be calculated based on the current constraint in case 2 ($I_2 = I_{max,desired}$).
5. For the calculated values for t_1, L_m and t_2, check whether the desired switching frequency f_s can be used in both scenarios, if not decrease t_1 or increase L_m and go to step 3.
6. For the chosen values for t_1, L_m, t_2 and f_s, that the added inductance is great enough to prevent charge flow back or not, see Eq. (2.37). If not change the value

of added inductance and go back to 2.

7. For the chosen parameters, check if the system is subject to swing or not: if yes decrease t_1 and go back to step 3.

By going through these steps, $t_1 = 38\%$, $t_2 = 15\%$, $L_m = 10\mu H$, $L_f = 4.5\mu H$ for this case study.

2.3 Comparison

The transferred charge of the conventional method can be compared to the transferred charge of the proposed method which is calculated before. While keeping the switching frequency and the maximum current similar in both methods, transferred charge by battery cell 1 in each cycle is compared for the conventional method and the proposed method, in the case when battery cell 1 has the highest voltage. To this aim, the transferred charge versus the series added inductance for bridges are illustrated in Fig. 2.20 for different voltage deviations in both methods. Here, $V_{base} = V_{max} = 4.5V$, $I_{base} = I_{max,desired} = 1.5A$ and $f_{base} = f_{s,desired} = 100kHz$ are assumed. Under these base values, $Q_{base} = I_{base} \times T_{base}$ and $L_{base} = V_{base} \times T_{base}/I_{base}$. From the graph and equations, it can be seen that ΔV and the series added inductance does not affect transferred charge in the conventional method while, as ΔV increases, the transferred charge would be higher in the proposed method. As a result, in the proposed method, at first when the voltage difference between bridges is high, the charge transfer is faster which is advantageous.

Since equations are derived in the ideal conditions, the simulations are done with ideal and non-ideal components to compare the transferred charge in the both condition. Assuming non-ideal components, the inter-bridge charge transfer occurs at a very low rate as it is shown in Fig. 2.21(b) also, compare Fig. 2.23(a) and Fig.

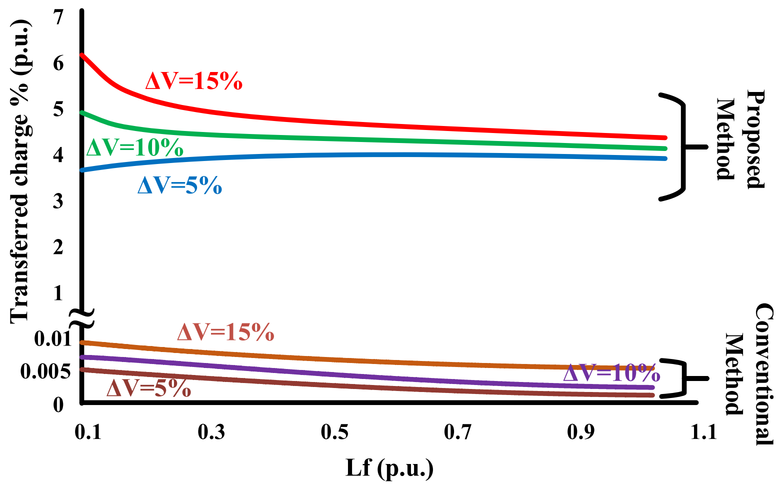

FIGURE 2.20: Analytical prediction of transferred charge vs. series added inductance under different voltage difference for both control method in ideal condition.

2.23(b). Charge transfer in [2] is closely linked device voltage drops and the low battery cell voltage of $4V$ whereas, the proposed method drastically increase the charge transfer rate as it is illustrated in Fig. 2.21 and Fig. 2.22. The equalization time is much shorter than the conventional method, with a higher power conversion efficiency. The dc voltage drop in all the bridge cells is high Fig. 2.21(b) since a $1mF$ capacitor was used in the simulations to replace an actual battery cell. Simulations using larger capacitors or actual battery cell models would not produce such a large drop in the dc voltages. Here, the simulations were done with small capacitances to reach the equilibrium point faster.

2.4 Simulation and Experimental Results

An experimental prototype was designed to verify the performance of the proposed controller. The system components were selected as per the design section procedure. The switching patterns for four MOSFET ($20V$, $5A$) modules were obtained using a TI F28335 Digital Signal Processor (DSP) at a switching frequency of $100kHz$, see Fig. 2.24. As the effect of different battery cell voltage unbalances is the main

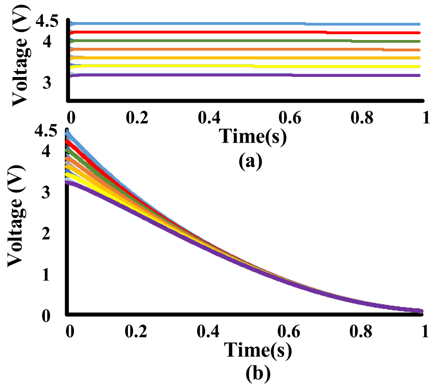

FIGURE 2.21: The performance of a system with 14 battery cells under the method in [2] (a) without parasitic components (b) with parasitic components.

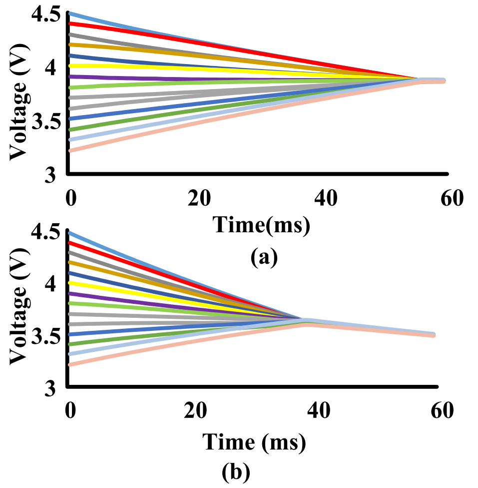

FIGURE 2.22: The performance of a system with 14 battery cells under proposed control method in [2] (1mF capacitors replaced actual battery cells): (a) without parasitic components (b) with parasitic components.

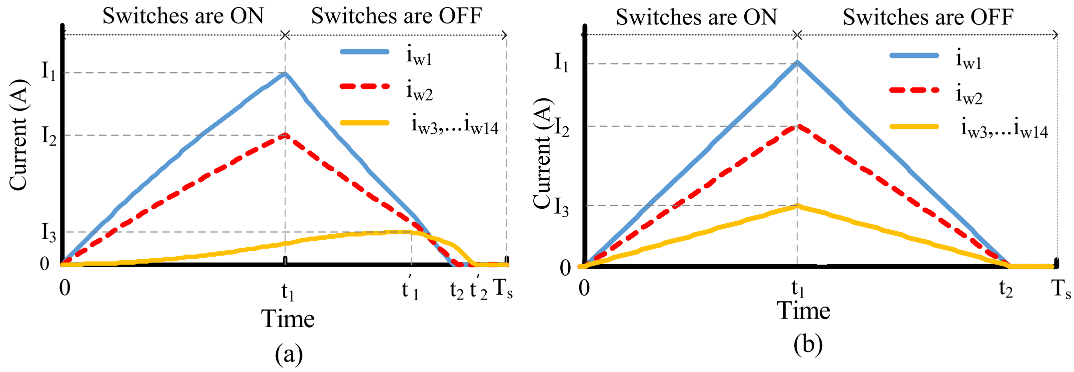

FIGURE 2.23: The current wave form of the proposed control method (a) without parasitic components (b) with parasitic components.

subject of investigations, 4 battery cells were implemented in the experimental system using three low ESR $5F$ super capacitors in parallel from SCM Series Supercapacitor. This allowed specific dc voltage unbalances to be obtained much faster than priming several battery cells at specific voltages. The 4 winding transformer in each bridge was implemented using an HP2- 0216L manufactured by Coil Craft company ($L = 10.6\mu H$). These transformers have six windings with windings 1 and 2 in BC as shown in Fig. 2.10(a)-(b). The coupled inductors that are used in this chapter are from Coilcraft company and they are very compact, $12.9 \times 16.3mm$. As a result, the prototype experimental circuit is also compact, Fig. 2.24. The circuit size, $60 \times 118mm$, can comfortably fit on 4 battery cells. Also, it is possible for this circuit design to handle higher power and current. The main design changes would be the size of the coupled inductors, while the other components like switches and diodes would not be subject to significant changes in size.

2.4.1 Experimental with Designed Parameters

To verify the design procedure and parameters, which are calculated in the design section, the prototype is built with the calculated parameters. The toroidal transformers have a low leakage inductance and a series added inductance was implemented by inserting two $4.5\mu H$ inductors into the centre-tap of the dc supply in each BC, see Fig. 2.24 and Fig. 2.10(a).

The experimental results of BC windings currents in Fig. 2.25 are close to simulations results and they match the design requirements. As it is shown in Fig. 2.25(a), the maximum current is less than $1.5A$; switching state 2 is long enough to make sure the current of the bridge returns to zero; currents flow during the entire switching cycle.

2.4.2 Leakage inductance effect

The effect of adding or having no added series added inductance, L_f can be observed in Fig. 2.25. As the toroidal transformer has a low leakage inductance (about 1%), the low leakage situation can be tested. The duration of the state 1 period is unchanged, on-time of the BC_1 switches, but the duration of state 2 period, the on time of switches in the second bridge, is much smaller when L_f

is removed. The shorter the period for state 2, less charge is returned to the dc supply of BC_1 during this state: less charge is also removed from the dc supply of BC_2 and more charge is transferred to BC_2 from BC_1. Therefore, the average current transferring charge from BC_1 to BC_2 is better than the case of a large effective series inductance as seen in Fig. 2.25.

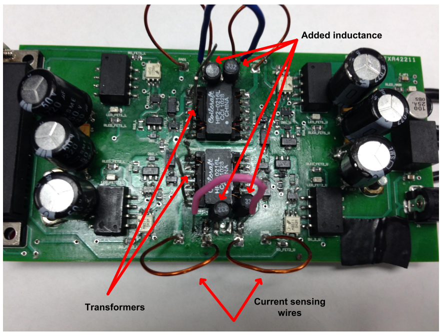

FIGURE 2.24: The prototype of the circuit.

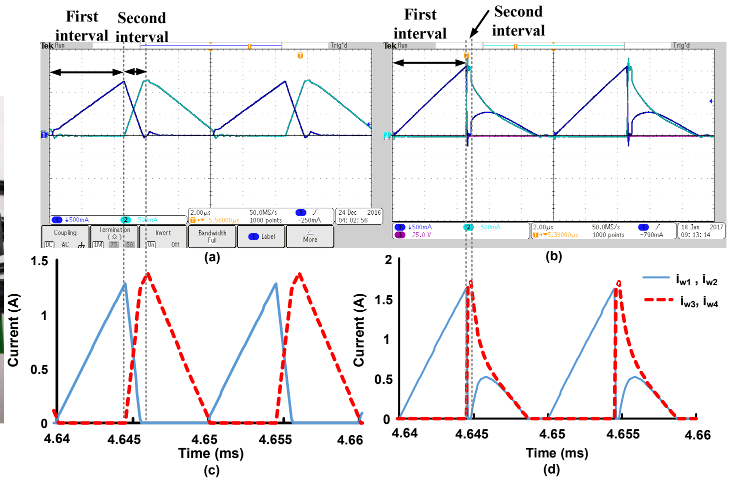

FIGURE 2.25: Experimental results - (a) L_f added (b) L_f removed; simulated results (c) L_f added (d) L_f removed.

2.4.3 Performance Comparison

To study the speed of voltage equalization, two bridge cells were used where a battery cell was approximated using four $15F$ capacitors (three $5F$ capacitors connected in parallel) to replace four battery cells in a 2 bridge cell system. The voltage of the first bridge was set to $5V$ and the voltage second bridge was set to $2.5V$. For both control methods, the performance of the system is shown in Fig. 2.26. As it can be seen, the equalization time in the proposed method is faster than the previous method in [2]. The equalization time in the proposed method is about 100 seconds while in the conventional method significant voltage differences remained at 100 seconds. Note that for the previous method, the voltages of both bridges are discharging over the period shown. For the proposed method, the lower bridge voltage is maintaining its voltage, and rising slightly, while the higher voltage bridge is discharging rapidly. This means that the higher voltage bridge is transferring charge to the lower voltage bridge. Therefore, the rate of charge transfer is much higher than the previous method. As it is shown there is a huge drop in the voltages of capacitors in Fig. 2.26, that is due to the fact that the capacity of the capacitors are small. These capacitors are replaced with 20Ah battery cells (EIG ePLB C020, see Fig. 2.27) and the results are shown in Fig. 2.28. When real battery cells are replaced with the capacitors there is no drop in the battery cell voltage. Also, when the battery cells voltage are equal the controller stops switching to prevent loss in the circuit.

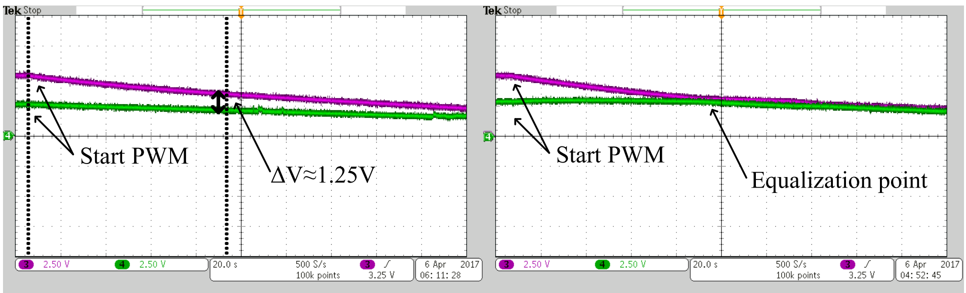

FIGURE 2.26: The performance of the system with four 15F capacitors under the (a) presented method in [2] (b) proposed method.

2.5 Conclusion

Analysis, design of a new control strategy for a battery cell voltage balancing circuit are presented. The modular circuit and its control strategy is relatively easy to implement but also, is much faster than the conventional control methods. The proposed distributed controller is also cost-effective since it just uses the

Figure 2.27: EIG ePLB C020 Battery cells

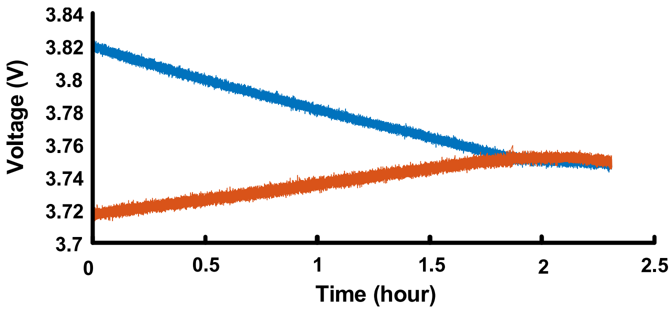

Figure 2.28: The performance of the system with four $20Ah$ battery cells.

local data, voltage of the bridge and its upper and lower bridges. Moreover, the number of voltage sensor is one for each pair of battery cells, which is half when compared to the other similar methods. Furthermore, this method offers ZCS in turn ON which reduces the turn ON loss of the switches. An equivalent circuit is introduced to simplify the calculations and make the system easier to analyze. The principle of operation of the circuit topology and controller are explained based on the main circuit and also the equivalent circuit. A design procedure is presented which provides the flexibility for using the system at different voltage and current requirements and finally, the design is optimized to get the best performance out of the system. The effect of the leakage inductance on the charge transfer rate and charge flow back are described and solution are provided to avoid them. A design example is provided and simulations and experimental results are provided to validate the design procedure. Also, a prototype, which uses the best design parameters that are calculated before, is made to get the experimental validation. It is shown that the new approach provides a much faster charge transfer in each cycle and more efficient power conversion when compared to a previous method.

CHAPTER 3

Transformer Coupled Series Connected Asymmetrical Bridge

A new rapid charge equalization circuit topology and control system is presented for battery voltage balancing. The presented method, similar to Cascaded method, is modular, scalable with a distributed control approach that uses parallel charge transfer technique. The method transfers charge from higher voltage cells to the lower voltage cells in each switching cycle. The transferred charge and the absorbed charge have a direct relationship to their voltages, highest voltage cells transfer more while the lowest voltage cells absorb more. Also, the proposed method uses a distributed control technique as opposed to a centralized controller. The topology is a plug and play and reduces the complexity of cell monitoring circuits. Moreover, the power circuit uses 1 switch and 1 diode per battery cell and one voltage sensor is used for a pair of battery cells. This method offers ZCS in turn ON to decrease turn On loss of the switches. All these features are similar to Cascaded method but there are several differences between Cascaded and Series method as follows: The number of connections to neighbor bridges is lower. This makes the wiring easier and decrease cost of the system. Furthermore, in the series method all bridges share the same current in their tertiary windings. Therefore, the effect of bridges on each other would be similar. This makes analysis, current waveforms prediction easier. Moreover, equalization time prediction possible in this method. The system circuit analysis, analytical analysis, and resultant design procedures are presented and relatively easier to implement compared to Cascaded method. Also, it is shown how the equalization time is used as one of the design constraints which is not possible in Cascaded method.

3.1 Structure and Operation

Structure and connections of a bridge modules are presented in Fig. 3.1. A single battery voltage Balancing Module (BM) or simply a bridge consists of an asymmetric half-bridge, two series connected battery cells, a toroidal transformer and two inductors L_f. The transformer has three windings: $w_{1,1}$ and $w_{2,1}$ are used to connect the centre tap of two battery cells to the asymmetrical bridge and, $w_{3,1}$ is used to connect the BM to its neighboring BMs. To decrease the number of connections compared to Cascaded method, BM are connected in series, see Fig. 3.2(a)-(b). As it is shown in Fig. 3.2(a), in Cascaded method, each bridge has four connections to its neighbor bridges while in the proposed method, Fig. 3.2(b), the number of connections are only two. Therefore, wiring in the system is less and cost of the system is less. To refer to these methods easier, Cascaded method is called "Cascaded method". The reason is that the windings connections are cascaded, see Fig. 3.2(a). In the proposed method, see Fig. 3.2(b), the connection is in series and will be referred to as "Series method".

Since this topology needs an even number of battery cells, in the cases where

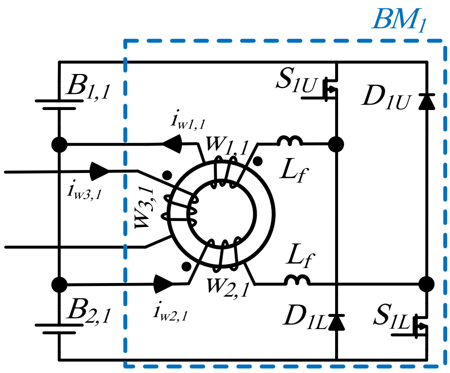

FIGURE 3.1: schematic of one module of the proposed method.

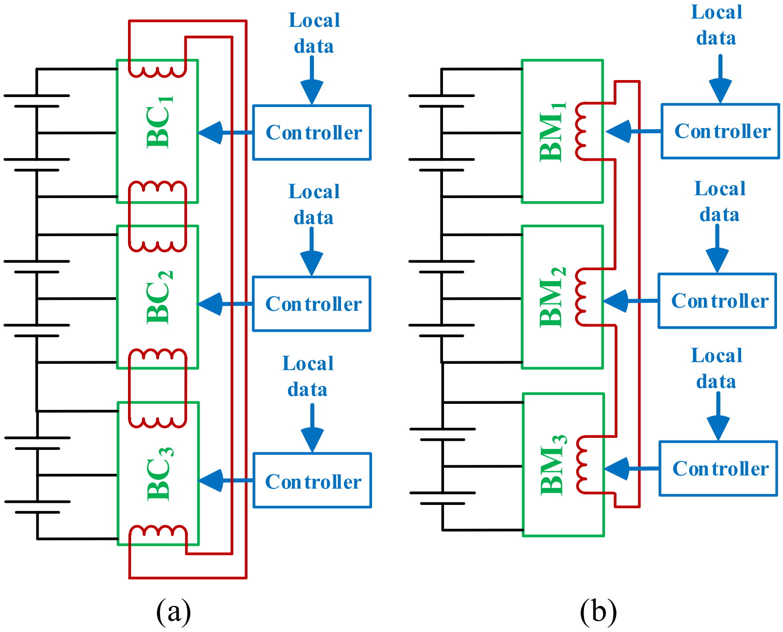

FIGURE 3.2: schematic of the (a) Cascaded (b) Series approaches.

there are odd number of battery cells it is possible to add a capacitor to the string of battery cells to effectively produce an even number for the battery cells. The converter connected to the capacitor will operate normally and will treat this cap as a very low capacity battery cell, which does not interfere with the rest of the circuit operation. The other option is to use the circuit in Fig. 3.3. Similar to Cascaded method, the analysis is presented for the first option.

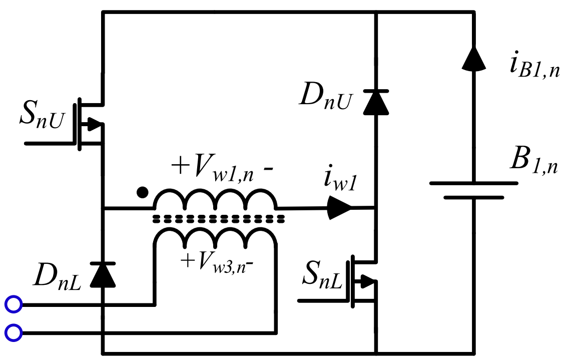

FIGURE 3.3: A solution to use Series method with an odd number of battery cells.

3.1.1 Equivalent Circuit

To make the circuit system analysis more straightforward, an equivalent circuit is presented. The equivalent circuit is used to calculate currents in the circuits then, the exchanged charged of battery cells are calculated using the calculated currents. This circuit is achieved by simplifying the presented circuit in Fig. 3.4(a). First step is to derive the simplified model of the coupled inductors. The coupled inductors in Fig. 3.4(a) are separated from the circuit to derive their equivalent model, see Fig. 3.4(b). Since all the windings are similar, the equivalent circuit of the coupled inductors in Fig. 3.4(b) is presented in Fig. 3.4(c). Since all the winding are the similar, it can be assumed L_l and L_m are leakage and mutual inductance of windings respectively by using Eqs. (2.1), (2.2), (2.3), (2.4), the following equations can be achieved.

The equations for coupled inductors are as follows:

$$\begin{cases} V_{w1,1} = (L_m + L_l)\dfrac{di_{w1,1}}{dt} + L_m\Big(\dfrac{di_{w2,1}}{dt} + \dfrac{di_{w3,1}}{dt}\Big) \\[2ex] V_{w2,1} = (L_m + L_l)\dfrac{di_{w2,1}}{dt} + L_m\Big(\dfrac{di_{w3,1}}{dt} + \dfrac{di_{w1,1}}{dt}\Big) \\[2ex] V_{w3,1} = (L_m + L_l)\dfrac{di_{w3,1}}{dt} + L_m\Big(\dfrac{di_{w2,1}}{dt} + \dfrac{di_{w1,1}}{dt}\Big) \end{cases} \tag{3.1}$$

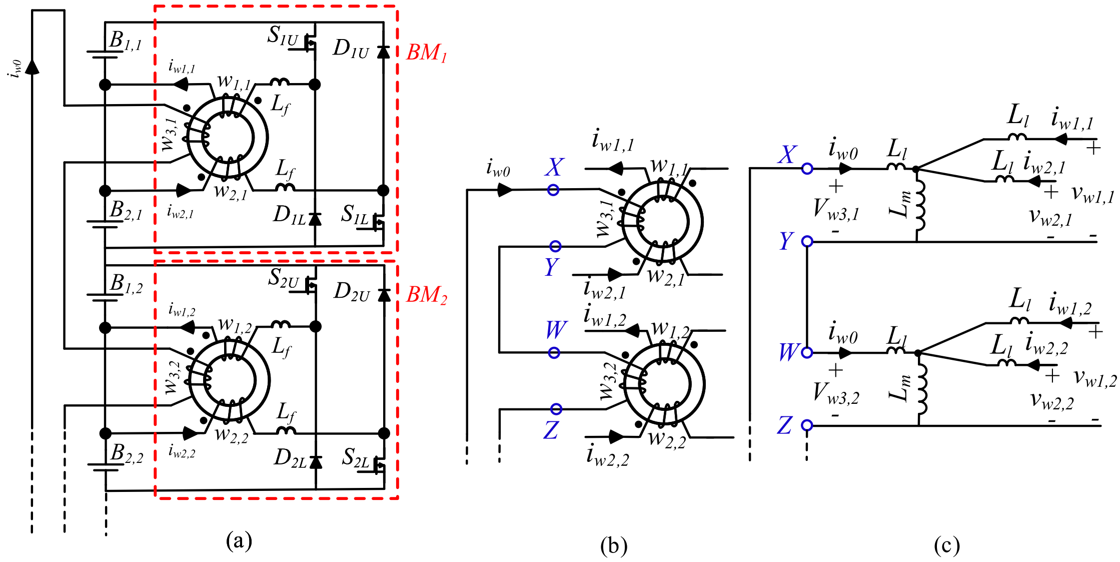

FIGURE 3.4: Schematic of (a) Two BMs connections (b) Coupled inductor connections (c) Equivalent circuit of coupled inductors.

Again, the connection of centre tap of battery cells is removed since there is no current through it. Therefore, it can be concluded that the equivalent circuit of Fig. 3.4(b) is shown in Fig. 3.4(c).

The next step to redraw the circuit when switches are ON and when diodes are ON. The circuit when switches are On is shown in Fig. 3.5(b) and the equivalent circuit when switches are ON is shown in Fig. 3.5(c). Also, the circuit when diodes are On is shown in Fig. 3.5(d) and its equivalent circuit is shown in Fig. 3.5(e).

To achieve the final equivalent circuit, BM_1 in Fig. 3.4(a) is redrawn in Fig. 3.6(a). The transformer and power converter can be represented using the achieved equivalent models as it is shown in Fig. 3.8(b). The combined action of the power converter and batteries voltages can be modeled with the voltages sources $E_{1,1}$ and $E_{2,1}$, typical waveforms for $E_{1,1}$ and $E_{2,1}$ in BM_1 are shown in Fig. 3.6(c). The action of $2n$ battery cells can be modeled by connecting the equivalent circuits together, see Fig. 3.6(a). A simplified version circuit of Fig. 3.6(a) is shown in Fig. 3.6(b), where the equivalent impedance of each bridge is $L_{eq} = \dfrac{L_m L_f}{2L_m + L_f}$ and the

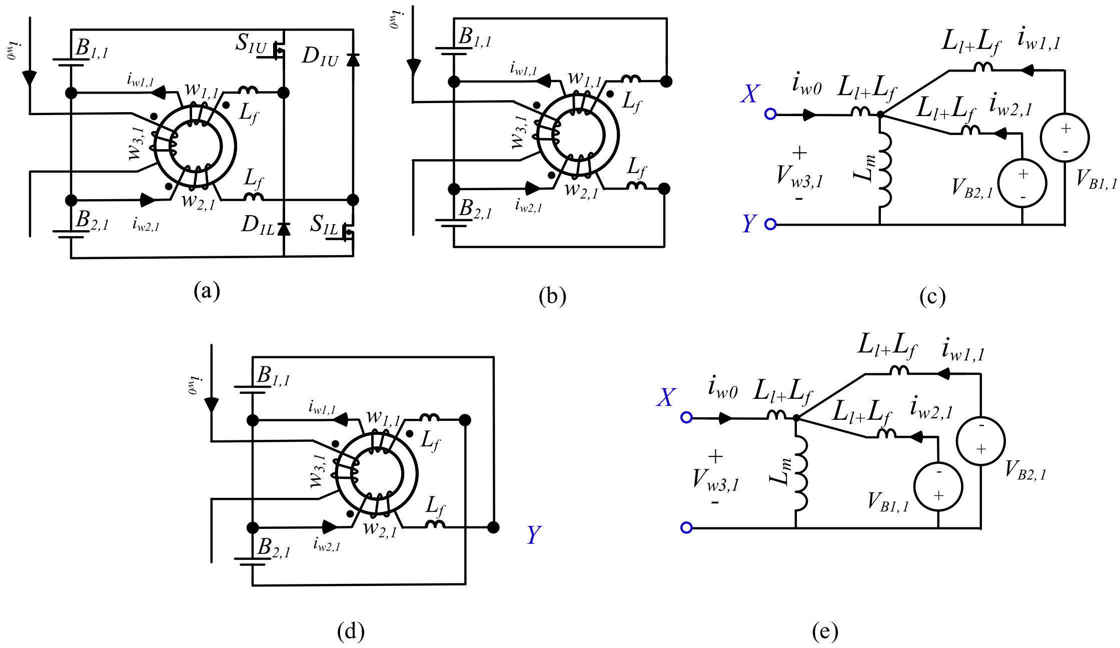

FIGURE 3.5: Schematic of the circuit (a) with switches and diodes (b) when switches are ON (c) equivalent circuit when switches are ON (d) when diodes are ON (e) equivalent circuit when diodes are ON

equivalent voltage source of bridge "i" would be $E_{eq,i} = \dfrac{(E_{1,i} + E_{2,i})\, L_m}{2L_m + L_f}$.

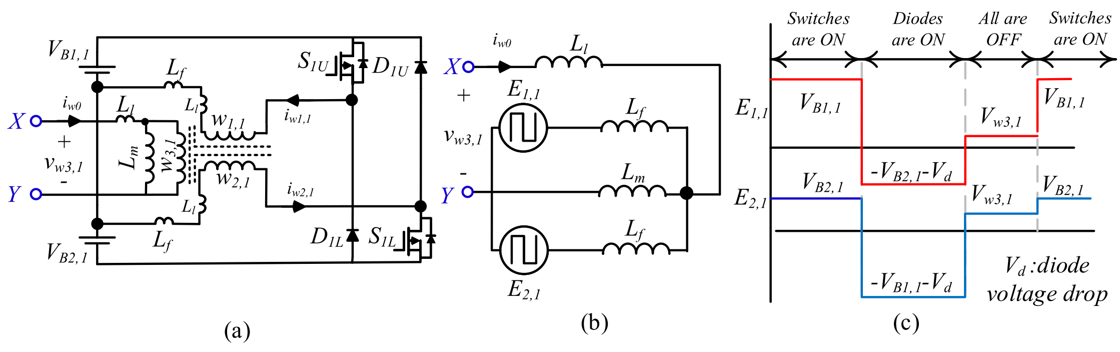

FIGURE 3.6: Equivalent circuit of a BM: (a) detailed representation, (b) general equivalent circuit (c) voltage waveform of $E_{1,1}$ and $E_{2,1}$ (L_m: magnetizing inductance for two windings, L_l: leakage inductance for two windings, L_f added series inductance).

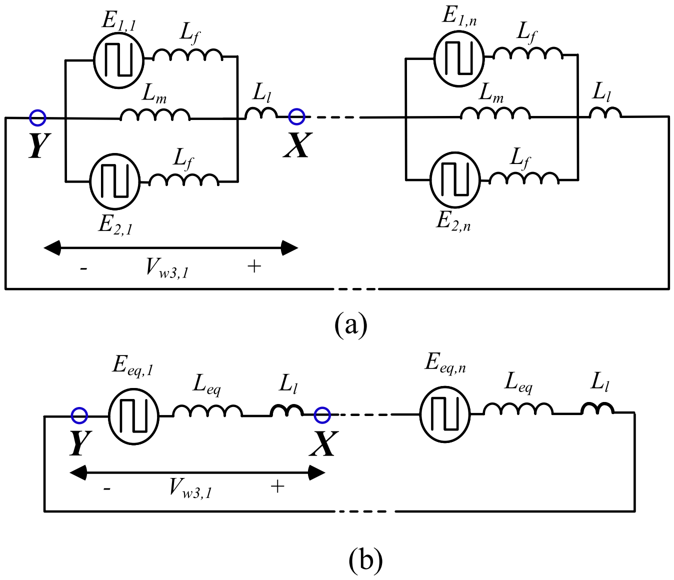

FIGURE 3.7: "n" bridge module topology model (a) equivalent circuit (b) simplified circuit where $L_{eq} = \dfrac{L_m L_f}{2L_m + L_f}$ and $E_{eq,i} = \dfrac{(E_{1,i} + E_{2,i})\, L_m}{2L_m + L_f}$.

The analysis of this circuit is easier than Cascaded method since the tertiary winding current is the same for all bridges. This means that the bridges have the same on each other and this effect is independent from the location of the bridges, compare Figs. 2.8 and 3.7 which are shown in Fig. 3.9. The current of the windings is easier to calculate in series method since all the bridges are connected in series. Also, all the bridges have the same effect on each other since the tertiary current which is the same in Series method. While in Cascaded method, this effect relates to the location of the bridges and their distance from each other. The reason behind this is that the bridges are connected together through windings of other bridges.

The idea is to use the equivalent circuit to calculate currents in each state. Then, the exchange charge of battery cells can be calculated using the calculated currents.

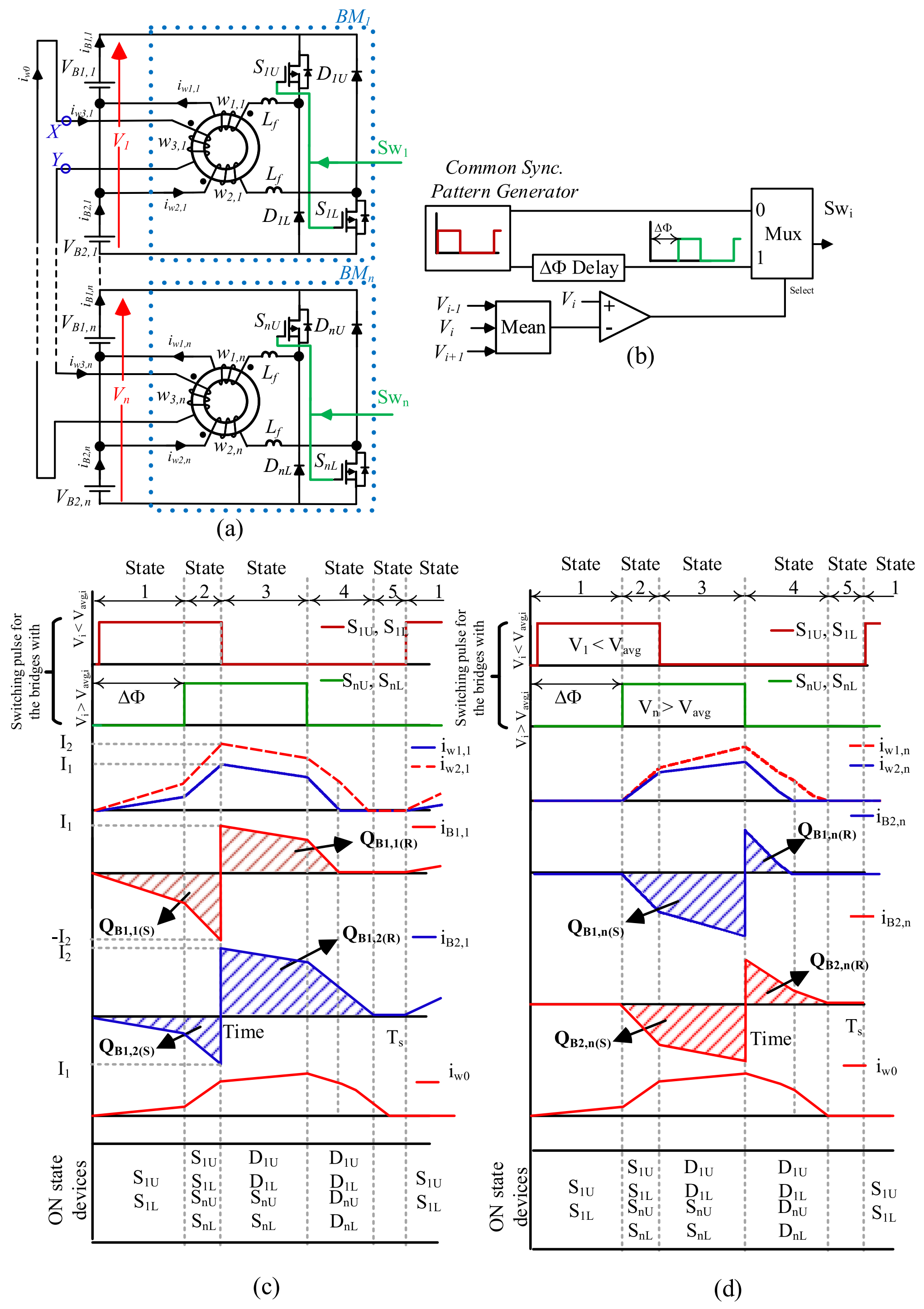

FIGURE 3.8: Proposed topology (a) Multi bridge module connections; (b) Controller of bridge module "i"; Current waveforms of the two-bridge system where $V_{B1,1} > V_{B2,1}$, $V_{B1,n} > V_{B2,n}$ and $V_1 < V_n$ (c) BM_1 (d) BM_n.

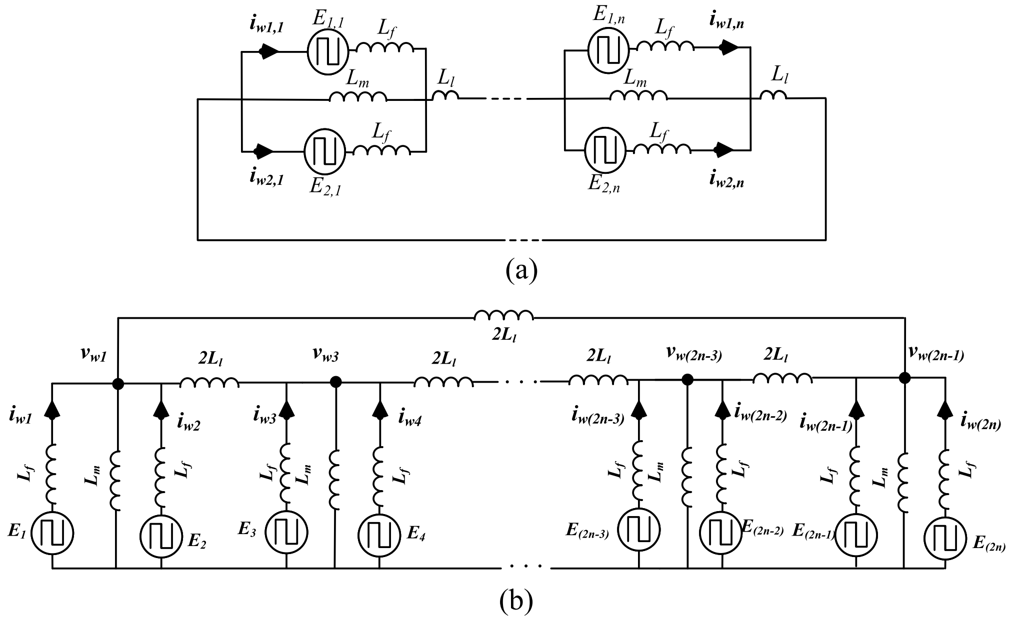

FIGURE 3.9: Multi bridge equivalent circuit (a) Series method (b) Cascaded method.

3.1.2 Charge Transfer Mechanism

The proposed circuit is designed to extract charge out of higher charged battery cells and inject it to lower charged battery cells. The proposed circuit distributes charge among all battery cells based on their voltages. The charge transfer procedure can be divided into two categories: (a) Intra-BM (between battery cells within the a BM), (b) inter-BM (between battery cells located in different BMs). These two are explained in the following sections.

3.1.2.1 Intra-BM

Similar to Cascaded method, it can be guaranteed that if both switches in a bridge are turned ON or OFF at the same time, charge will be transferred from higher charged to lower charged battery cell in a bridge. It is proved that when switches are ON, the inductor windings connected to the higher charged battery cell has a higher current, when switches are turned OFF and diodes are ON, the connection of battery cells and inductors will be toggled and the inductor with the higher current will be connected to lower charged battery cell, see Fig. 3.6(a). Therefore, higher charged cells pass charge to lower charged battery cells. To compare the exchanged charge of battery cells in a bridge, Assume BM_1 in Fig. 3.8(a) where $V_{B1,1} < V_{B2,1}$ and V_1 is the lowest. In state 1, both switches of BM_1 are ON and other bridges switches are OFF. The slopes of $i_{w1,1}$ and $i_{w2,1}$ can be calculated based on Fig. 3.7(b) as follows:

$$\begin{cases} V_{B1,1} = L_f \dfrac{di_{w1,1}}{dt} + V_{w1,1} \\ V_{B2,1} = L_f \dfrac{di_{w2,1}}{dt} + V_{w2,1} \end{cases} \xrightarrow[V_{B1,1}<V_{B2,1}]{V_{w1,1}=V_{w2,1}} \frac{di_{w1,1}}{dt} < \frac{di_{w2,1}}{dt} \tag{3.2}$$

where, $V_{wi,j}$ is the voltage of winding i in bridge j. This voltage is the effect of other bridges on bridge j. Also, due to the fact that leakage inductance is negligible, voltage of the couple inductor windings in a bridge are equal. The slopes of the current in the second state is higher as the voltage of $V_{w3,1}$ decreases.

$$\begin{aligned} V_{w3,1}|_{state1} &= \frac{(n-1)E_{eq,1}}{(n-1)L_m + L_{eq}} > E_{eq,1} - \frac{\sum\limits_{k=1}^{n} E_{eq,k}}{n} \\ &= V_{w3,1}|_{state2} \xrightarrow{Eq.(3.2)} \begin{cases} \dfrac{di_{w1,1}}{dt}|_{state1} > \dfrac{di_{w1,1}}{dt}|_{state2} \\ \dfrac{di_{w2,1}}{dt}|_{state1} > \dfrac{di_{w2,1}}{dt}|_{state2} \end{cases} \end{aligned} \tag{3.3}$$

Based on Eq. (3.2) and (3.3), it can be claimed that $I_2 > I_1$. Similarly, it can be proved that $I_{w1,1}$ goes back to zero faster than $i_{w2,1}$ i.e., $t_{off2} > t_{off1}$. The exchanged charge of battery cells in bridge 1 can be compared as follows:

$$\begin{cases} Q_{B1,1} \approx I_1 t_{on} - I_2 t_{off2} \\ Q_{B2,1} \approx I_2 t_{on} - I_1 t_{off1} \end{cases} \Rightarrow Q_{B1,1} < Q_{B2,1} \tag{3.4}$$

If Q is negative, the battery cell absorbs charge and if it is positive, it transfers charge. This means that $B_{2,1}$ absorbs more charge than $B_{1,1}$. Thus, by using such a pattern, charge goes from the higher voltage battery cell to lower voltage battery cell in a bridge.

3.1.2.2 Inter-BM

By applying the switching pattern shown in Fig. 3.8(c)-(d) charge is transferred form higher charged to lower charged bridges. The proposed switching pattern increases the stored charge in the inductors in the lower voltage bridges and increases the duration of the third switching state where the lower voltage battery cells are absorbing charge. These two operating features lead to an increase in the charge transferred to lower voltage bridges. The chosen switching pattern sequence is defined as follows: First, the lower voltage bridge switches are turned ON, second, all switches are turned ON to maximize the stored energy in the inductors, third, the lower charged bridges are turned OFF to absorb the stored inductor energy, forth, all the switches are turned OFF and currents go back to zero until the next cycle starts, see Fig. 3.8(c)-(d). In the first and second states energy is stored in the inductors while in the second state more energy is stored in the inductors as the slope of the currents are higher in the second state, This can be proved using Eq. (3.3). Assume that bridge 1 has the lowest voltage, in the second state the lowest possible voltage on bridge 1 coupled inductor occurs therefore, the slope of the currents in bridge 1 is maximized and more energy is stored in the windings of bridge 1. In the third state, battery cells in bridge 1 absorb charge until their currents reach zero. So, as the duration of this interval increases, the absorbed charge will be increased, see Fig. 3.4. The slope of the currents are minimized by turning all switches in all bridges ON. This is due to the fact that the second term in the equation of current slopes of bridge 1 in Eq. (3.5) is maximized.

$$V_{w,i,j} = E_{eq,i} - \frac{\sum_{k=1}^{n} E_{eq,k}}{n} \xrightarrow{Eq.(3.2)} \frac{di_{wi,j}}{dt} = \frac{1}{L_f}\left(E_{eq,1} - \frac{\sum_{k=1}^{n} E_{eq,k}}{n} - E_{i,j}\right)\Bigg|_{\substack{i=1,2 \\ j=1...n}} \tag{3.5}$$

In Fig. 3.8(c)-(d), the amount of absorbed and transferred charge of $B_{i,j}$ are shown by $Q_{Bi,j(R)}$ and, $Q_{Bi,j(S)}$, respectively. It can be seen that the amount of transferred charge in the second state is maximized while the amount of absorbed charge for the lower bridge in the third state is maximized. Finally, to make all the currents reach zero at the end of a cycle, all the switches are turned OFF, see state 4 Fig. 3.8(c)-(d). When all the switches are OFF, the rest of the stored energy will be distributed between all the battery cells based on their voltages, inter and intra-BM charge transfer. Finally, in state 5, all switches and diodes are OFF and currents are zero. This state is necessary to guarantee ZCS in turn ON and operation under fixed switching frequency. To calculate the amount of exchanged charge for battery cell, $Q_{Ex,Bi,j}$ it is possible to check the area under $i_{Bi,j}$, which represent exchanged charge of battery cell i in BM_j. For example, the exchanged charge of battery cell 2 in Figs. 3.8 (c)-(d) equals to:

$$Q_{Ex,B2,1} = Q_{B2,1S} - Q_{B2,1R} \tag{3.6}$$

where, $Q_{B2,1S}$ is transferred charge and $Q_{B2,1R}$ is the absorbed charge. If $Q_{Ex,Bi,j}$ is positive, it means that the battery cell transferred charge and if the value is negative, it means that the battery cell absorbed charge. For example in the studied case where $V_{B1,1} < V_{B2,1} < V_{B2,n} < V_{B1,n}$, by applying the discussed switching pattern, $B_{1,1}$ and $B_{2,1}$ are absorbing charge while $B_{2,n}$ and $B_{2,n}$ are transferring charge. Furthermore, $B_{1,1}$ absorbs more charge than $B_{2,1}$ since it has lower voltage and, $B_{1,n}$ transfers more charge than $B_{2,n}$ since it has higher voltage, see Figs. 3.8 (c)-(d). Therefore, by using the chosen switching pattern Inter-BM charge transfer occurs that transfer charge from higher charged battery cells to the lower charged battery cells. Therefore, charge transfers between all the battery cells based on their voltages no matter they are in a bridge or not.

3.1.3 Distributed Control System

Based on the previous explanations the strategy of the controller should be as follows: to transfer charge within a bridge, both switches should be turned ON or OFF simultaneously. Also, to transfer charge between bridges, a sequence of three switching states is used: First, switches of all bridges are turned ON. Second, switches of the lower voltage bridges are turned OFF while the other switches are kept ON. Third, all switches are turned OFF. The objective is to design a distributed controller with the aforementioned switching strategy where switching decisions for each bridge are made in that bridge based on the available local data. To synchronize all the controllers, it is assumed that a common synchronization signal, the red signal in 3.8(b), is generated and sent to all modules. The controller of each BM_i monitors the total DC voltage of BM_i, $V_{1,i} + V_{2,i}$ which is referred to as V_i, and compares it with the local average of the three neighboring bridge voltages: $(V_{i-1} + V_i + V_{i+1})/3 = V_{avg,i}$. If V_i is lower than $V_{avg,i}$, the controller sends the common sync. pattern, the red signal in Fig. 3.8(b), to both switches of the BM_i. If V_i is greater than $V_{avg,i}$, the controller delays the common sync pattern and sends it to both switches of BM_i, the delayed switching pattern is the green signal in Fig. 3.8(b). Thus, a switching cycle can be divided into 5 states, State

1: the bridges with lower voltage turn ON at the beginning of the switching cycle while the bridges with higher voltage are OFF, State 2: all switches are ON, State 3: Switches of the lower voltage bridge are turned OFF while the other switches are ON, State 4 and 5: all switches are OFF. State 1 is added, to the three steps discussed before, to increase the current in the lower voltage bridges at the end of first state and, to increases the current at the end of second state. This will increase the duration of the third and fourth states where the battery cells in lower voltage bridges are absorbing charge, hence, more charge will be absorbed by lower voltage bridges. The controller does not change these patterns during the balancing procedure so, they should be designed to make sure the circuit constraints such as currents of inductors are always within an allowable range. Since there is no central controller, the first controller which detects the unbalanced voltages, generates the red and green signals and sends a synchronization signal to all the other controllers. Therefore, there is no central controller or specific master controller in the system and the system.

3.2 Design Procedure for Choosing Circuit Parameters

The main objective of this section is to find the proper rating for switches, diodes, inductors along with the duty cycle and $\Delta\phi$ which are used in the controller, see Fig. 3.8. These parameters, which will be referred to as design parameters, are calculated based on the system design constraints. The system constraints are maximum allowable current and voltage of the components, switching frequency and maximum equalization time. All the calculations are presented in general, for a system containing a series of "$2n$" series connected battery cells, "n"-bridge system. The analysis uses a simplified system equivalent model, see Fig. 3.7(b), to calculate the switch and inductor current and voltage waveforms as functions of the design parameters where the currents and voltages are maximum; worst cases. The predefined system constraints are then used to calculate a range for all the design parameters. The best solution is the one which offers the lowest equalization time.

3.2.1 Justification for Worst Case Design Scenarios

Circuit constraints, such as I_{max}, V_{max} and, f_s, are calculated as functions of the design parameters, "$L_m, L_f, dutycycle, \Delta\phi$". By applying the circuit constraints on the resultant functions, a range of possible design parameters can be determined. In the beginning, the worst case scenarios are justified then, analysis of the worst case scenarios are presented and I_{max}, V_{max} and, f_s are calculated. Several assumptions are made to make the analysis easier without loss of generality. It is assumed that (a) the battery cell voltages have a maximum and a minimum; (b) the transformer leakage inductance is assumed negligible due to the compactness and size of the magnetic cores used. The design parameters to be determined are: the winding magnetizing inductance and the effective series inductance L_m, L_f, respectively, Duty cycle and phase shift used in the synchronization patterns. The system constraints can be defined as follows:

(I) The maximum peak current of inductors and switches should not exceed, $I_{max,desired}$.

(II) Switching frequency should be fixed at $f_{s,desired}$.

(III) All currents should reach zero at the end of each cycle.

(IV) The maximum allowable voltage on windings and switches are $V_{max,winding,desired}$, $V_{max,switch,desired}$, respectively.

(V) The maximum equalization time should be about $T_{equalization}$.

There is no current sensor in this topology, therefore, to make sure that the currents of inductors and switches never exceed their maximum limit and all the currents reach zero at the end of a cycle, L_m, L_f , Duty cycle and phase shift used in the system sync. patterns should be calculated for the worst case scenarios. Worst case scenarios for the currents, voltages and switching period occur when currents and voltage reach their maximum and, the switching period is the longest. Also, the worst case scenario for the equalization time is the situation where it takes longest time for battery cells to reach equalization point. Three extreme case scenarios exist:

Case 1: Battery cell 1 has lower voltage than V_{max} and the others have V_{max}.

Case 2: Battery cell 1 has V_{max} and the others have lower voltage.

Case 3: Battery cell 1 has V_{max} and the others have V_{min}.

Case 1 and 2 are the extreme cases for currents, voltage and switching period while the third case is the extreme case for the equalization time. To justify the extreme case scenarios, assume Fig. 3.7(a)-(b), maximum voltage occurs when all battery cells are at their maximum and all switches are ON except switches and diodes of one bridge. This is due to the fact that all equivalent voltages sources are in series. Similarly, the maximum current occurs at the end of the states where all the switches are ON. This maximum current should be studied for both cases. This is due to the fact that for example if diodes in the first state of case 2 are ON the maximum current occurs in the second state of case 2. To be more specific, if this condition is met, the diodes in the second state of case 2 are ON and maximum current occurs at the end of this state.

$$\frac{L_m \sum_{i=2}^{n} E_{eq,i}}{L_m + (n-1)L_{eq}} \overset{?}{\geq} V_{Bj,1} + V_{D,on} \Big|_{\ j=1,2} \tag{3.7}$$

The longest switching period occurs in case 1 where all switches except bridge 1 switches are turned ON in the second state. In case 1, all switches except bridge 1 switches are turned ON in state 1 while, in case 2 all bridges except bridge 1 switches are turned ON in the second state. In both cases currents go up when switches are ON and go down when switches are OFF, therefore, as the switches turn ON later, currents go back to zero later. Thus, the worst case scenario for the switching cycle occurs in case 1 where switches are turned ON in the second state. Also, the worst case scenarios for the equalization time occurs when one battery cell voltage is at the maximum and the other cells are at their minimum, case 3. In this case, the currents are minimized, therefore, the transferred charge is minimized and, the equalization time is maximized. Therefore, maximum switching period and voltage occur in case 1 and case 2 should be studied along with case 1 for the maximum current. Also, the maximum equalization time occurs in case 3. By calculating the maximum current, voltage, switching period and, equalization time, the best values for design parameters can be found.

3.2.2 Worst Case Scenarios Analysis

As it is explained, the maximum current, voltage and, switching period in worst case scenarios should be calculated based on the design parameters. Then, based on the predefined system constraints, a range for each design parameters can be found. The analysis of case 1 is as follows:

Case 1: In this case, all the battery cells at V_{max} except battery cell 1 which has lower voltage. Therefore, bridge 1 the common sync. pattern, the red pattern in Fig. 3.8(b), and rest of the controllers of bridges choose the phase delayed signal, the green pattern in Fig. 3.8(b).

In state 1, the controller of bridge 1 chooses the blue pattern and, bridge 2

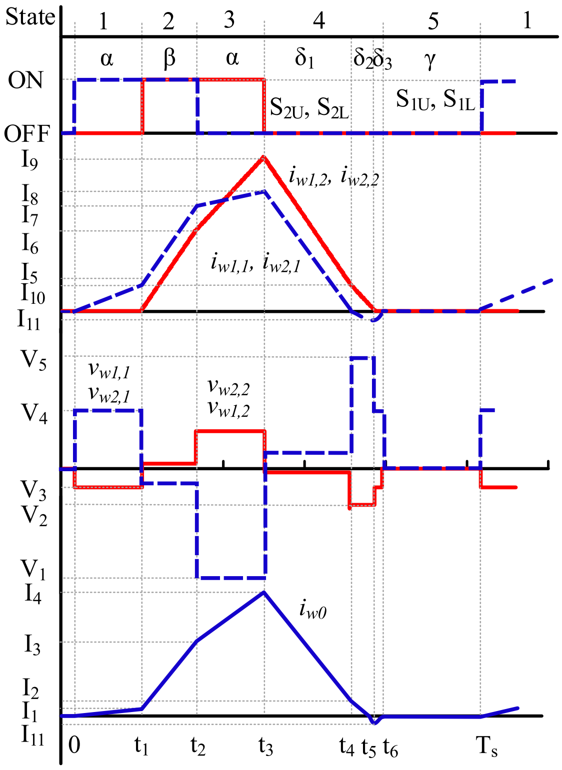

FIGURE 3.10: Typical waveforms for a 2-bridge system in case 1.

chooses the red pattern in Fig. 3.10. The duration of each state is shown on Fig. 3.10. In the first state, BM_1 switches are turned ON and $i_{w1,1}$ and $i_{w2,1}$ increase. It is considered that battery cell 1 has the lower or equal voltage compared to the other battery cells which have the highest voltage, V_{max}. To study the worst condition for the maximum current, voltage and, longest switching period to go back to zero, the voltage of battery cell 1 is considered equal to V_{max}. The duration of the first state is also considered as "α", see Fig. 3.10. The slop of i_{w0} in the first state, di_{w0}/dt, and the value of i_{w0} at the end of this state, I_1, can be calculated as it is shown below, see Fig. 3.10.

$$\frac{di_{w0}}{dt} = \frac{E_{eq,1}}{L_{eq} + (n-1)L_m + nL_l} \Rightarrow I_1 = \frac{di_{w0}}{dt} \times \alpha \tag{3.8}$$

where E_{eq} and L_{eq} are shown in Fig. 3.7. Therefore, the currents slopes of $i_{w1,1}$

and $i_{w2,1}$ and their values at the end of this state, see Fig. 3.10, can be calculated as below.

$$\begin{aligned} \frac{di_{wi,1}}{dt} =& \frac{E_{eq,1} + L_{eq}\dfrac{di_{w0}}{dt} + V_{Bi,1}}{L_l + L_f} \Bigg|_{\, i=1,2} \\ \Rightarrow I_5 =& \frac{di_{w1,1}}{dt} \times \alpha \end{aligned} \tag{3.9}$$

Generally, the current of w_0 and wi, j at the end of state m can be calculated based on these formula:

$$I_m = \frac{\sum_{k=1}^{n} E_{eq,k}}{nL_{eq} + nL_l} \times \Delta t_m + I_{m-1} \quad for\; w_0 \tag{3.10}$$

$$I_m = \frac{-E_{eq,j} + L_{eq}\dfrac{\sum_{k=1}^{n} E_{eq,k}}{nL_{eq} + nL_l} - E_{i,j}}{L_l + L_f} \times \Delta t_m + I_{m-1}\, for\; w_{i,j} \tag{3.11}$$

where $E_{eq,k}$, $E_{i,j}$ and, L_{eq} during state m can be calculated as shown in Figs. 3.6(b)-(c), 3.7(a)-(b), Δt_m is the duration of state m and, I_{m-1} is the current at the beginning of state m. This procedure can be done until state 3 where the maximum voltage on the windings occurs. The maximum voltage should be tolerated by the lower voltage bridge inductors and it is can be calculated as below:

$$\begin{aligned} \frac{di_{wi,j}}{dt} &= \frac{V_{Bi,j} - E_{eq,j} + L_{eq}\dfrac{-E_{eq,1} + \sum_{i=2}^{n} E_{eq,i}}{nL_{eq} + nL_l}}{L_l + L_f} \\ \Rightarrow V_{w1,1,(s3)} &= V_{B1,1} + (L_l + L_f) \times \frac{di_{w1,1}}{dt} \end{aligned} \tag{3.12}$$

In state 4, the switches of all bridges are OFF, therefore, the diodes in all bridges are ON. As it is shown in Fig. 3.10, state 4 is divided into three intervals. In the first interval currents of first bridge go back to zero. Therefore, duration of this interval is:

$$\delta_1 = \frac{-I_8}{\frac{\sum_{k=1}^{n} E_{eq,k}}{nL_{eq} + nL_l}} \tag{3.13}$$

In the second interval, if the imposed voltage on the inductors of the lower voltage bridge is high enough, diodes of the switches in the lower voltage bridge are turned ON and will stay ON till the currents of all other bridges go back to zero. So, if the following equation holds true, diodes are ON and the duration of the second interval is:

$$\begin{gathered} V_{wi,1} = \frac{L_m \sum_{i=2}^{n} E_{eq,i}}{(n-1)L_{eq} + L_m} > V_{Bi,1} + 2V_{D,on}\Big|_{i=1,2} \\ \Rightarrow \delta_2 = \frac{-I_2\Big((n-1)L_{eq} + L_m\Big)}{\sum_{i=2}^{n} E_{eq,i}} \Rightarrow \delta_3 = \frac{I_{11}(nL_{eq} + L_m)}{\sum_{i=1}^{n} E_{eq,k}} \end{gathered} \tag{3.14}$$

When currents in all bridges except bridge 1 go back to zero, the next interval starts and last until the currents of first bridge go back to zero. The duration of the third interval can be calculated as shown above. If Eq. (3.14) holds false, the second interval lasts until currents of all bridges go back to zero and the duration of the third interval is zero. Finally, in state 5, all currents are zero until the next switching cycle starts. To maximize the switching frequency, the unused state in the switching cycle, state 5, can be eliminated in both case by setting $\gamma = 0$. This elimination is valid when it is guaranteed that the currents go back to zero at the end of state 4. This is considered in the worst case scenarios analysis so, it is safe to eliminate state 5. This state is defined in case of uncertainty of the value of the magnetizing and added inductance which will be explained thoroughly in sensitivity analysis section. To conclude this case, the maximum current in this case is I_4, I_8 or I_9, the maximum period is $2\alpha + \beta + \delta_1 + \delta_2 + \delta_3 + \gamma = T_s$ and the maximum voltage on the inductor is $V_{w1,1}(s3)$.

Case 2: As it is discussed in case 1, it is enough only to check the maximum current in the second case scenario. The maximum current which occurs in the second state can be calculated as functions of the design parameters. The formulas for calculating the currents are similar to the previous case, see Eq. (3.10) and (3.11). The only important point in this case is that, in state 1, if Eq. (3.14) holds true, diodes are ON and current will flow in the first bridge.

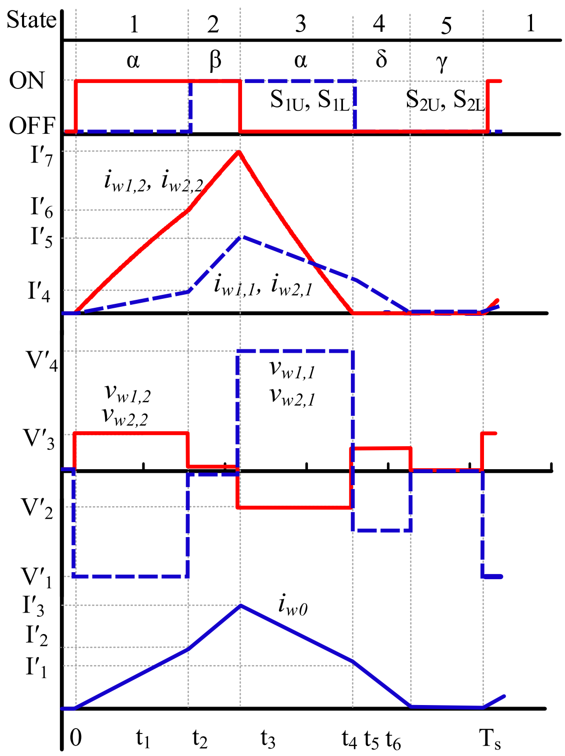

Figure 3.11: Typical waveforms for a 2-bridge system in case 2 when diodes of BM_1 are ON in the first state.

Using Eq. (3.10) and (3.11), the maximum currents in this case, I_7' or I_3' see Fig. 3.11, can be calculated as functions of design parameters. Therefore, all the constraints, which are discussed at the beginning of the section: I_{max}, V_{max} and, $f_{s,min}$, are calculated as functions of design parameters. There are 3 equations, I_{max}, V_{max} and, $f_{s,min}$, and 4 unknown, L_m, L_f, α and β. Thus, by applying the constraints on the obtained formulas, all the design parameters can be calculated as a function of L_f. Then, by calculating the equalization time for all the solution in case 3, the best solution which offers the lowest equalization time can be achieved. Next step is to calculate the equalization time.

3.2.3 Analytical Prediction of Voltage Equalization Time

The best solution among all the calculated solutions, is the one which offers the lowest equalization time in the worst case scenario for equalization time, case 3. Also, the equalization time should be always smaller than the predefined value in the system constraints. If the minimum calculated equalization time in case 3 is less than the predefined value, the design is good but if it is bigger than the predefined value, the constraints should be modified. The worst case scenario for equalization time occurs in case 3, where all the battery cell voltages are at the minimum except one of them which is at its maximum voltage. This leads to lower current in bridges, due to the nature of series voltage source connection, consequently, the rate of charge transfer decreases.

To predict the equalization time, current waveforms of the battery cells should be calculated, then the transferred charge of each battery cell can be calculated. By using the following equation, the new voltage of the battery cell at the beginning of the next cycle can be calculated.

$$\Delta V_{Bi,j} = \frac{Q_{Ex,Bi,j,cycle1}}{C} \Rightarrow V_{Bi,j,cycle2} = V_{Bi,j,cycle1} + \Delta V_{Bi,j,cycle1} \tag{3.15}$$

where $Q_{Ex,Bi,j,cycle1}$ is the exchanged charge in the first cycle, C is the capacity of the battery cell, $\Delta V_{Bi,j,cycle1}$, $V_{Bi,j,cycle1}$ and, $V_{Bi,j,cycle2}$ are the voltage variation, voltage at the beginning of the first cycle, voltage at the beginning of the second cycle of battery cell i in BM_j. This procedure is repeated cycle by cycle until the battery cells reach equal voltage. For instance, the exchanged charge of battery cell 1 in bridge 2 in case 1, $Q_{B1,2}$ can be calculated as follows, see Figs. 3.8 (c)-(d) and Eq. (3.6):

$$Q_{Ex,B1,2} = \frac{\beta I_6}{2} + \frac{\alpha(I_6 + I_9)}{2} - \frac{\delta_1(I_9 + I_{10})}{2} - \frac{\delta_2 I_{10}}{2} \tag{3.16}$$

Thus, to calculate the exchange charge of $B_{1,1}$ in the first cycle, I_6, I_9, I_{10}, δ_1 and, δ_2 for the first cycle should be calculated. Using the calculated value and Eq. (3.16), the exchanged charge in the first cycle can be calculated. Based on the exchanged charge, the battery cells voltage at the end of this cycle can be calculated and these calculations should repeated for next cycle. However, it is assumed that the voltage of battery cells do not change during a cycle, this assumption is valid when the capacity of battery cells are large. The effect of this simplification is bold when the battery cells are substituted by low capacity capacitor as it is studied in experimental section.

3.2.4 Design Procedure

To conclude the design procedure, an step to step procedure is presented. The first step is to calculate the currents and voltages waveforms to calculate switching period duration and, maximum voltage and currents in the worst case scenarios as functions of L_m, L_f, α and β, which are design parameters, as follows:

$$\begin{cases} T_s(L_m, L_f, \alpha, \beta) \\ = \alpha + \beta + \alpha + \delta + \gamma < T_{s,designed} \\ I_{\max}(L_m, L_f, \alpha, \beta) \\ = max(I_4, I_8, I_9, I'_3, I'_7) < \mathrm{I}_{max,designed} \\ V_{\max}(L_m, L_f, \alpha, \beta) \\ = V_{w1,1,(s3)} < V_{\max,winding,designed} \end{cases} \Rightarrow \begin{cases} Duty - cycle = \frac{\alpha+\beta}{\alpha+\beta+\alpha+\delta+\gamma} \times 100 \\ Phase - shift = \frac{\alpha}{\alpha+\beta+\alpha+\delta+\gamma} \times 360 \end{cases} \tag{3.17}$$

It is assumed that the maximum and minimum voltages of battery cells are known and that the leakage inductance of the transformer/coupled inductor are negligible and can be neglected. Furthermore, the maximum switching frequency is defined and γ is set to zero. γ is an unused time in the switching cycle, therefore, it can be set to zero to achieve the maximum switching frequency. There are 4 unknowns: "α", "β", "L_m", "L_f" while there are only 3 independent equations. Therefore, assuming the following are given, "$V_{max,winding,desired}$", "$T_{equalization,desired}$", "$I_{max,desired}$", "$f_{s,desired}$", all the design parameters can be calculated based on L_f. Then, by calculating the equalization time, the best solution can be achieved. The system design steps are summarized in the flowchart of Fig. 3.12:

3.2.5 Design Example

A controller for a 4-bridge system which contains four $5F$ capacitors has the following design constraints: "$V_{max,winding} \leq 3V$", "$I_{max} \leq 2A$", "$f_s \geq 100kHz$", $T_{equalization} \leq 100sec$. An experimental test system is implemented using two BMs

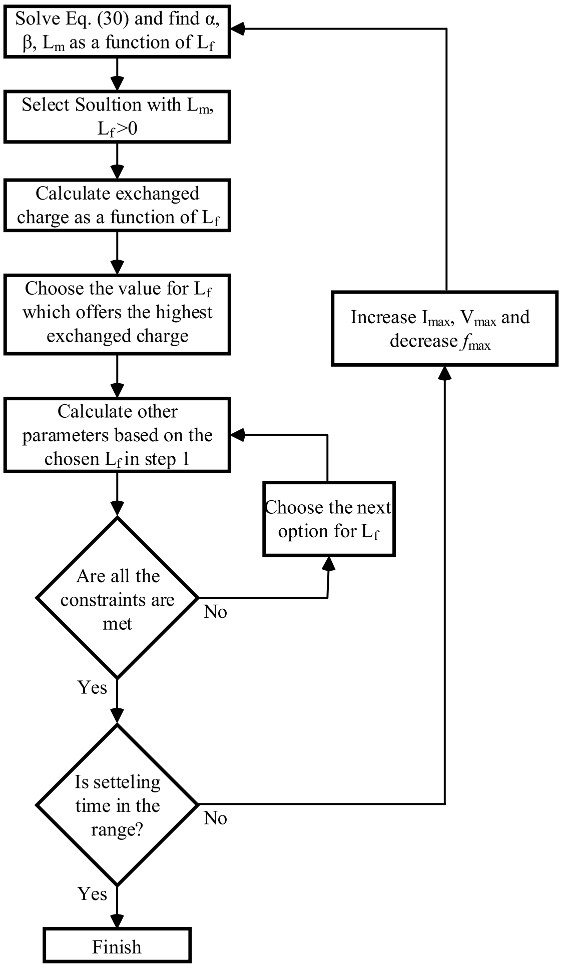

FIGURE 3.12: Design Flowchart.

with four $5F$ capacitors used in each module with a maximum voltage of $4.5V$ and a nominal voltage of $4V$. By solving Eq. (3.17), "$Duty\ cycle$", "$Phase - shift$" and "L_m" can be found as functions of L_f as follows:

$$\begin{cases} L_m(L_f) = 0.6842 \times L_f \\ \alpha(L_f) = 2.8188 \times 10^{-6} - 9.7 \times 10^{-3} \times L_f \\ \beta(L_f) = 0.2251 \times L_f - 8.3684 \times 10^{-7} \\ 0 < L_f < 20\mu H \end{cases} \tag{3.18}$$

Based on these functions, the diagrams of Fig. 3.13(b)-(d) can be drawn. Then, by calculating the equalization time for all the solutions, the diagram in Fig. 3.13(a) can be drawn. To minimize the equalization time L_f can be found form Fig. 3.13(a). The minimum equalization time is achieved when L_f is around $8\mu H$, see Fig. 3.13 (a).

These functions are drawn in the diagrams of Fig. 3.13. To minimize the equalization time L_f can be found form Fig. 3.13 (a). Using Fig. 3.13(b)-(d) and based on the chosen L_f the rest of the control variables can be found. Thus, the best design to minimize the equalization time while all the constraints are met is: Duty cycle = 37%, phase-shift = 100°, $L_m = 5.7\mu H$ and $L_f = 8\mu H$.

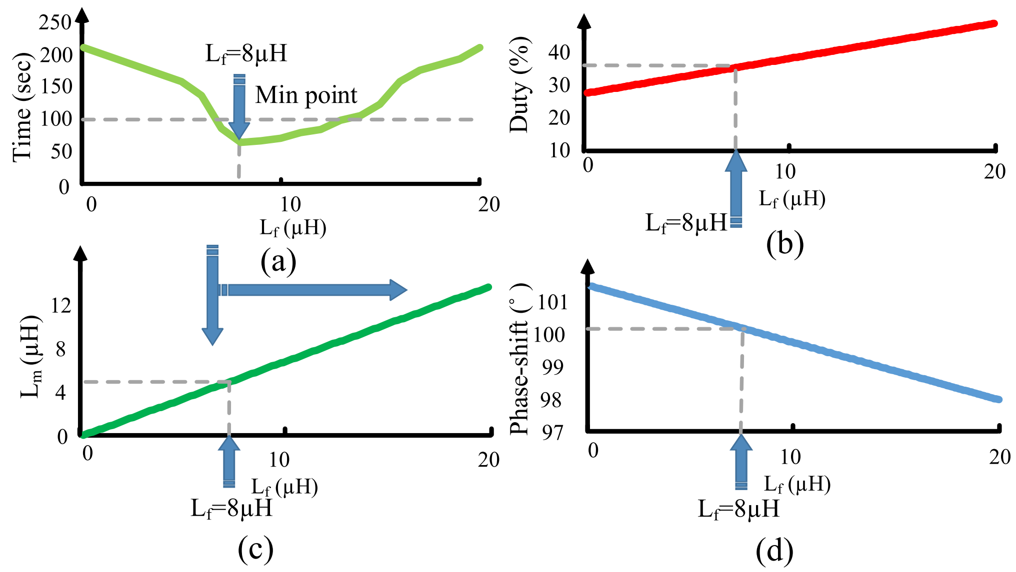

FIGURE 3.13: design guideline for a 2-bridge system.

The system with designed parameters and ideal component i.e., no voltage drop and no parasitic resistance, is simulated in Fig. 3.14 and the simulation results are compared to the analytical calculations. The predicted waveform along with the simulated waveforms are presented in Fig. 3.14 where the battery cells are replaced

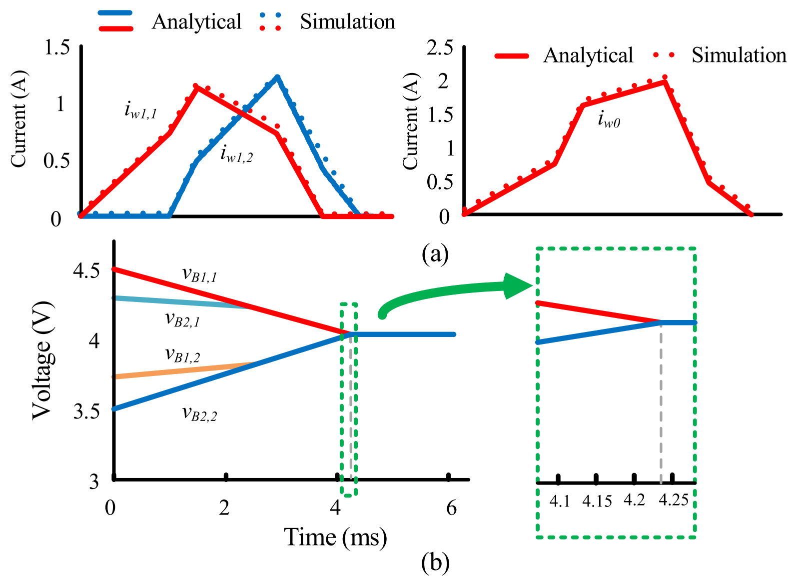

FIGURE 3.14: Simulation and theory comparison for the designed system with $1mF$ capacitors (a) Simulated and analytical waveforms (b) simulated equalization time.

with $1mF$ capacitors. The analytical and simulated waveforms are similar which validates the analytical calculation. Thus, the analytical calculations can be used to predict the current and voltage waveforms well as to predict the equalization time. In contrast to and Cascaded method, in this method it is possible to predict the equalization time. The reason behind this is that the tertiary windings of the coupled inductor share the same current, therefore, the effect of bridges on each other is the same and is independent of location of the bridges. The predicted equalization time is around $4.2ms$ which is accurate compared with the simulation results in Fig. 3.14. It is worth mentioning that the small percentage of error is due to the simplification in the equalization procedure, where the voltage of the battery cells are updated at the end of each cycle while in the reality, the voltage of battery cells change during a switching cycle. The simplification adopted would only lad to inaccurate results only if the capacity of battery cells are small, i.e., or conversely $\Delta Q/C$ is big. However the capacity of the battery cells are significantly large as to make the effects of this simplification insignificant.

3.3 Sensitivity Analysis

The effect of parameters variation on the performance of the system is studied and results are shown in Fig. 3.15. All of the discussed analysis and calculation are based on the fact that all inductors and components which are used in the bridges are similar however, in the reality, this assumption is not accurate. The parameters which are subject to change are L_m and L_f and, their variation effect on the circuit constraints such as, maximum voltage, frequency and, equalization time is studied. To make it general, this study has been done in per-unit calculation; the base values are defined as follows: $I_{base} = 2A$, $V_{max} = 5V$, $L_m = 5.7\mu H$, $L_f = 8\mu H$, $duty = 37\%$, and $T_{eq,base}$, the equalization time with the aforementioned parameters, is $71sec$. The parameters which are subject to change are L_m and L_f, the variation range considered for each one is ±%25pu and their variation effect on I_{max}, Frequency and T_{eq} are studied. The effect of these two variables on the frequency is negligible and the effect of L_m on I_{max} is minimal, see Fig. 3.15. The variation effect of L_m on T_{eq} would not cause any large derivation from the predicted values. The effect of L_f on T_{eq} and, I_{max} are more considerable and should be considered in the worst case calculations. Since there is no current sensors in this circuit, by considering a safety margin for the chosen components, the variation effect of L_m and L_f on the system performance can be managed.

3.4 Experimental Results

The presented analysis and design procedure are validated by comparing the results of an experimental prototype to the results of the simulations and analytical calculations and results are shown in Figs. 3.16 and 3.19. Also, the results of the proposed method are compared to the results of cascaded circuit and results are shown in Table. 3.4. The prototype is implemented based on the designed

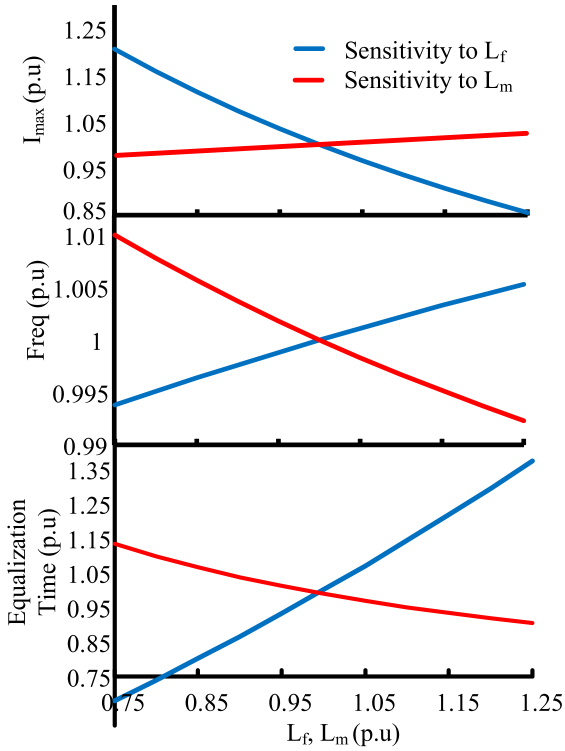

FIGURE 3.15: Sensitivity analysis of the designed system.

parameters which are calculated in design example section, see Fig. 3.17. The analysis is modified and, the voltage drop of diodes are added while the parasitic resistance of the component are neglected since the chosen component have very low resistance. The predicted currents waveforms closely match to the experimental results, see Fig. 3.16 (c), (d). The calculated equalization time is 71.2610sec which is about 7% less than the experimental results due to the effect of parasitic resistance of components. As a result of analysis, if there is no diode voltage drop the equalization time is faster. As it is shown there is a huge drop in the voltages of capacitors in Fig. 3.16(e), that is due to the fact that the capacity of the capacitors are small. These capacitors are replaced with 20Ah battery cells (EIG ePLB C020, see Fig. 3.18) and the results are shown in Fig. 3.19. When real battery cells are replaced with the capacitors there is no drastic drop in the battery cell voltage of cells and when the battery cells voltage are equal the controller stops switching to prevent loss in the circuit.

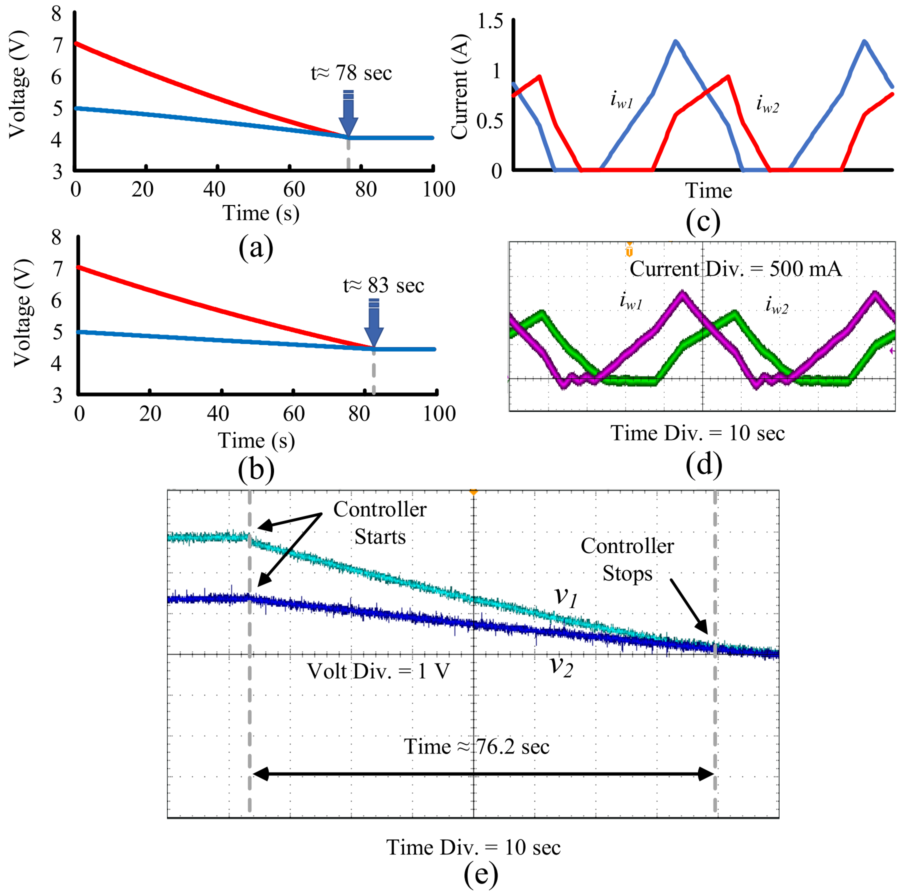

FIGURE 3.16: Performance comparison of (a) Series method and (b) Cascaded method for a 2-bridge system with $5F$ capacitors and similar constraints (c) predicted waveform by theory (d) experimental results of current waveforms (e) equalization time of 2 BMs with two $5F$ capacitors as battery cells.

3.5 Comparison

a comprehensive comparison between the proposed method and the previously published paper is presented. First, a comparison between the proposed method and popular cell to cell, string to cell, cell to string and cell to string to cell methods

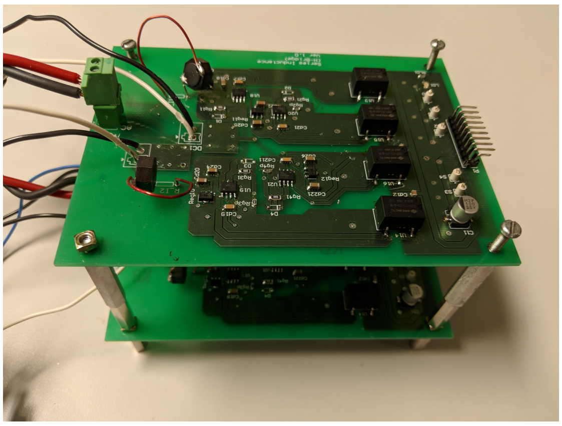

FIGURE 3.17: Two BMs covers 4 battery cells.

FIGURE 3.18: EIG ePLB C020 Battery cells

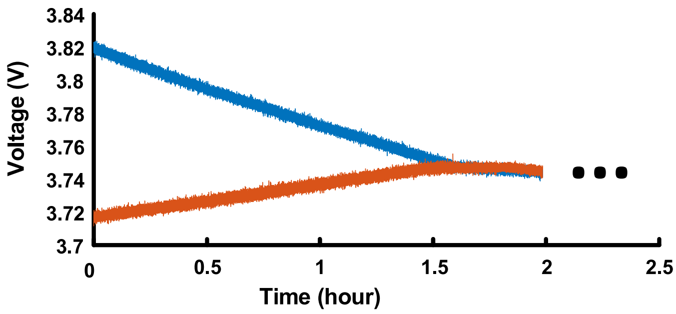

FIGURE 3.19: Performance of the system with four $20Ah$ cells.

is presented in Table. 3.1. In this table, methods are compared from different aspects such as modularity, charge transfer features and number of components in

TABLE 3.1: Comparing different methods for a system with $2n$ battery cells.

Method / Feature	Cell to Cell			Cell to String	String to Cell	Cell to String to Cell		
	[73]	[41]	[74]	[43]	[75]	[68]	Cascaded Method	PRO-POSED
Modularity	✓	✓	✓	×	×	✓	✓	✓
Non-neighbor Batteries Charge Transfer	×	✓	✓	✓	✓	✓	✓	✓
Parallel Charge transfer	✓	×	✓	×	×	✓	✓	✓
Supports Unlimited Number of Battery cells	✓	×	×	×	×	✓	✓	✓
Charge Transfer Between all Cells in a Cycle	×	×	✓	×	×	✓	✓	✓
Number of Switches / Diodes	$\frac{4n}{0}$	$\frac{2n}{2n}$	$\frac{4n}{8n}$	$\frac{2n}{1}$	$\frac{8n}{2}$	$\frac{16n}{16n}$	$\frac{2n}{2n}$	$\frac{2n}{2n}$
Number of Sensors	$2n$	$2n$	$2n$	$2n$	$2n$	$4n$	n	n
Central/Distrib-uted Controller	Dist.	Cent.	Cent.	Cent.	Cent.	Dist.	Dist.	Dist.
Equalization Speed	Slow	Slow	Fast	Slow	Slow	Fast	Fast	Fast
Cost	Low	High	High	Low	High	High	Low	Low
Neighbor Cells Charge Transfer Efficiency	High	High	Avg	Avg	Avg	Avg	Avg	Avg
Far Away Cells Charge transfer Efficiency	Low	Low	Avg	Avg	Avg	High	High	High

the circuit.

From Table. 3.1 it can be concluded that the Cell to String to Cell methods are the best methods to use. But if the efficiency of the circuits are compared, Cell to Cell methods show the best performance. For example, the efficiency of the proposed circuit is measured experimentally and results are shown and compared to the similar method in Table. 3.2. Two efficiencies are calculated: sequential and far-away cells (intra and inter-bridge in this method) charge transfer. In sequential charge transfer, charge exchanges between two neighbor cells while in far-away charge transfer, charge exchanges between non-neighbor cells in a cycle. There are methods which have higher sequential charge transfer efficiencies compared to the proposed method but by investigating those method it can be concluded that either those methods use cell to cell charge transfer method or they are so expensive. For example, in [76], battery cells are only able to transfer charge to their neighbor cells therefore, the charge transfer efficiency of these converters would drastically drop when battery cell with higher and lower charge are far away. Also, there are methods with high efficiency which can transfer charge between non-neighbor cells with high efficiency, such as [77], but they can exchange charge only between two cells in a cycle, which decreases the speed of equalization when variety of cell voltages are high in the string of battery cells. In addition to that, methods using a central controller can only support a limited number of cells while in the method with distributed control, such as the proposed method, this problem is solved. In addition to that, parallel charge transfer is the ability of the circuit to exchange charge between all battery cells in a cycle. These features increase the speed of equalization of the system and when it combines with high efficiency of far-away charge transfer, it can increase the speed and efficiency of the system. The proposed method, has high efficiency for far-away cell charge transfer and also, supports parallel charge transfer, therefore, compared to the similar method, shows superior speed of equalization and efficiency. Also, it is possible to substitute the diodes in the circuit by switches to improve the efficiency of the circuit but at the cost of increase the size and cost of the circuit. In that case, the most prominent loss factors are the turn off loss of the switches and conduction loss of the inductors and switches which are not comparable to the diode conduction loss.

Therefore, it is better to use methods which have the feature of parallel charge transfer and ability to charge transfer between all cells in a cycle while the efficiency

TABLE 3.2: Comparing efficiency, control method and, charge transfer features.

Method / Efficiency	[78]	[62]	[76]	[79]	[77]	Proposed
Sequential Charge Transfer	%55	%56	%90	%90	%93	%70
Far-away Cell Charge Transfer	%55	%56	Low	%90	%93	%65
Controller	Cent.	Cent.	Dist.	Cent.	Cent.	Dist.
Parallel Charge Transfer	✓	×	✓	×	×	✓

of them are good.

Another aspect which should be taken into account is cost of the system. Cost comparison between the proposed method, Cascaded method, [74] which is a high performance method and, [41] which is among the cheapest methods are presented in Table. 3.3. The feedback cost stated in Table. 3.3, is the cost of isolating or conditioning the feedback signal when a central controller is used. For example in cases that the number of battery cells are high, assume n battery cells, there is a long distance between the battery cells and the controller. To prevent EMI/RFI all the feedback signals should be isolated or digitized. This process adds some cost to the circuit which is a hidden cost. On the other hand, the controller should have n inputs to be able to process all the input signal, therefore, number of battery cells is limited by the number of controller inputs. In the contrast, the proposed distributed controller needs only three feedback signals which are local. Therefore, there is no such a cost for the proposed controller. Also, there are methods which are not expensive but the they are not fast, like cell to cell methods [41], on the other hand, there are methods which are fast but the cost of the system is high, like [74]. The method described in [2] has a very low rate of charge transfer resulting in a low speed of equalization compared to the proposed method. Cascaded method has also, improved the speed of equalization compared to [2] while using fewer transformer windings and connections. However, the coupled inductors used in Cascaded method have 4 windings and each bridge has 4 connections to its neighbor bridges while the coupled inductors used in the proposed method has only 3 windings and then, there are only 2 connections to neighboring bridges. Also, the cost of the Series method is lower than cascaded method. Moreover, the design procedure is more straightforward in the proposed method and the equalization time prediction, can be done with a good accuracy. Simpler analysis and prediction of equalization time can be achieved since the tertiary windings current is the same in all bridges therefore, effect of each bridge on other bridges is not related to the location of the bridge. In cascaded method, each bridge has the maximum effect on the neighbor bridges since they are cascaded. Consequently, the analysis of this method would be much easier than method in Cascaded method.

The performance of the cascaded method, is compared to the proposed method. In the Cascaded method, voltages of battery cells converge faster when the voltage difference is high, beginning of the equalization process. this is due to the nature of cascaded connection of the windings. However, when the voltage difference between battery cells decreases, the rate of charge transfer decreases. On the other hand, the inductances used in the series method are larger than the cascaded method since the applied voltage on them are greater. Therefore, in high voltage applications where the voltage are greater, size of the inductors in cascaded method is smaller consequently, size of the circuit is smaller.

Table 3.3: Comparison of basic costs for a system which covers 4 battery cells as of February 2019 [3].

Component \ Method	Proposed method	Cascaded Method	[41]	[74]
Inductors (1.5A)	\$0.6	\$0.6	\$0.9	\$0.6
Coupled Inductors (1.5A)	\$5.54	\$11.08	-	\$2.8
MOSFET (5A, 20V)	\$3.68	\$3.68	\$5.52	\$7.36
Diode (3A, 20V)	\$2.88	\$2.88	\$4.32	\$11.52
Cap. (16V, 47μF)	-	-	\$0.54	\$0.72
Voltage Sensor (Opamp + 4Res)	\$2.68	\$2.68	\$5.36+ \$feedback	\$5.36+ \$feedback
Total Cost	\$15.38	\$20.92	\$16.64+ \$feedback	\$28.36+ \$feedback

Table 3.4: Comparing two methods.

Feature \ Method	Cascaded	Series
Equalization Time Prediction	×	✓
Equalization Time	$T_{Cascaded} > T_{Series}$	
Number of Connection to Neighbor Bridges	4	2
Inductors value	Small	Large
Number of windings in Each Bridge	4	3
Analysis Complexity	Complex	Simple

3.6 Conclusion

A modular battery voltage balancing method is proposed, using lower number of components compared with other existing techniques. This method similar to the Cascaded method is modular, uses distributed controller, exchange charge between all battery cells in a cycle and offers ZCS in turn ON but the size of inductors in series method in larger compared to Cascaded method. Although, this method would be faster than cascaded method but at the cost of larger inductor. A distributed control system is presented which operates based on only local feedbacks data with half of the voltage sensors. An equivalent circuit is presented to simplify the analysis of the circuit for all the possible conditions and states. The presented analysis provides a means for developing a design procedure. A case study is provided using the resultant design procedure which is also flexible enough to be used for different battery voltage cells. One of the most significant advantages of the proposed charge balancing technique is that the equalization time can be considered as one of the design parameters. A design example is presented and, the designed circuit is built as a prototype. The simulations and analytical results are validated using the results of the experimental setup. The results confirm that the proposed method is faster than cascaded method. The design procedure presented is relatively straightforward and accurate while the results can be closely predicted using analytical calculations.

Chapter 4

Transformer Coupled Parallel Connected Sepic Module

A charge balancing circuit is proposed which is based on parallel connection of transformer coupled Sepic modules. This topology, similar to Cascaded and Series connections, is modular and able to exchange charge between all cells in a cycle. The charge exchange between all cells makes the system fast. In each module, charge goes from higher charged cell to lower charged cell and a switching pattern is used to transfer charge between modules, from battery cells with higher the total charge to modules with lower charge. The proposed topology is modular and scalable therefore, a distributed controller is designed to make the system modular. Distributed control technique unlike a centralized controller provides features such as plug and play, reduced complexity and low cost of cell monitoring circuits. All the aforementioned features are common between Parallel method and cascaded and Series method but there are some differences. The difference between this method and Cascaded and Series methods is that in this method, fewer active components is used, its efficiency is higher and has higher speed of equalization but it does not offer ZCS in turn ON. The power converter uses 1 switch, 2 diodes and, 1 voltage sensor a pair of battery cells. This topology, however, has a higher voltage stress on the switches compared to Cascaded and Series methods. Analysis and an straightforward design procedures are presented. A prototype of the circuit is built and experimental results are used to validate calculations and design procedure.

4.1 Circuit Topology

The proposed circuit is named based on the basic circuit and the transformer windings connection. The basic topology is Single-Ended Primary-Inductor Converter (SEPIC) and the secondary windings of the transformers are connected in parallel therefore the method is called "Sepic-based Parallel". The way transformers are connected enables modules to transfer identical amount of charge to other modules regardless of their location, unlike Cascaded method where a bridge transfers more charge to its neighbor bridges. The Sepic topology which is a unidirectional converter consists of a boost converter followed by an inverted buck-boost converter, see Fig. 4.1. The advantage of this converter compared to the buck-boost converter is that this converter output is non-inverting.

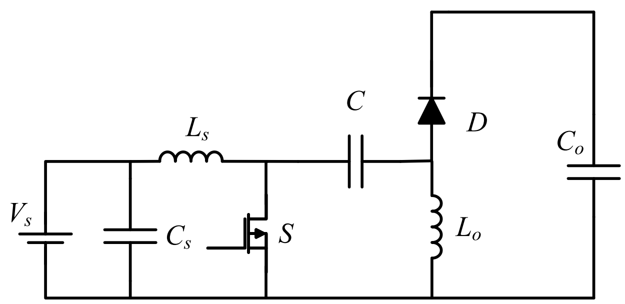

FIGURE 4.1: Sepic Converter.

It is possible to stack this converter to support more battery cells, see Fig. 4.2. As it shown in Fig. 4.2, in circuit 1 the connection of the switch and inductor is removed. To create a path for inductors currents, another connection from C_o to C_s is added. In Fig. 4.2, a red cross is on the removed connection and the added connection is shown by a green arrow. The resultant circuit still operates as a Sepic converter. The resultant circuit is connected to a conventional Sepic converter shown as circuit 2 as it is shown by an orange arrow. The area which is shown by blue dashed square is similar in both converters, therefore, only one of them is kept. The final circuit is shown in the right hand side of Fig. 4.2 which will be referred to as a module. In this module, it is possible to transfer charge from higher charged battery cell to lower charged battery cell.

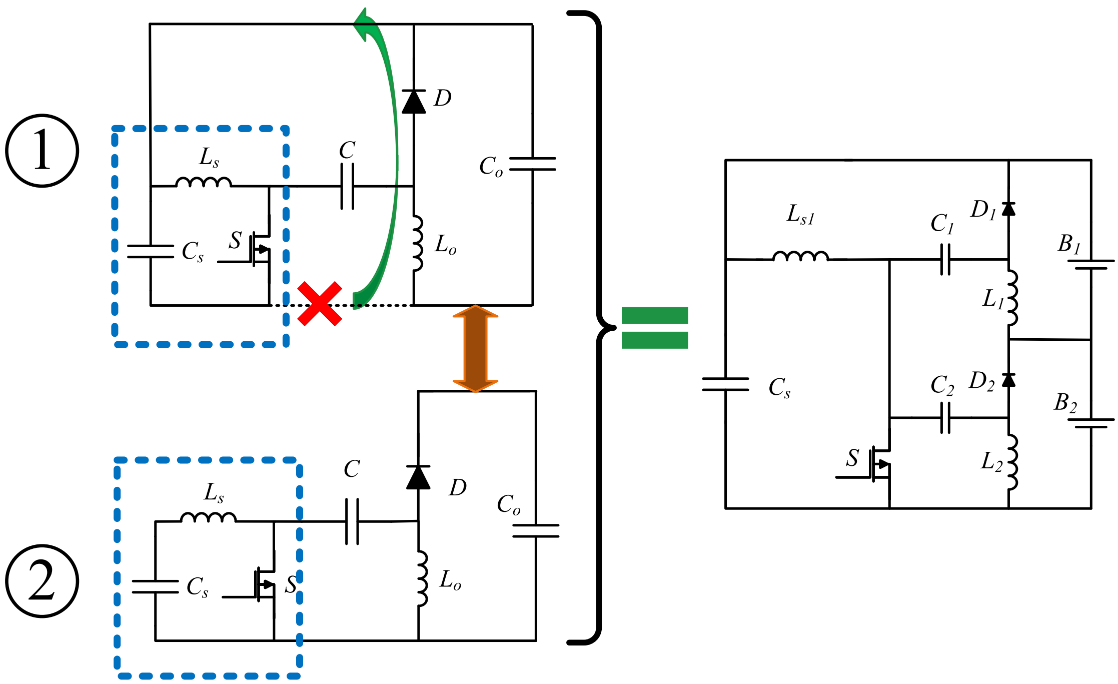

FIGURE 4.2: Connection of two Sepic converter.

The developed module in Fig. 4.2 covers only two battery cells. The idea is to make some changes to be able to connect modules together. It is possible to

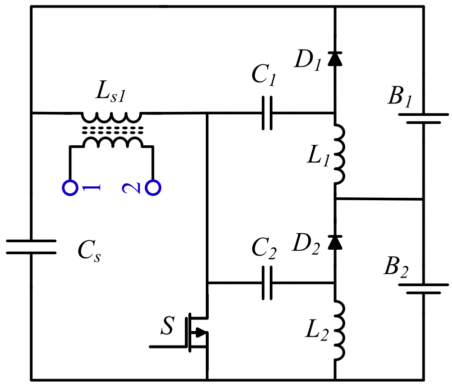

FIGURE 4.3: One module of the proposed converter.

stack more converters to cover more battery cells as it is proposed in [67], Fig. 1.7(c). The problem with this strategy is that as the number of stacked converter increases, the rating of the components should increase. This leads to a larger and more expensive circuit.

The proposed solution here is to substitute L_{s_1} with a coupled inductor as it is shown in Fig. 4.3. Finally, modules can be connected together using the coupled inductor as it is shown in Fig. 4.4. In Fig. 4.4(b), it is shown that secondary windings of coupled inductors are connected to a shared bus in the way that all coupled inductors are in parallel.

The inductor which is chosen to be replaced with a coupled inductor is L_s since the current of this inductor is always unidirectional. If the direction of the current is bidirectional, a condition may happen that the direction of the current in the coupled inductors are different. This leads to demagnetizing the coupled inductor and decrease the stored charge. In other words, it may charge the higher charged cell and discharge the lower charge cell.

Also, only two battery cells exist in a module. The reason behind this is that, it is intended to exchange charge between all battery cells in a cycle. This is explained in detail in single module principal of operation.

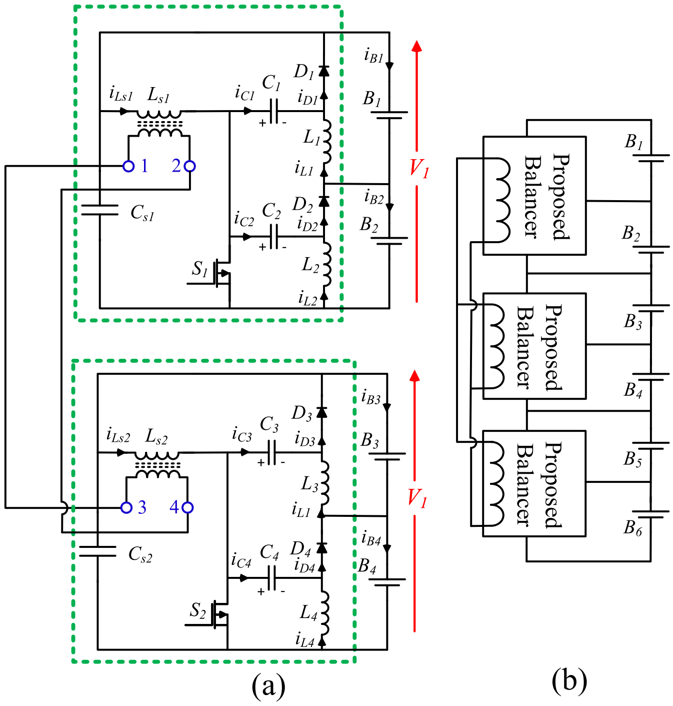

FIGURE 4.4: Two module of the proposed converter.

The circuit in [67], Fig. 1.7(c), can transfer charge from string of series connected battery cells to only one battery cell in a cycle. Therefore, the speed of equalization of [67] is lower than the proposed method which is able to transfer charge between all battery cells in a cycle. Also, the size of the inductors and switches in the proposed circuit would be smaller than the method in [67]. The proposed method improves the performance of the method in [67] and makes it possible to add more battery cells without any changes in the rating of the components, and maintaining the exchange charge between all battery cells in a cycle. These features are achieved by connecting module in Fig. 4.1 as it is shown in Fig. 4.4. The proposed method has 1 switch per 2 battery cells which is fewer than Cascaded an Series methods. In addition, in Cascaded method, bridges transfer more charge to their neighbor bridges while the exchanged charge in the proposed method does not depend on the location of the bridge. Furthermore, the proposed method improves the speed of equalization of the method in [67], Fig. 1.7(c), by proposing a solution to exchange charge between all battery cells in a cycle. Therefore, the proposed method is faster and more cost-effective compared to methods in Cascaded and Series methods.

4.2 Principal of Operation

The main objective of a charge balancing circuit is to equalize charge between all battery cells. In the next sections, it is shown that by applying a specific switching pattern, charge is transferred from higher voltage cells to lower voltage cells. Since the charge transfer procedure is complicated, first the basic operation of a single module is presented and then, the operation of a multi module system is presented in general.

4.2.1 Single Module Operation

To make the charge transfer procedure more clear, the basic operation of a single module of the proposed circuit in the case that $V_{B_1} > V_{B_2}$ is shown in Fig. 4.5 and waveforms are shown in Fig. 4.6. Note that, it is assumed that the voltage of capacitors and current of inductors are constant during a switching cycle.

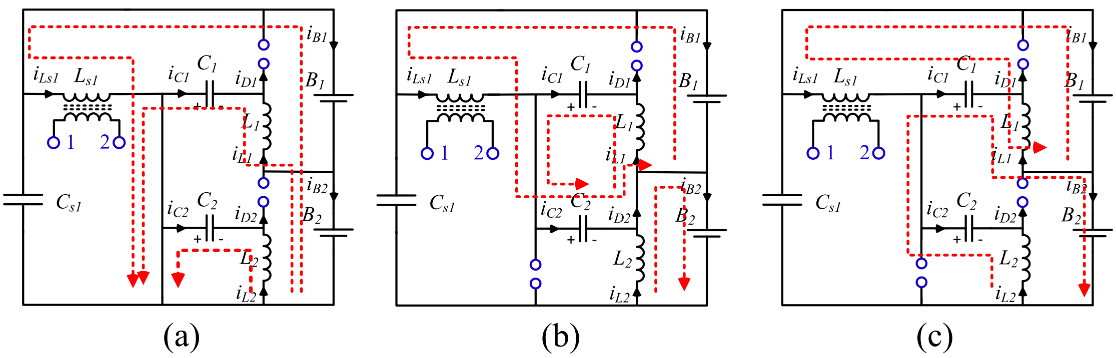

FIGURE 4.5: Basic operation of the proposed circuit in the case $V_{B_1} > V_{B_2}$ (a) When the switch is ON (b) When the diode is ON (c) When the switch and diodes are OFF.

As it is shown in Fig. 4.5(a), when the switch is ON, currents of the inductors, L_i, go through the capacitors C_i and the switch. Battery cells charge inductors and discharging capacitors in this state, see Fig. 4.6. In the next state, Fig. 4.5(b), when the switch is turned OFF, Fig. 4.5(b), the diode which is connected to the lower voltage battery cell turns ON and charges the lower voltage battery cells, see Fig. 4.6. At the moment when the switch is turned OFF, voltage of the inductors increase to turn ON the diodes.

Since it is assumed that voltage of capacitors are constant during a switching cycle, diodes cannot turn ON at the same time. The reason behind that is shown in Fig. 4.7. The average voltage of inductors during a switching cycle is zero.

Therefore, voltage of capacitors are as follows:

$$\begin{cases} V_{c_1} = V_{B_1} \\ V_{c_2} = V_{B_1} + V_{B_2} \end{cases} \tag{4.1}$$

When both diodes are ON, voltage of the point “A” and “B” in Fig. 4.7 should be the equal. While by calculating voltage of these two point in Fig. 4.7:

$$\begin{cases} V_A = V_{C_1} + V_{B_1} + V_{B_2} = 2V_{B_1} + V_{B_2} \\ V_B = V_{C_2} + V_{B_2} = V_{B_1} + 2V_{B_2} \end{cases} \Rightarrow V_A = V_B \Rightarrow V_{B_1} = V_{B_2} \tag{4.2}$$

Therefore, both diodes can only conduct simultaneously when the voltage of battery cells are equal. In unequal conditions, the diode which is connected to the lower voltage battery cell turns ON.

In the next state, Fig. 4.5(c), the current of the diode reaches zero and the diode turns OFF (DCM operation mode), Fig. 4.6. In this state, the applied voltage

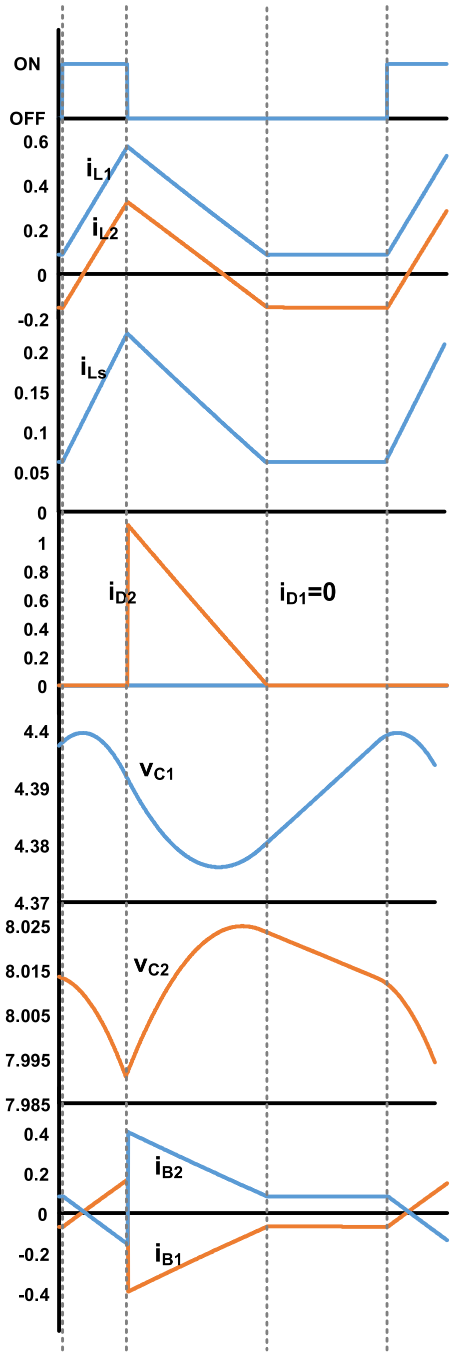

Figure 4.6: Current waveforms of a single module system.

on the inductors are zero, hence all currents are constant until the next switching cycle.

Only two battery cells is placed in each module to be able to exchange charge

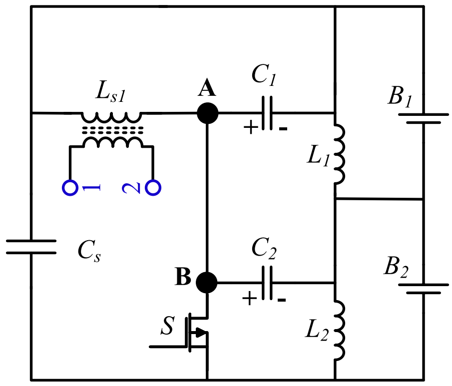

FIGURE 4.7: The schematic of a module when both diodes are ON.

between all battery cells in a cycle. To explain the reason behind this, Assume that there are three or more battery cells in a module. Based on discussed principal of operation of a module, in each cycle, charge goes from battery cells in the module to the lowest charged cell. Therefore, one of the objective of the circuit which is to exchange charge between all battery cells in a cycle would not be satisfied. By placing two battery cells in module, it can be said that charge goes from higher charged cell to lower charged cell in module.

4.2.2 Multi Module Operation

Referring to figure 4.4, assume $V_{B_1} > V_{B_2} > V_{B_3} > V_{B_4}$, consequently, the module voltages $V_1 > V_2$. Using the proposed control patterns the idea is to prove that $I_{B_1} < I_{B_2}$, $I_{B_3} < I_{B_4}$ and $I_{B_1} + I_{B_2} < I_{B_1} + I_{B_2}$ for all conditions. In other words, charge is transferred from a higher voltage cell to a lower voltage cell in a module and at the same time, charge is transferred from higher voltage modules to lower voltage modules. Therefore, charge transfer procedure is divided into two categories: (a) Charge transfer between battery cells within a module or Intra-module, (b) Charge transfer between battery cells which are located in separate module or inter-module, see Fig. 4.8.

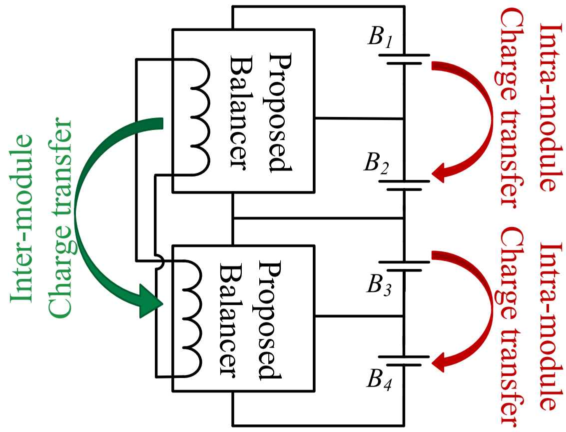

FIGURE 4.8: Charge exchange paths.

To elucidate the charge exchange procedure, assume the green gate command in Fig. 4.9 is applied to the switch of the first module and the red gate command in Fig. 4.9 is applied to the switch of the second module. When S_1 is ON, the charge is stored in L_s, L_1 and, L_2. During the next switching state, S_2 is turned ON while S_1 is turned OFF and it will be proved that, inductors in module 2 are charged while inductors in module 1 are discharged. Some of the stored charge in the inductors of module 1 will be transferred to the lower battery cell in module 1 and the rest of that will be transferred to module 2. Finally, in the last state, when all switches are OFF, the stored charge in the inductors of module 2 will be transferred to the lower battery cell in module 2. The details of switching waveforms are shown in Fig. 4.9. Also, to achieve fixed switching frequency, the converter operates in DCM mode, this means that the current of diode reaches zero before the end of a switching cycle.

To show that the charge will be transferred from higher charged cell to lower charged cell, the exchange charge of battery cells in the circuit should be calculated. The transferred charge to B_i is:

$$Q_{absorbed,B_i} = \int_0^{T_s} i_{B_i}(t)dt \tag{4.3}$$

The average current of a battery cell in a switching cycle is:

$$\begin{cases} I_{B_1} = I_{L_1} - I_{L_s} \\ I_{B_2} = I_{B_1} + I_{D_2} - I_{L_1} \end{cases} \Rightarrow I_{B_i} = I_{D_i} - I_{L_s} \tag{4.4}$$

where I_{B_i}, I_{D_i} and, I_{L_s} are the average current of B_i, D_i and, L_s, respectively. Moreover, $I_{D_i} = I_{L_i}$, where I_{L_i} is the average current of L_i. To calculate I_{L_i} and I_{L_s}, these currents in all states should be calculated. There are 5 states which are shown in Fig. 4.9. The switching cycle for each module is divided to T_{on} when the switch is ON, T_α when the switch is OFF and diode is conducting, and T_β where the diode current goes to zero. As it is mentioned before, to achieve fixed switching frequency, in the last state all currents are DC, see T_β in Fig. 4.9. To separate switching states for the higher and lower voltage module, subscript "H" and "L" are used for the higher voltage (module 1) and lower voltage module (module 2), respectively. Also, assume $D_j = \frac{T_{on_j}}{T_s}$, $D_{\alpha_j} = \frac{T_j}{T_s}$, and $D_{\beta_j} = \frac{T_{\beta_j}}{T_s}$, where "$j$" is "$H$" or "$L$". During T_{β_L} before T_{on_H} starts, the transformer voltage of the lower voltage module is zero, therefore, the current of L_{s_j} and, L_{i_j} would be constant and will be referred to as $I_{L_{s_{\beta_j}}}$ and, $I_{L_{i_{\beta_j}}}$ respectively, where "j" can be "H" or "L". Therefore, I_{L_s} and I_{L_i} are:

$$\begin{cases} I_{L_{s_j}} = I_{L_{s_{\beta_j}}} + \left.\dfrac{D_H^2 T_s di_{L_{s_j}}}{2dt}\right|_{@1} + \left.\dfrac{D_L^2 T_s di_{L_{s_j}}}{2dt}\right|_{@2} \\ + \left.\dfrac{(D_{\alpha_H} - D_L)^2 T_s di_{L_{s_j}}}{2dt}\right|_{@3} + \left.\dfrac{(D_L + D_{\alpha_L} - D_{\alpha_H})^2 T_s di_{L_{s_j}}}{2dt}\right|_{@4} \\ I_{L_i} = \dfrac{D_H^2 T_s V_H}{2L_i} - \dfrac{D_{\alpha_H}^2 T_s (V_{B_i} + V_{D_i})}{2L_i} - \dfrac{\left. I_{L_{s_H}} \right|_{@4}}{2} + I_{L_{i_\beta}} \qquad for\ i = 1, 2 \\ I_{L_i} = \dfrac{D_L^2 T_s V_L}{2L_i} - \dfrac{D_{\alpha_H}^2 T_s (V_{B_i} + V_{D_i})}{2L_i} - \dfrac{\left. I_{L_{s_L}} \right|_{@1}}{2} + I_{i_{L_\beta}} \qquad for\ i = 3, 4 \end{cases} \tag{4.5}$$

where $|_{@i}$ is used to refer to state i in Fig. 4.9.

To calculate I_{L_s} and I_{L_i}, the slope of the current in different switching state should be calculated. To calculate the slope of the currents, the effect of modules on each other should be studied. Since all the secondary windings of the transformers are connected to the a same bus, the effect of a module on the other ones does not depend on the location of the modules. Assume l and m are leakage and magnetizing inductance of a coupled inductor. Since all the windings are similar, it can be concluded that l and m for all of them are equal.

Therefore, the equation for n modules can be written as in Eq. (4.6).

$$\begin{bmatrix} V_{L_{s_1}} \\ V_{L_{s_2}} \\ \vdots \\ V_{L_{s_n}} \end{bmatrix} = \begin{bmatrix} R & M & \dots & M & M \\ M & R & \dots & M & M \\ \vdots & \vdots & \ddots & \vdots & \vdots \\ M & M & \dots & R & M \\ M & M & \dots & M & R \end{bmatrix}_{n\times n} \times \frac{d}{dt} \begin{bmatrix} i_{L_{s_1}} \\ i_{L_{s_2}} \\ \vdots \\ i_{L_{s_n}} \end{bmatrix} where \begin{cases} M = \dfrac{m^2 + ml(n+1)}{(n+1)(l+m)} \\ R = l + M \end{cases}$$

$$\Rightarrow \frac{d}{dt} \begin{bmatrix} i_{L_{s_1}} \\ i_{L_{s_2}} \\ \vdots \\ i_{L_{s_n}} \end{bmatrix} = \begin{bmatrix} a & b & \dots & b & b \\ b & a & \dots & b & b \\ \vdots & \vdots & \ddots & \vdots & \vdots \\ b & b & \dots & a & b \\ b & b & \dots & b & a \end{bmatrix} \times \begin{bmatrix} V_{L_{s_1}} \\ V_{L_{s_2}} \\ \vdots \\ V_{L_{s_n}} \end{bmatrix} where \begin{cases} a = \dfrac{R + (n-1)M}{2(n-1)M^2 + nMR + L^2} \\ b = \dfrac{-M}{2(n-1)M^2 + nMR + R^2} \end{cases} \tag{4.6}$$

The slope of the current of a transformer in Fig. 4.4 can be calculated based on the applied voltage on the primary windings of the transformers in each switching state.

Another unknown expression in Eq. 4.5 are $I_{L_{s_\beta}}$ and $I_{L_{i_\beta}}$, the current of inductors and coupled inductors when the diodes and switches are OFF. To calculate $I_{L_{s_\beta}}$ and $I_{L_{i_\beta}}$, the following equation is valid from the end of T_{α_L} to the beginning of T_{on_H}:

$$\begin{cases} I_{L_{s_{\beta_H}}} = -I_{L_{1_\beta}} - I_{L_{2_\beta}} \\ I_{L_{s_{\beta_L}}} = -I_{L_{3_\beta} - I_{L_{4_\beta}}} \end{cases} \tag{4.7}$$

If all battery cells have equal voltage, all diodes will turn ON at the same time otherwise, in transients, only the diode which is connected to the battery cell would turn ON. In transients, only the diodes which are connected to lower voltage

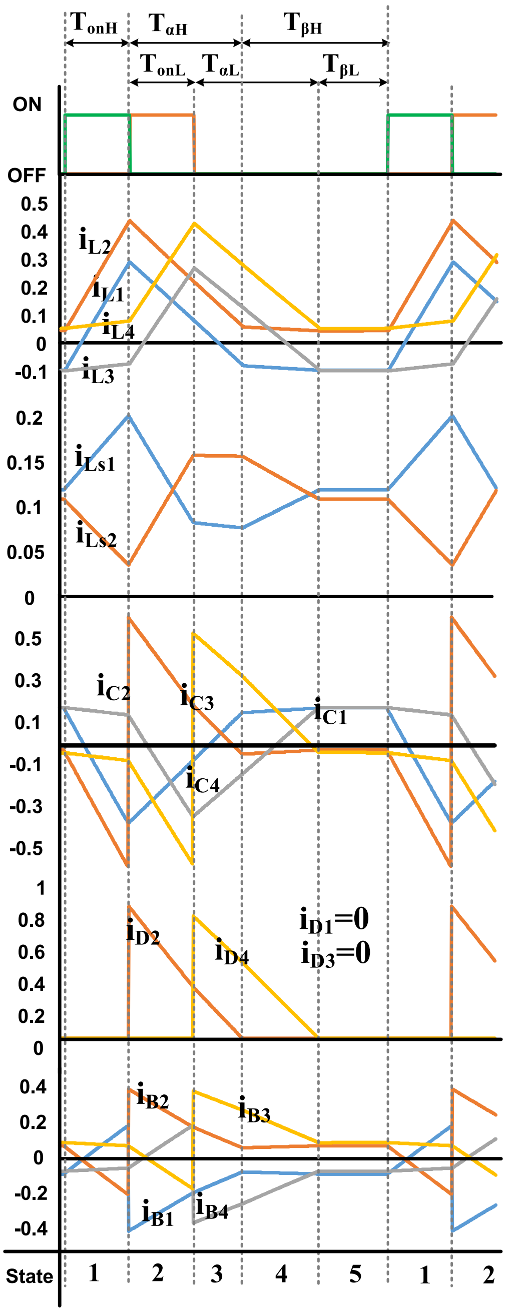

FIGURE 4.9: Current waveforms of a 2 module system.

battery cell would turn ON, D_2 and D_4. Thus, I_{D_1} and I_{D_3} are always zero and this results in $I_{L_1} = 0$ and $I_{L_3} = 0$. To calculate I_{L_2} and I_{L_4}, $I_{L_{2_\beta}}$ and $I_{L_{4_\beta}}$ should be calculated:

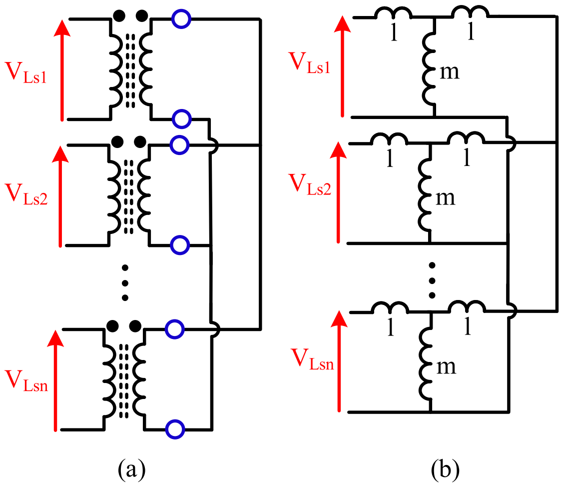

FIGURE 4.10: Transformer connection.

$$\begin{cases} I_{L_{2_\beta}} = I_{c_2} - \dfrac{D_H^2 T_s V_H}{2L_2} + \left(I_{L_{s_H}} + I_{L_1}\right)\Big|_{@2,3} + \dfrac{I_{L_{s_H}}}{2}\Big|_{@4} \\ I_{L_{4_\beta}} = I_{c_4} - \dfrac{D_L^2 T_s V_2}{2L_4} + \left(I_{L_{s_L}} + I_{L_{3_L}}\right)\Big|_{@3,4} + \dfrac{I_{L_{s_L}}}{2}\Big|_{@1} \end{cases} \tag{4.8}$$

Since the average current of a capacitor during a switching cycle is zero:

$$\begin{cases} I_{L_{2_\beta}} = -\dfrac{D_H^2 T_s V_H}{2L_2} + \left(I_{L_{s_H}} + I_{L_1}\right)\Big|_{@2,3} + \dfrac{I_{L_{s_H}}}{2}\Big|_{@4} \\ I_{L_{4_\beta}} = -\dfrac{D_L^2 T_s V_2}{2L_4} + \left(I_{L_{s_L}} + I_{L_{3_L}}\right)\Big|_{@3,4} + \dfrac{I_{L_{s_L}}}{2}\Big|_{@1} \end{cases} \tag{4.9}$$

Another unknown in Eq. (4.5) is D_α. To calculate that, average voltage and volt-sec of the inductors are used. The average voltage of an inductor in a switching cycle is zero, therefore the average voltage of capacitors (V_c) can be calculated as:

$$
\begin{cases}
V_{c_1} = V_{B_1} \\
V_{c_2} = V_{B_1} + V_{B_2} \\
V_{c_3} = V_{B_3} \\
V_{c_4} = V_{B_3} + V_{B_4}
\end{cases}
\tag{4.10}
$$

Moreover, the voltage-sec of inductors in a switching cycle must be zero, hence:

$$
\begin{cases}
D_H V_1 + \dfrac{(D_L + D_{\alpha_L} - D_{\alpha_H}) V_{L_{s_H}}\Big|_{@4}}{2} = D_{\alpha_H}(V_{B_1} + V_{D_1}) \\
D_L V_2 + \dfrac{D_H V_{L_{s_L}}\Big|_{@1}}{2} = D_{\alpha_L}(V_{B_3} + V_{D_3})
\end{cases}
\tag{4.11}
$$

Based on Eqs. (4.10) and (4.11):

$$
\begin{cases}
D_{\alpha_L} = \dfrac{D_L V_2 + \dfrac{D_H (V_{L_{s_L}})\Big|_{@1}}{2}}{V_{B_3} + V_{D_3}} \\
D_{\alpha_H} = \dfrac{D_H V_1 + \dfrac{(D_L + D_{\alpha_L}) V_{L_{s_H}}\Big|_{@4}}{2}}{V_{B_1} + V_{D_1} + \dfrac{V_{L_{s_H}}\Big|_{@4}}{2}}
\end{cases}
\tag{4.12}
$$

Since $I_{D_i} = I_{L_i}$ and assuming that $L_1 = L_2 = L$ and $D_H = D_L$, by writing KCL for the capacitors the following equations can be achieved.

$$\begin{cases} I_{D_2} = I_{L_2} = \dfrac{D_{\alpha_H}^2 T_s V_H}{2L_2} - \dfrac{D_{\alpha_H}^2 T_s (V_{B_2} + V_{D_2})}{2L_2} + I_{L_{s_H}} \Bigg|_{@2,3} \\ I_{D_4} = I_{L_4} = \dfrac{D_{\alpha_L}^2 T_s V_L}{2L_4} - \dfrac{D_{\alpha_L}^2 T_s (V_{B_4} + V_{D_4})}{2L_4} + I_{L_{s_L}} \Bigg|_{@3,4} \end{cases} \tag{4.13}$$

These equations can be simplified as:

$$\begin{cases} I_{D_2} = I_{L_2} = \dfrac{D_{\alpha_H}^2 T_s (V_{B_1} - V_{D_2})}{2L} + I_{L_{s_H}} \Bigg|_{@2,3} \\ I_{D_4} = I_{L_4} = \dfrac{D_{\alpha_L}^2 T_s (V_{B_3} - V_{D_4})}{2L} + I_{L_{s_L}} \Bigg|_{@3,4} \end{cases} \tag{4.14}$$

Using Eqs. (4.5) and (4.7):

$$\begin{cases} I_{L_{s_H}} = \dfrac{D_H^2 T_s di_{L_{s_H}}}{2dt} \Bigg|_{@1} + \dfrac{D_H^2 T_s V_H}{L} \\ I_{L_{s_L}} = \dfrac{D_L^2 T_s di_{L_{s_L}}}{2dt} \Bigg|_{@2} + \dfrac{D_L^2 T_s V_L}{L} \end{cases} \tag{4.15}$$

Based on Eqs. (4.4), (4.14), (4.15), it can be concluded that:

$$I_{L_1} = I_{L_3} = 0 \xrightarrow{\text{Eq. (4.4)}} \begin{cases} I_{B_1} = -I_{L_{s_1}} \\ I_{B_2} = I_{L_2} - I_{L_{s_1}} \\ I_{B_3} = -I_{L_{s_2}} \\ I_{B_4} = I_{L_4} - I_{L_{s_2}} \end{cases} \tag{4.16}$$

Since I_{L_s} is always positive, see Fig. 4.5 and Eq. 4.15, by using Eq. (4.14) it can be concluded that:

$$\begin{cases} I_{L_2} > 0 \\ I_{L_4} > 0 \\ I_{L_{s_1}} > 0 \\ I_{L_{s_2}} > 0 \end{cases} \xrightarrow{\text{Eq. (4.16)}} \begin{cases} I_{B_1} < I_{B_2} \\ I_{B_3} < I_{B_4} \end{cases} \tag{4.17}$$

In other words, using the switching pattern shown in Fig. 4.9, in a module charge goes from a higher voltage battery cell to a lower voltage battery cell, i.e., intra-module charge transfer. Also:

$$\begin{cases} I_{L_2} > I_{L_4} \\ I_{L_{s_1}} > I_{L_{s_2}} \end{cases} \xrightarrow{\text{Eq. (4.16)}} \begin{cases} I_{B_1} < I_{B_3} \\ I_{B_2} < I_{B_4} \end{cases} \Rightarrow I_{B_1} + I_{B_2} < I_{B_3} + I_{B_4} \tag{4.18}$$

These mean, charge goes from higher voltage module to lower voltage module i.e, inter-module charge transfer.

4.3 Control strategy

The main objective of the controller is to keep the fixed switching frequency by operating in DCM mode. Furthermore, to transfer charge from higher charged to lower charged cells, the switching scheme should be as follows: In the first state, the switch of all higher voltage modules should be turned ON. In the second state, when the switches of higher voltage modules are turned off, the switch of the lower voltage modules should be turned ON. Finally, all switches should be turned OFF. Moreover,the controller should be a distributed controller where switching decisions for each module are made in that module based on the available local data. The controller uses local data prevent using a central controller and its costs. To synchronize all the controllers, it is assumed that a common synchronization signal, the green signal in 4.9, is generated and sent to all modules by the first controller which detects the local unbalanced voltages. Therefore, there is no central controller or specific master controller in the system and the system would be plug and play. The controller of each module monitors the total DC voltage of the battery cells of its module along with the total DC voltage of its neighbor battery cells, see Fig. 4.11. For example, in Fig. 4.4, controller of second module, monitors V_1, V_2 and, V_3. The voltage of the module, in this example V_2, will be compared with the local average of the three neighboring module voltages: $\frac{V_1+V_2+V_2}{3}$. If V_2 is greater than $\frac{V_1+V_2+V_2}{3}$, the controller sends the common sync. pattern, the green signal in Fig. 4.9, to the switch of second module. If V_2 is lower than $(V_1 + V_2 + V_2)/3$, the controller delays the common sync pattern and sends it to the switch of the second module, the delayed switching pattern is the red signal in Fig. 4.9.

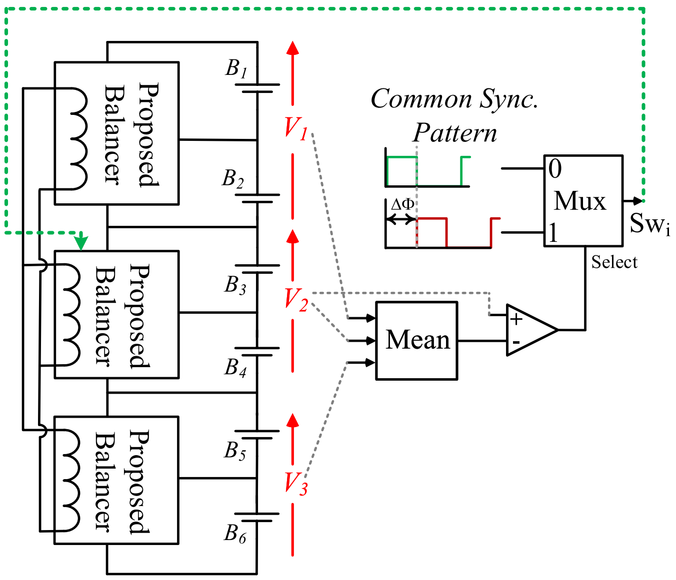

FIGURE 4.11: Proposed Controller.

4.4 Design

To make the design of the converter more straightforward, a step to step procedure is presented. The analysis which are used to justify intra and inter-module charge exchange can be used to select the components and set the controller settings. The design inputs are: V_{max} and V_{min} of battery cells, number of battery cells ($2n$), switching frequency ($f_s = \frac{1}{T_s}$), maximum ripple current (ΔI_{max}), and maximum allowable current (I_{max}). The design outputs are: capacity of capacitors (C), inductance of the inductors (m, l, L_i), Duty cycles range D_H and D_L and rating of the components. For simplicity it is assumed that $D_L = D_H = D$. The design step are as follows:

1) Duty-cycle: The circuit should operate in DCM mode, to maintain a fixed switching frequency. To achieve this goal, $D + D_\alpha < 1$. Using Eq. (4.12) a range for D can be calculated. Then by choosing a D within that range, these inequalities should hold true.

$$\begin{cases} D_{\alpha_H} < 1 - D \\ D_{\alpha_L} < 1 - D \end{cases} \Rightarrow \begin{cases} D < \dfrac{V_{B_3} + V_{D_3}}{(V_{B_3} + V_{D_3} + V_2) + \dfrac{D(V_{L_{s_L}})|_{@1}}{2}} \\[2em] D < \dfrac{V_{B_1} + V_{D_1} + \dfrac{(1 - D_{\alpha_L})V_{L_{s_H}}|_{@4}}{2}}{(V_1 + V_{B_1} + V_{D_1} + \dfrac{V_{L_{s_H}}|_{@4}}{2})} \end{cases} \tag{4.19}$$

2) Inductors: To calculate inductances, the maximum allowable current and maximum peak-to-peak should be used. Using Eq. (4.5) and the fact that ΔI_{L_i} and ΔI_{L_s} are maximum when switch of the module they located in is ON, m, l an L_i can be calculated as it is shown in Eq. (4.20). This can be proved using Eq. (4.5), the slope of the currents is positive when switch of the module they located in is ON. Note that L_i are equal.

$$\begin{cases} \Delta I_{L_{s_j}} = \left.\dfrac{D_H^2 T_s di_{L_{s_j}}}{2dt}\right|_{@1} < \Delta I_{L_{s_{jmax}}} & j = H, L \\ \Delta I_{L_j} = \dfrac{D_H^2 T_s V_H}{2L_j} < \Delta I_{L_{jmax}} & j = 1, 2 \\ \Delta I_{L_j} = \dfrac{D_H^2 T_s V_L}{2L_j} < \Delta I_{L_{jmax}} & j = 3, 4 \end{cases} \tag{4.20}$$

Also, the maximum current of the inductors can be approximately calculated using Eqs. (4.15) and (4.20):

$$\begin{cases} \hat{I}_{L_{s_j}} = I_{L_{s_j}} + \dfrac{\Delta I_{L_{s_j}}}{2} < I_{L_{s_{jmax}}} & j = H, L \\ \hat{I}_{L_j} = I_{L_j} + \dfrac{\Delta I_{L_j}}{2} < I_{L_{jmax}} & j = 1, 2 \\ \hat{I}_{L_j} = I_{L_j} + \dfrac{\Delta I_{L_j}}{2} < I_{L_{jmax}} & j = 3, 4 \end{cases} \tag{4.21}$$

3) Capacitors: V_C is assumed to be a constant during a switching cycle. To maintain the constant value of V_C for an entire switching period, C, L, and L_s, must be chosen such that the resonant frequency f_r is much lower than the switching frequency f_s. f_r can be approximately calculated from the impedance during T_β. The circuit during T_β is shown in Fig. 4.12, the resonant may happen between the coupled inductor, capacitor and inductor which are connected in series. The equivalent impedance of the coupled inductor is M as it is calculated in Eq. (4.6). The angular resonant frequency can be calculated as follows:

$$\omega_r = 2\pi f_r = \frac{1}{(C_i)^2(M + L_i)} \tag{4.22}$$

Therefore, the capacitance of C is:

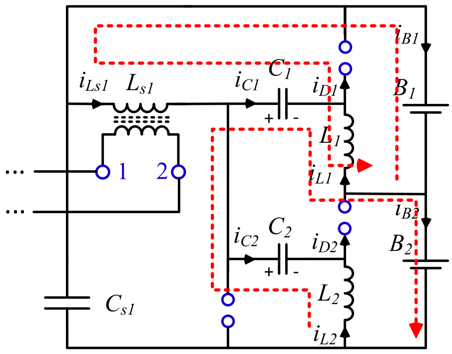

FIGURE 4.12: Currents direction in the circuit during T_β.

$$C_i = \frac{1}{(2\pi f_r)^2(M + L_i)} \tag{4.23}$$

Moreover, the voltage of C_s is assumed to be constant during a switching cycle. Therefore, C_s should be large enough to validate this assumption:

$$C_s \geq 3C_i \tag{4.24}$$

4.5 Experimental Results

An experimental prototype was designed and built to verify the topology, design procedure, and the performance of the proposed circuit along with its controller. The system components were selected based on the design section procedure. The system design parameters inputs are as follows: There are four $20Ah$ battery cells (EIG ePLB C020, see Fig. 4.13) which are used as the string of battery cells. The maximum and minimum voltage of battery cells are: $3.5V < V_{B_i} < 4.5V$. The maximum ripple of the inductor currents are $\Delta I_{L_s} \leq 0.2A$, $\Delta I_{L_i} \leq 0.6A$. The maximum current of the inductors is $I_{L_{max}} \leq 1A$. The switching patterns for four MOSFET ($20V$, $5A$) modules were obtained using a TI F28335 DSP at a switching frequency of $100kHz$. The output design parameters are as follows: using Eq.

(4.19) results in $D = 0.2$, using Eq. (4.20) and Eq. (4.21) result in $m = 100\mu H$, $l = 1\mu H$ and $L_i = 33\mu H$, using Eqs. (4.23) and (4.24) result in $C_i = 30\mu F$ and $C_s = 150\mu F$. The prototype of the circuit is shown in Fig. 4.14. The experimental current waveforms of the system are shown in Fig. 4.15 and these waveforms validate the simulation, calculations and design procedure. The performance of the system with $20Ah$ battery cells is shown in Fig. 4.16.

FIGURE 4.13: Four cells of $20Ah$ Li-ion EIG ePLB C020 Battery cells.

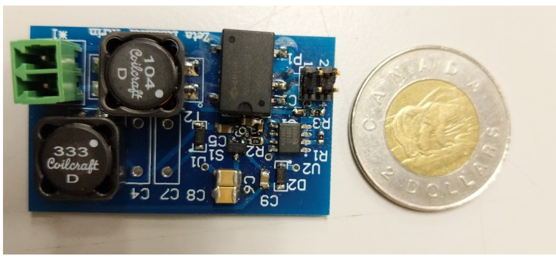

FIGURE 4.14: A module of the proposed circuit.

The experimental waveforms of the inductors and transformers current validate the calculations and design procedure, see Figs. 4.15.

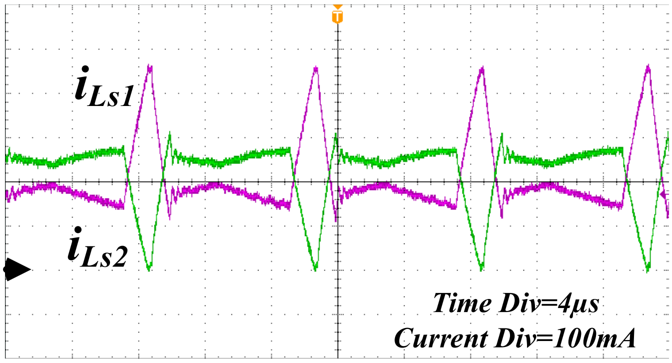

FIGURE 4.15: Experimental coupled Inductor current waveforms of the prototype circuit.

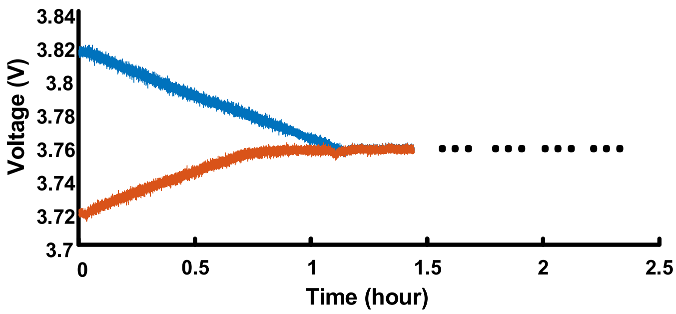

FIGURE 4.16: Experimental performance of the prototype circuit with 20Ah battery cells.

4.6 Comparison

The proposed method is compared to similar methods comprehensively from different aspects. Table 4.1 demonstrates various features and the number of components.

Table 4.1: Comparing different methods for a system with $2n$ battery cells.

Feature \ Method	[41]	[67]	[68]	[77]	Cascaded/Series	[74]	Proposed Method
Scalability	✓	×	✓	×	✓	✓	✓
Charge transfer to far away cells	×	✓	✓	×	✓	✓	✓
Synchronous Charge transfer	✓	×	✓	×	✓	✓	✓
No limitation on Number of Battery cells	✓	×	✓	×	✓	×	✓
Number of Switches / Diodes	$4n/0$	$1/2n$	$16n/16n$	$n/2n$	$2n/2n$	$4n/8n$	$n/2n$
Number of Sensors	$2n$	0	$4n$	$2n$	n	$2n$	n
Control Strategy	Cent.	-	Dist.	Cent.	Dist.	Cent.	Dist.
Equalization Speed	Slow	Average	Fast	Slow	Fast	Fast	Fast
Cost	Low	Low	High	High	Low	High	Low

Table 4.2: Comparing efficiency, control method and, charge transfer features.

Efficiency \ Method	[78]	[62]	[76]	[79]	[77]	Proposed Method
Neighbor Charge Transfer	%55	%56	%90	%90	%93	%85
non-neighbor Cell Charge Transfer	%55	%56	Low	%90	%93	%83
Controller	Cent.	Cent.	Dist.	Cent.	Cent.	Dist.
Synchronous Charge Transfer	✓	×	✓	×	×	✓

From Table. 4.1 it can be concluded that Cascaded and Series methods are similar to Parallel method from features point of view. Since cascaded and series methods are the only method which has similar features such low cost, modularity, fast speed of equalization, charge exchange between all battery cells in a cycle and distributed controller. Therefore, a comparison between the proposed method and Cascaded and series is necessary. From the number of switches prospective, the proposed method is better since it uses one switch per two battery cells. From Number of passive component point of view, the proposed method requires 3 low voltage capacitors while cascaded and series methods do not need any capacitors. So, the proposed method has 3 capacitors more and 1 switch fewer than cascaded and series methods. Since cost of capacitors are low and size of them is small compared to a switch and it gate driver system, the proposed method is better from number of components point of view. Finally, the performance of the circuits should be compared. Comparing the cascaded and series equivalent circuits, Figs. 2.8, 3.7,with the equivalent circuit in Fig. 4.10, it can be concluded that when the charge is transferred between two non-neighbor module/bridges, number of magnetic devices which should process the charge is higher in Cascaded method. To clarify this, assume that the charge is exchanged between "module p" and "module q" in Fig. 4.17.

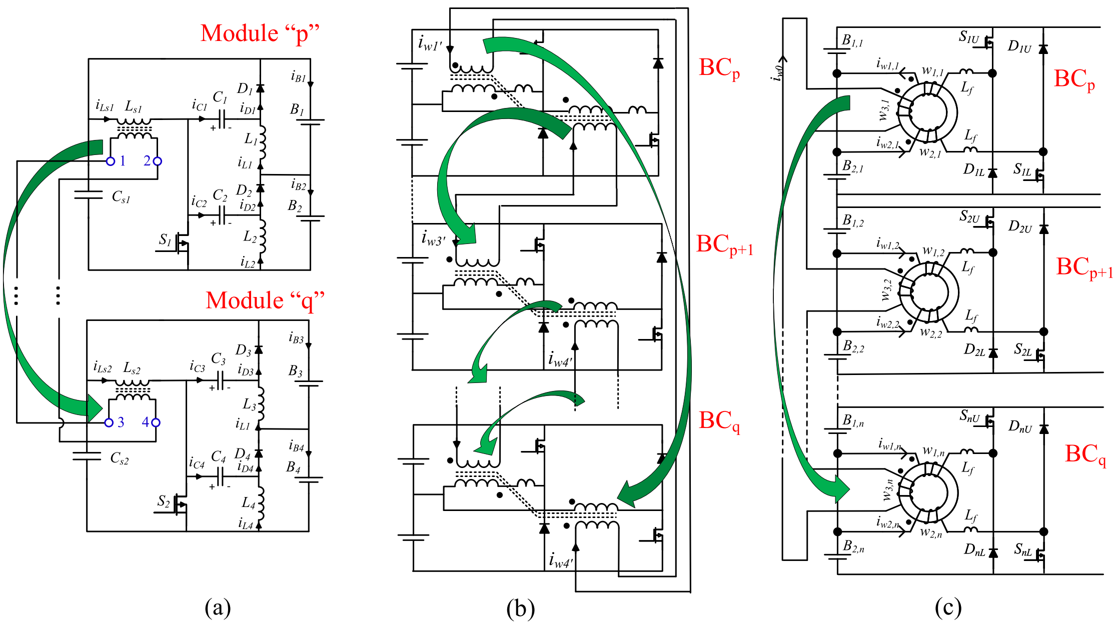

FIGURE 4.17: Charge transfer path comparison (a) Parallel method (b) Cascaded method (c) Series method.

The passive components that has to process power is higher in Cascaded method, as it is shown in Fig. 4.17. The number of magnetic devices which are on the transferred charge path, depends on the location of two bridges in cascaded method, see Fig. 4.17. This number is always constant in Parallel and series method and equals to 2. Therefore, parallel and series method has lower losses compared to cascaded method due to the lower number of magnetic devices which process the power. Thus, assuming the identical constraints such as maximum inductor current, the equalization time of the parallel and series method will be lower.

Another comparable approach is [67]. In the method of [67], if the number of battery cell increases, components rating increase too, while in the proposed method there is no need to increase the rating of the components. Moreover, in [67], the charge exchange occurs between the string of battery cells and the lowest voltage battery cells but in the proposed method, all the battery cells exchange charge. This is due to the fact that there are only two battery cells in each module, and the battery cell which has the lower voltage in each module absorbs charge, intra-module charge transfer, and at the same time charge is transferred to lower voltage module as inter-module charge transfer.

Efficiency of the converters is another important feature to be considered. Efficiency of the inter-module and efficiency of the intra-module charge transfer should be measured. Two efficiencies are mentioned in Table. 4.2, the neighbor charge transfer efficiency is a measure of loss in transferring charge between neighboring modules. The non-neighbor charge transfer efficiency measures the loss of the conversion in transferring charge between module which are not close to each other. There are methods such as [79] which have high neighbor charge transfer efficiency but the non-neighbor charge transfer efficiency is low. The reason lies in the principal of operation of these converter. These converter transfer charge neighbor by neighbor therefore, if the module are not close the charge will be converted several times before reaching the lower voltage module which causes excessive losses in the circuit. Moreover, methods such as [80] transfer charge

TABLE 4.3: Comparison of basic costs for a system which covers 4 battery cells as of February 2019 [3].

Component \ Method	Proposed method	Cascaded method	[41]	[74]
Coupled Inductors ($1.5A$)	\$2.8	\$11.08	-	\$2.8
MOSFET ($5A$, $20V$)	\$1.84	\$3.68	\$5.52	\$7.36
Diode ($3A$, $20V$)	\$2.88	\$2.88	\$4.32	\$11.52
Cap. ($16V$, $47\mu F$)	\$0.36	-	\$0.54	\$0.72
Inductor	\$0.6	\$0.6	\$7.2	\$0.6
Voltage Sensor (an Op-amp with 4 resistors)	\$2.68	\$2.68	\$5.36+ feedback cost	\$5.36+ feedback cost
Total Cost	\$11.16	\$20.92	\$16.64+ feedback cost	\$28.36+ feedback cost

between non-neighbor modules directly but they can only exchange charge between two cells or the string of battery cells and one cell. The disadvantage of these methods is that the speed of equalization is low since they cannot exchange charge between all battery cells in one cycle. Furthermore, a cost comparison is done in Table. 4.3. Three methods are chosen to be compared to the proposed method: Cascaded method which is the closest one from features point of view, [41] which shows very good performance and has the advantage of ZCS and, [74] which is a comprehensive and high performance method. As it is shown in Table. 4.3, identical components are used to compare cost of the different methods. Also, since one of the advantages on the proposed is that it needs fewer voltage sensors, cost of voltage sensors is also added in Table. 4.3. The simplest voltage sensor which composed of an op-amp and 4 resistors is assumed as the voltage sensor which is used in the circuits.

Feedback cost in Table. 4.3 is one of hidden costs in the system. For example, if there are 100 battery cells and the controller is central, the voltage feedback signals should be isolated or even digitized to be transferred from battery cells to the controller. This is due to the fact that the feedback signals are subject to EMI/RFI when they are transferred in a long distance. In this case, either a complicated and expensive controller should be used to process all the 100 feedback signals or the number of battery cells will be limited by the controller inputs. In contrast, using the proposed distributed controller approach, there are only 3 local feedback signals with no hidden cost associated with isolation, digitization or conditioning signals. Moreover, many of the low cost methods such as [74] cannot transfer charge between all cells in one cycle resulting in a lower speed of equalization. In summary, methods which are able to exchange charge between all battery cells, also called Synchronous charge transfer, would be the best choice because they have lower number of component and overall cost.

4.7 Conclusion

A new simple and low component count battery voltage balancing circuit is proposed. The proposed modular circuit provides Synchronous charge transfer at a high efficiency and is based on variants of Sepic converter topology and magnetic coupling. The input inductor of Sepic Converter is replaced by a transformer and the secondary windings of the transformers are connected to a shared link. Therefore, all the modules and battery cells can exchange charge. A distributed control system is presented that operates based on only local feedbacks data with half of the voltage sensors compared to the similar methods. The analysis of the circuit is presented to be used for developing a design procedure. The simulations and analytical results are validated using an experimental prototype. The results confirm that the proposed method is faster than previously published techniques. The design procedure presented is relatively straightforward and accurate while the results can be closely predicted using analytical calculations.

CHAPTER 5

Comparison

All the proposed method can be categorized into Cell to String to Cell methods. Methods in this category are able to exchange charge between all battery cells in a cycle. Each one of them uses different strategy to exchange charge which has their own advantage. Therefore, the proposed methods should be compared to the methods in this category. The advantages of the proposed methods over the other Cell to String to Cell methods are as follows:

- All the proposed converters are modular. Compared to the other method in this category which are not modular, proposed methods are modular and do not have any limitation on the number of battery cells. For example, the method in [66] uses a multi-windings transformer, which the number of windings increases as the number of battery cells increases. Therefore, this method is not modular.

- Controllers of the proposed methods are distributed and uses local data to control the circuit. This prevents the limitation of the centralized controller and keeps the system modular. For example, the method in [66] needs a central controller. A central controller have a limited number of inputs, so, the number of supported battery cells is limited. Moreover, all the feedback signals should be sent to the central controller and this makes the wiring hard.

- Number of sensors is very low in the proposed methods. Only 1 voltage sensors per two battery cells is used and there is no current sensors. The current is limited using the design procedure. For example, method in [68] uses 4 sensors per two battery cells which increase the cost of the circuit.

- The used coupled inductors are low voltage, therefore, size of the coupled inductors and the circuits would be small. For example method in [65] uses high voltage transformers which makes the system bulky and expensive.

- Number of switches and diodes are low compared to the other methods in this category. Only one/two switch(es) and two diodes per two battery cells are used. This decrease the cost of the system compared to the other methods in this category. For example, method in [68], uses 16 switches per two battery cells which makes the system large and expensive.

Also, the proposed methods should be compared to be able to choose the best method for an specific application. Therefore, a comprehensive comparison between the proposed methods is presented. The proposed methods are compared from different aspects such as cost, number of components, efficiency and component rating.

TABLE 5.1: Comparing component count of proposed methods for a system contains $2n$ battery cells.

Component \ Method	Cascaded	Series	Parallel
Coupled Inductor	n	n	n
Inductor	$2n$	$2n$	$2n$
Switch	$2n$	$2n$	n
Diode	$2n$	$2n$	$2n$
Capacitor	-	-	$3n$
Connection to neighbor bridges/modules	4	2	2

5.1 Number of Active Components

Circuit diagrams of the proposed circuits are shown in Fig. 5.1. From the number of components perspective, parallel method is the best method, see Table. 5.1. Parallel method has 1 switch fewer than the other ones, but it needs 3 more capacitors per 2 battery cells compared to the other methods. The reason that Parallel method is chosen as the best method from the component count perspective is that the extra gate driver system adds more components and costs to the circuit compared to the 3 extra capacitors.

5.2 Wiring

To be able to exchange charge between all battery cells, all converters are connected to their neighbor bridges/modules or a common bus. In cascaded method, converters are connected together through the tertiary and quaternary windings. Therefore, each bridge has 4 connections to its neighbor bridge. In series method, bridges are connected together through their tertiary windings. Thus, each bridge has two connections to its neighbor. In parallel method, modules are connected to each other through their tertiary windings which is connected to a same bus. Hence, each module has two connections to the common bus.

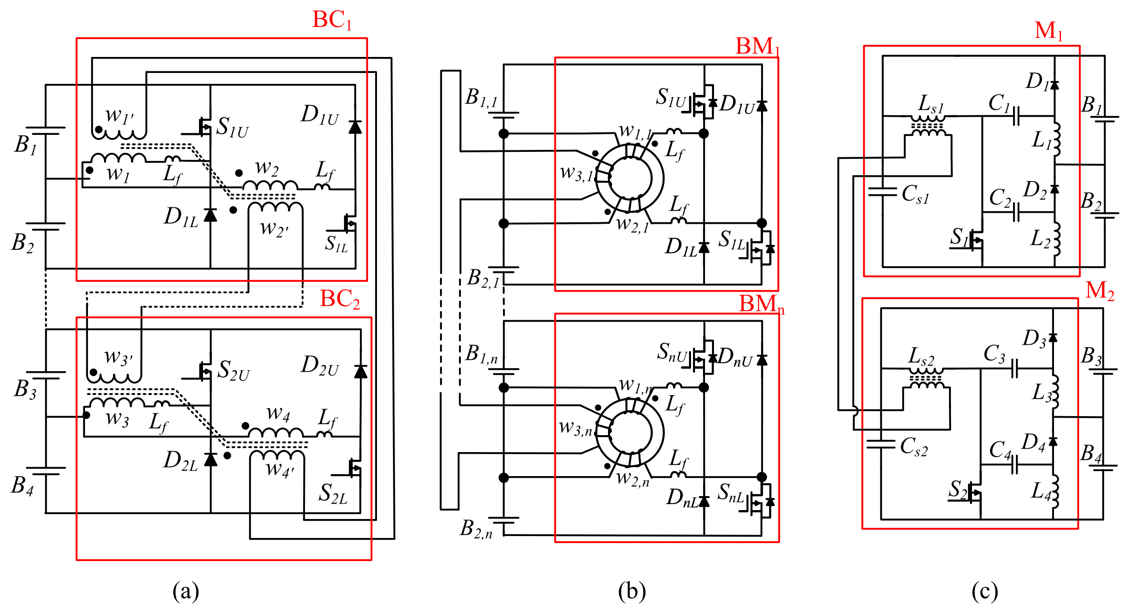

FIGURE 5.1: Circuit diagram of the proposed methods (a) Cascaded method(b) Series method (c) Parallel method.

Consequently, from the wiring point of view, parallel and series method would be better choices since they have fewer connections and less wiring.

5.3 Reliability

Reliability of these circuits form number of active components and number of connections can be studied.

5.3.1 Number of Active Components

Number of active components is important since more active components increase the risk of failure and decrease the reliability. When an active component fails, two case scenarios may happens for the active component: 1) open circuit 2) short circuit. If the active component becomes open circuit, other bridges can continue to operate without a problem. This is due to the fact the bridges/modules are connected through the tertiary and quaternary windings of coupled inductors. But if the active component becomes short circuit, the circuit cannot operate anymore. This is due the fact that a constant DC source (a battery cell) is connected to an inductor.

To conclude this, fewer number of switches leads to higher reliability of the circuit. Consequently, parallel method has higher reliability compared to cascaded and series methods since it has 1 switch fewer per two battery cells.

It can be deduced that, in total, reliability of parallel method is higher than the other methods due to fewer number of switches and fewer number of connections compared to other methods. In the second place is series method which has fewer connections to its neighbor bridges compared to the cascaded method.

5.3.2 Number of Connections

From number of connection angle, the fewer connections leads to higher reliability. Cascaded method has 4 connection to its neighbor bridges while the other methods has only 2 connections. The shared bus in series method should be considered in the reliability studies. The shared bus in series method should be protected since if that wire is disconnected, circuits cannot operate. Considering that battery cells are in a protected container, it can be assumed that the shared bus is protected. Therefore, the risk of shared bus disconnection is low, see Fig. 5.2.

5.3.3 Switch Failure

In case of switch failure, switch break down, the bridge would not operate properly. Therefore, battery cells voltage in the bridge would not be equalized. However, other bridges can follow the equalization process since the upper and lower bridges of the defective bridge have connections to other bridges. The daisy

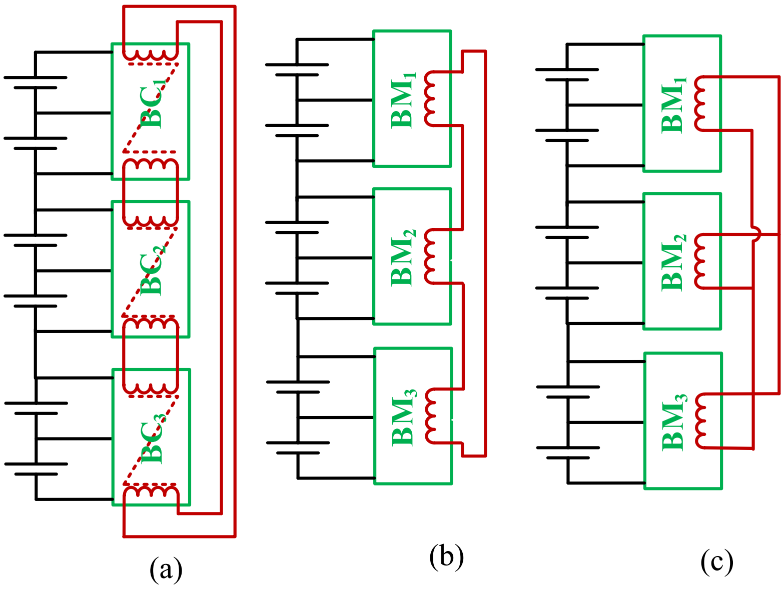

FIGURE 5.2: Circuit connection of the proposed methods (a) Cascaded method(b) Series method (c) Parallel method.

chain connection of bridges are made to make sure if a bridge fails, the other bridges can continue equalization process, see Fig. 5.2.

5.3.4 Coupled Inductor Failure

If a coupled inductor fails, in the Cascaded and Parallel methods the bridge which contains the defective coupled inductor would not operate but the other bridges can follow equalization process. However, in the Series method, since all bridges are in series, if a coupled inductor fails, all bridges would be affected and may not operate properly, see Fig. 5.2.

To conclude this, the parallel method has the highest reliability. In the second place is the Cascaded method which has lower reliability compared to the Parallel method. Finally, Series method has the lowest reliability compared to the Parallel and Cascaded methods.

5.4 Cost of Circuits

From the cost angle, parallel method is the best method as it has fewer switches and uses coupled inductor with only two windings as opposed to the cascaded and series methods that use coupled inductors with three or four windings. Moreover, Parallel method uses only 1 switch and 1 gate driver system while the other methods use two switches and two gate driver systems. This makes Cascaded and series method more expensive than parallel method. The converters cost comparison is summarized in Table .5.2. The table shows that cascaded method is the most expensive then the Series and the least expensive is the Parallel method.

TABLE 5.2: Comparison of basic costs of the proposed methods for a system which covers 4 battery cells as of February 2019 [3].

Component \ Method	Parallel method	Cascaded method	Series Method
Coupled Inductors ($1.5A$)	\$2.8	\$11.08	\$5.54
MOSFET ($5A$, $20V$)	\$1.84	\$3.68	\$3.68
Diode ($3A$, $20V$)	\$2.88	\$2.88	\$2.88
Cap. ($16V$, $47\mu F$)	\$0.36	-	-
Inductor	\$0.6	\$0.6	\$0.6
Voltage Sensor (an Op-amp with 4 resistors)	\$2.68	\$2.68	\$2.68
Total Cost	\$11.16	\$20.92	\$15.38

5.5 Voltage Stress of Components

Comparing the voltage stress of the components in the proposed methods shows that the cascaded and series methods apply lower stress on components, see to Fig. 5.1. In parallel method, the maximum voltage on the switch in a module occurs when battery cells are at their maximum voltage and D_1 is ON, see Fig. 5.1(c). The applied voltage on the switch in this condition is $3V_{max} + V_{d,on}$. In cascaded and series methods the maximum voltage on the switches in a bridge occurs when the diode is ON and this voltage is $V_{max} + V_{d,on}$, see Fig. 1.3(a)-(b). Therefore, the maximum voltage which should be tolerated by a switch in cascaded and series methods are lower as shown in Table. 5.3. Cascaded and Series method are the best method from the switches voltage stress point of view. To compare series and cascaded methods, the maximum voltage on their coupled inductors should be compared. To calculate the maximum voltage on the coupled inductor of cascaded method, Eq. (2.8) and the equivalent circuit of Fig. 5.3, repeated here for convenience, can be used.

TABLE 5.3: Maximum voltage on a switch in the proposed methods.

Method / Component	Cascaded	Series	Parallel
Maximum Voltage on the switch	$V_{max} + V_{d_{on}}$	$V_{max} + V_{d_{on}}$	$3V_{max} + V_{d_{on}}$

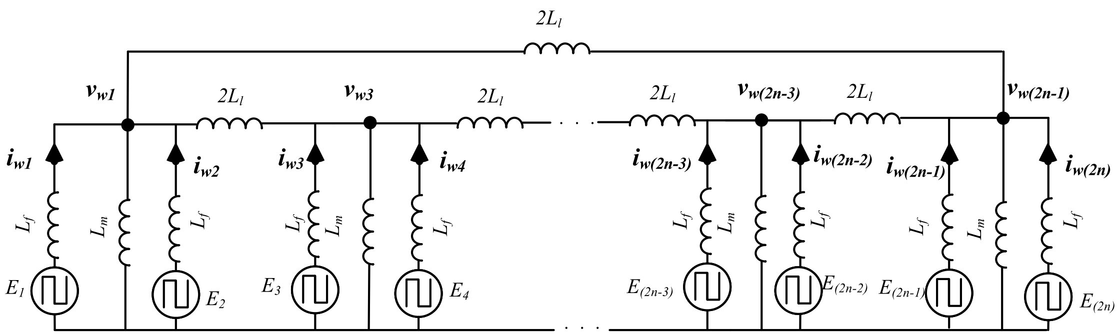

FIGURE 5.3: The equivalent circuit of a system with "n" bridges and "$2n$" battery cells.

Therefore, the maximum voltage on a coupled inductor of a bridge can be calculated as follows:

$$[V_i] = [Y_{ij}]^{-1} \left[\frac{E_{(2i-1)} + E_{(2i)}}{L_l + L_f} \right]$$
$$V_{L_{max}} = max \left(\sum_{k=1}^{n} Y_{ij}^{-1}(1,k) \left[\frac{E_{(2k-1)} + E_{(2k)}}{L_l + L_f} \right] \right) \qquad 1 < i, j < n \tag{5.1}$$

In series method, the maximum voltage on a coupled inductor of a bridge can be calculated using the equivalent circuit which is presented before, see Fig. 5.4:

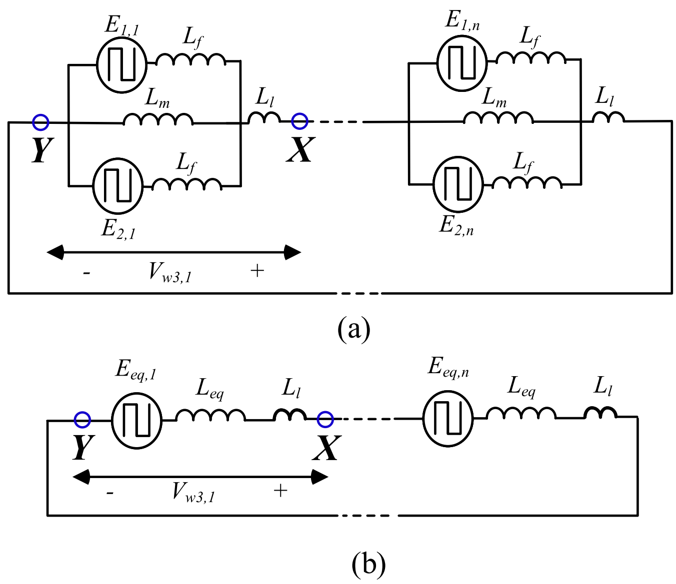

FIGURE 5.4: "n" bridge module topology model (a) equivalent circuit (b) simplified circuit where $L_{eq} = \dfrac{L_m(L_l + L_f)}{2L_m + L_l + L_f}$ and $E_{eq,i} = \dfrac{(E_{1,i} + E_{2,i})\,L_m}{2L_m + L_l + L_f}$.

$$V_{L_{max}} = max \left(L_{eq} \sum_{k=2}^{n} \frac{E_{eq,k}}{(n-1)L_{eq} + 2nL_l + L_m} \right) \tag{5.2}$$

To have a better idea about the voltage stress on the coupled inductor, assume that there are 100 bridges (200 battery cells), the maximum voltage on the coupled inductors is calculated for a range of operating points. The range of operation is defined as $0 < \Delta V_{pu} < 0.1pu$. The diagram of the maximum voltage on the coupled inductors based on the voltage difference is drawn in Fig. 5.5:

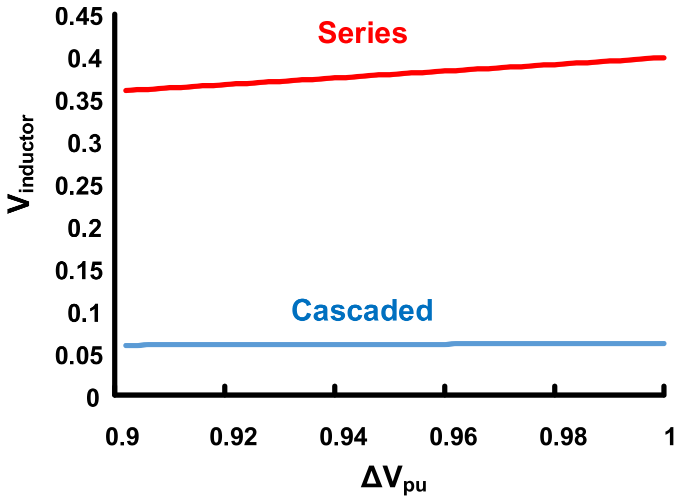

FIGURE 5.5: The maximum applied voltage on a coupled inductors in cascaded and series methods.

As it is shown in Fig. 5.5, the applied voltage on the inductors of Cascaded method is almost constant. This can be verified by checking the equivalent circuit of cascaded method in Fig. 5.3. V_i are around the average voltage of E_1 to E_n. Therefore, the voltage stress does not change significantly when more battery cells are added to the circuit. On the other hand, in series method, all bridges are in series, therefore, as the number of battery cells increases the applied voltage on the inductors increases.

5.6 Zero Current Switching

By checking the current waveforms of the switches, it can be concluded that Cascaded and Series method has advantage of ZCS in turning On. Therefore, the stress on the switches in these two methods would be less than the stress on the switch in Parallel method.

5.7 Size of Circuit

Inspecting the designed examples of the proposed methods show that for identical design constraints such as maximum current and switching frequency, the required inductance in Parallel method is larger compared to the cascaded and series methods. Therefore, from the inductance value prospective, the cascaded and series methods are the best. Table. 5.4 shows the inductance value which are used in the proposed methods.

Table 5.4: Comparison of basic costs of the proposed methods for a system which covers 4 battery cells as of February 2019.

Method / Component	Cascaded	Series	Parallel
Coupled Inductor	$10\mu H$	$5\mu H$	$100\mu H$
Inductors (L_f, L_i)	$4.5\mu H$	$8\mu H$	$22\mu H$

Using the values in Table. 5.4, it can be concluded that parallel method uses the largest inductors. Since the design constraints are identical, the size of the inductors in parallel method is larger. To compare the size of the inductor in cascaded and Series methods, size of their coupled inductors should be compared. From the results in the voltage stress section, it can be concluded that the voltage rating of the coupled inductors in series methods is higher. Also, in the design procedure of a coupled inductor, the following equation is used [81]:

$$V = k(NA)(f_s B) \tag{5.3}$$

where k is a constant, N is number of turns, A is cross section and, B is magnetic field. To keep the core loss fix, $(f_s B)$ should be constant [81], therefore, when voltage increases, the number of turns or cross section area increase. This increase in the number of turn or cross section area of inductors leads to larger size of coupled inductors. Therefore, due to the higher voltage, the size of the coupled inductors in series method will be larger.

Therefore, from the physical size standpoint, the best method is cascaded methods and the series method is in the second place and finally Parallel method is in the third place. It is worth mentioning that the prototype circuits which are built and tested may be bigger than the size they can be built. For example, Parallel circuit is shown and size of that is compared to a coin. The parallel circuit is the biggest circuit, this means that the other circuits can be built with smaller size.

5.8 Magnetic Design Complexity

Comparing the magnetic design complexity of the proposed methods proves that the cascaded and series methods have the most complicated magnetic structure. The reason is that cascaded and parallel methods use coupled inductors with more than two windings which makes the magnetic design more complicated as opposed to parallel method with only two windings, see Fig. 5.6. Moreover, when the inductance of the coupled inductor increases, the design would become more challenging.

5.9 Efficiency of Converters

From efficiency of a single module perspective, parallel method is the best because there is no circulating current. In Series and Cascaded methods, charge is taken out from higher and lower voltage cells to be stored in the inductors. Then the

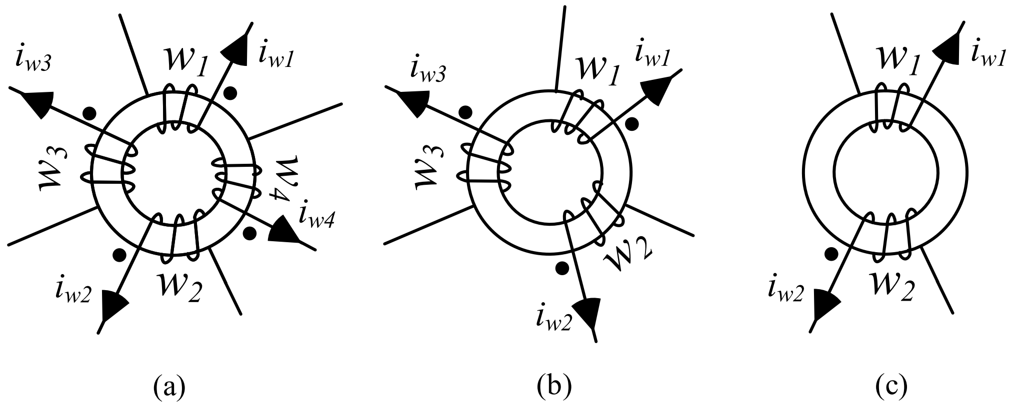

FIGURE 5.6: The coupled inductor used in (a) Cascaded method (b) Series method (c) Parallel method.

stored charge is distributed between battery cells in a way that the higher charged cell absorbs less charge and the lower charged cell absorbs more charge. However, in parallel method, the charge is taken out of all battery cells and is transferred only to the lower charged cells. Less circulation current in parallel method leads to less loss in the circuit. One of the main source of losses in the circuit is the diode conduction losses. In parallel method, only one diode in a module conducts in a cycle while in Series and Cascaded methods both diodes conduct in a cycle. Therefore, Parallel method has the lowest loss and highest efficiency. It is possible to substitute the diodes in the Cascaded and Series method to improve the efficiency of the circuit but the cost and size of the circuit increase. In that case, the turn off loss and conduction loss of the switches and inductors would be the prominent factor in the circuit loss. These two factors are not comparable to conduction loss of the diodes in the circuits. Therefore, by this substitution efficiency of the circuit increases. However, this improve in the efficiency of the circuit comes at the cost of increase in the size and cost of the circuit.

Neighbor to neighbor efficiency of cascaded method is similar to series method but efficiency of non-neighbor charge transfer in Cascaded method depends on the location of the bridges because the number of magnetic devices which process

TABLE 5.5: Comparing efficiency, control method and, charge transfer features.

Component \ Method	Cascaded	Series	Parallel
Neighbor Charge Transfer	%70	%70	%85
Non-neighbor Cell Charge Transfer	$\leq$ %65	%65	%83

power varies when location of the bridges varies, see Fig. 4.17. Therefore, the overall performance of series method is better than cascaded method.

In summary, Parallel method shows the best efficiency among all proposed methods. Since the non-neighbor charge transfer efficiency of the Series method is higher than Cascaded method, the second place goes to Series method and cascaded method is in the third place.

5.10 Equalization time

Speed of equalization in parallel method is faster than the proposed methods because of the higher efficiency of Parallel method and the fact that there is no circulating current in the system. Circulating current decrease the speed of equalization since it decreases the net exchanged charge in the system. The equalization time of the proposed methods are shown in Figs. 5.7, 5.8 and 5.9 when identical constraints are used to design the circuits. As it is predicted, the speed of equalization of the parallel method is faster than the other two method. Speed of equalization of series method is faster than cascaded method due to the higher efficiency and lower number of magnetic devices which process the power.

5.11 Conclusion

To summarize all comparisons, results are gathered in Table. 5.6. The proposed methods are ranked in each subject to make it easier to be compared. As an

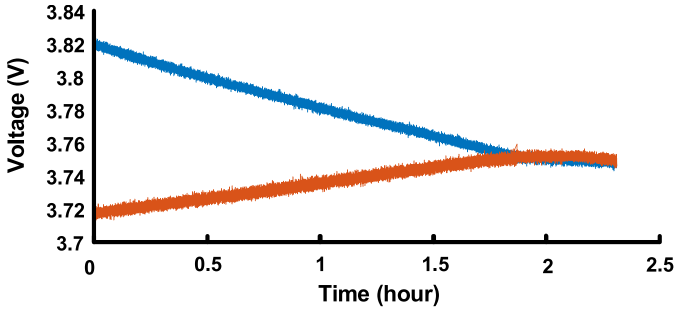

FIGURE 5.7: The performance of the system under cascaded method.

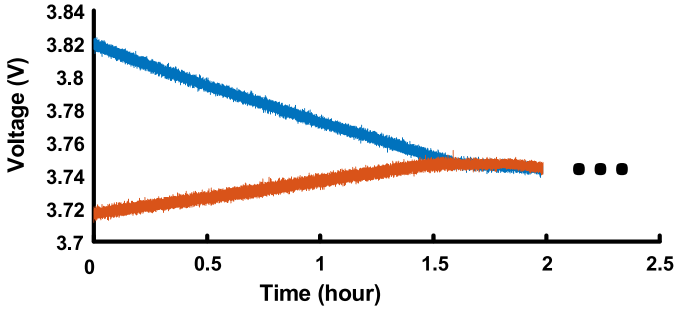

FIGURE 5.8: The performance of the system under series method.

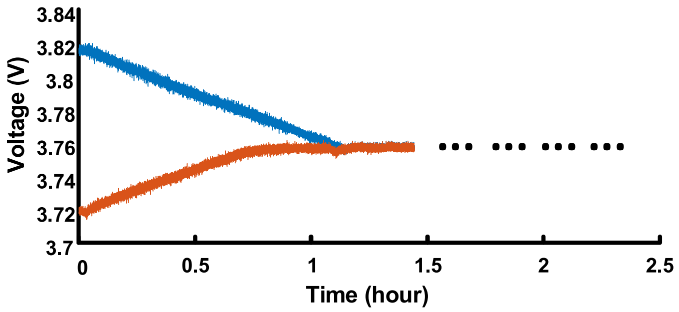

FIGURE 5.9: The performance of the system under parallel method.

example, for the identical design constraints, parallel method has the largest inductor size. Therefore, if size of the circuit is important, cascaded method can be used. In different condition, if the performance of the system is a more important parameter, parallel method should be used. In other case, if the size of the circuit and performance of the system are both important, series method should be used. Since in the design of the circuits there are multiple constraints on size, performance and cost of the circuit, the best method should be chosen based on the weight of constraints in an optimization process. In this process, Table. 5.6 can be used to choose the best method. As an example, in electric racing car, the Cascaded method would be a better choice. The reason behind that is the size of the circuit. In racing car it is important to keep everything small and light, therefore, the Cascaded method is a better choice. As another application, in an electric vehicle where efficiency and cost of the system are the most important factors, the Parallel method is the best choice. In high voltage applications, such as energy storage unit where ZCS, Voltage stress of components and efficiency are the most important factors, the Series method would be the better choice.

Table 5.6: Comparison of the proposed methods.

Subject \ Method	Cascaded	Series	Parallel
Number of Switch/Diode	$2n/2n$	$2n/2n$	$n/2n$
Wiring & Connections	4	2	2
reliability	Average	Low	High
Cost	High	Average	Low
Voltage Stress	Low	Average	High
ZCS	Yes	Yes	No
Size	Small	Average	Large
Magnetic Design Complexity	Complex	Complex	Simple
Efficiency	Low	Average	High
Equalization Time	Slow	Average	Fast

CHAPTER 6

Conclusion & Future Work

The lithium-ion battery cells are the best choice for the EVs, energy storage and similar applications. One of the challenges in using this kind of battery cells is that lithium-ion battery cells' performance is greatly affected by over-charging and over-discharging. Therefore, to increase the cells' lifetime and to obtain the best performance out of a string of connected battery cells, using battery balancing systems is necessary. The main objective of this study is to propose battery voltage balancing circuits with the following features: modularity; high efficiency; low component count; charge exchange among all cells in a cycle; and, a distributed controller.

6.1 Conclusion and Contribution

Three circuits, along with their controller, are proposed for balancing the voltage of a series connected battery cells. These circuits are analyzed to develop comprehensive design procedures. The output of these design procedures are used to build prototype circuits. The prototype circuits are tested and the experimental results are used to validate the design procedures and analysis. The main contributions and conclusions of this thesis are summarized below:

(i) The proposed circuits are modular. Hence, they can be extended to cover more battery cells without any changes in the circuits. In these methods there are some inter-bridge/module windings that are responsible for connecting the bridges/modules together. To add more battery cells to the system, it is sufficient to connect the inter bridge/module windings of the converters to the inter bridge/module winding of neighbouring bridges/modules. Consequently, no other modification is needed to add more battery cells to the system. Due to this characteristic the circuit can be referred to as: "Plug and Play".

(ii) The proposed controllers are modular and use local data: voltage of the neighbouring bridges/modules and voltage of the bridge/module itself. Therefore, the arrangement can be called "distributed controllers". Moreover, the first controller detects the unbalanced voltages and will generate the synchronization signal and send it to all of the bridges. Thus, there is no master/slave controller in the circuit to cause a problem in case of failure of a controller. As a result the system is more reliable. Furthermore, a distributed controller has an important advantage over a central controller. The problem with central controller is that it has limited number of inputs and consequently it can support only a limited number of battery cells. However, in the proposed method there is no limitation to the number of battery cells that can be utilized.

(iii) In the proposed methods, the component count is as low as 2 switches/1 switch, 2 diodes, 1 coupled inductor and 1 voltage sensor per 2 battery cells. Not only the size of the system is small, but also the cost of the system is low.

The low number of sensors decreases the cost of the auxiliary circuits as well. The cost of the auxiliary circuitry is one of the hidden cost in the system. Auxiliary circuitry, is comprised of the conditioning, isolating or digitizing circuits. These circuits are used to connect the output of the sensors to the controller.

(iv) A comprehensive design procedure for each method is presented. The design procedure is flexible and can be used to design the circuit and its controller for different battery cells, voltage or power levels. The inputs of the design procedures are number, maximum and minimum voltage of the battery cells, and the maximum and minimum allowable voltage and current in the circuit. The output would be the rating of the components and controller settings.

(v) The proposed controller does not need any current sensors. The current is limited in the circuit through the design procedure and by studying the worst case scenarios.

(vi) The proposed circuits transfer charge among all the battery cells during a cycle. The charge is distributed among all the battery cells based on their voltages. Therefore, these methods have lower equalization time than the methods which transfer charge between two cells, neighbour cells or a cell and the string in a cycle.

(vii) In the second method, it is possible to calculate the equalization time. This is due to the topology and configuration of the second proposed method. In the second method, bridges are connected in series. Therefore, the current that goes to the bridges is identical. In comparison, in the first method, the bridges are parallel and the currents that go to the bridges are not identical. This advantage is used in the design procedure in the second method to predict and minimize the equalization time.

6.2 Future Work

There are a number of directions that this research could proceed in. Three of the most promising are outlined below.

(i) It is possible to add current sensors to the circuit and use the SOC instead of the battery cellsâ voltage as the controller inputs. This makes the system more expensive but in a situation where the voltage and SOC variation are not commensurate, the SOC would be a better choice as a controller input.

(ii) Photovoltaic (PV) modules are generally connected in a series in order to produce the high voltage. In cases where a very small section of the PV module is shaded, the generated power of the whole PV module decreases dramatically. The concept of balancing the charge of a series of connected battery cells can be used to solve the power generation drop in a partly shaded PV system. Therefore, all the proposed circuits can be used as a Generation Control Unit (GCU) in PV systems.

(iii) The possibility of using this converter as a micro-converter for a PV system to set the maximum power point while performing the role of a generation control unit should be studied. In that case, not only would the output power of each panel be maximized but also the cost of the system would decrease. This is due to the fact the maximum power point tracker converter can be eliminated.

Bibliography

[1] https://docs.google.com/spreadsheets/d/1PHYhxyW63t4FDG7oaL_jH0hWoW3t4B3vBDDxLNAsRJU/edit#gid=0m, accessed: 2019-07-16.

[2] J. Ewanchuk and J. Salmon, "A modular balancing bridge for series connected voltage sources," *Power Electronics, IEEE Transactions on*, vol. 29, no. 9, pp. 4712–4722, 2014.

[3] http://www.digikey.ca, accessed: 2019-02-15.

[4] S. F. Tie and C. W. Tan, "A review of energy sources and energy management system in electric vehicles," *Renewable and Sustainable Energy Reviews*, vol. 20, pp. 82–102, 2013.

[5] F. A. Azidin, M. A. Hannan, and A. Mohamed, "Renewable energy technologies and hybrid electric vehicle challenges," *Przeglkad Elektrotechniczny*, vol. 89, no. 8, pp. 150–156, 2013.

[6] W. Y. C. C. Chau, KT, "An overview of energy sources for electric vehicles," *Energy Conversion and Management*, vol. 40, no. 10, pp. 1021–1039, 1999.

[7] K. Chau, Y. Wong, and C. Chan, "An overview of energy sources for electric vehicles," *Energy Conversion and Management*, vol. 40, no. 10, pp. 1021–1039, 1999.

[8] B. Dunn, H. Kamath, and J.-M. Tarascon, "Electrical energy storage for the grid: A battery of choices," *Science*, vol. 334, no. 6058, pp. 928–935, 2011. [Online]. Available: http://science.sciencemag.org/content/334/6058/928

[9] T. H. Phung, J. C. Crebier, and Y. Lembeye, "Voltage balancing converter network for series-connected battery stack," in *IECON 2012-38th Annual Conference on IEEE Industrial Electronics Society.* IEEE, 2012, pp. 3007–3013.

[10] C. Mi, B. Li, D. Buck, and N. Ota, "Advanced electro-thermal modeling of lithium-ion battery system for hybrid electric vehicle applications," in *Vehicle Power and Propulsion Conference, 2007. VPPC 2007. IEEE.* IEEE, 2007, pp. 107–111.

[11] M. Broussely, P. Biensan, F. Bonhomme, P. Blanchard, S. Herreyre, K. Nechev, and R. Staniewicz, "Main aging mechanisms in li ion batteries," *Journal of power sources*, vol. 146, no. 1, pp. 90–96, 2005.

[12] L. Lu, X. Han, J. Li, J. Hua, and M. Ouyang, "A review on the key issues for lithium-ion battery management in electric vehicles," *Journal of power sources*, vol. 226, pp. 272–288, 2013.

[13] A. Affanni, A. Bellini, G. Franceschini, P. Guglielmi, and C. Tassoni, "Battery choice and management for new-generation electric vehicles," *IEEE Transactions on Industrial Electronics*, vol. 52, no. 5, pp. 1343–1349, 2005.

[14] H. Rahimi-Eichi, U. Ojha, F. Baronti, and M.-Y. Chow, "Battery management system: An overview of its application in the smart grid and electric vehicles," *IEEE Industrial Electronics Magazine*, vol. 7, no. 2, pp. 4–16, 2013.

[15] Y. Xing, E. W. Ma, K. L. Tsui, and M. Pecht, "Battery management systems in electric and hybrid vehicles," *Energies*, vol. 4, no. 11, pp. 1840–1857, 2011.

[16] J. Kim, J. Shin, C. Chun, and B. Cho, "Stable configuration of a li-ion series battery pack based on a screening process for improved voltage/soc balancing," *IEEE Transactions on Power Electronics*, vol. 27, no. 1, pp. 411–424, 2012.

[17] C.-M. Young, N.-Y. Chu, L.-R. Chen, Y.-C. Hsiao, and C.-Z. Li, "A single-phase multilevel inverter with battery balancing," *IEEE Transactions on Industrial Electronics*, vol. 60, no. 5, pp. 1972–1978, 2012.

[18] J.-H. Kim, J.-W. Shin, C.-Y. Jeon, and B.-H. Cho, "Screening process of li-ion series battery pack for improved voltage/soc balancing," in *The 2010 International Power Electronics Conference-ECCE ASIA-*. IEEE, 2010, pp. 1174–1179.

[19] J. Shim and K. A. Striebel, "Characterization of high-power lithium-ion cells during constant current cycling: Part i. cycle performance and electrochemical diagnostics," *Journal of power sources*, vol. 122, no. 2, pp. 188–194, 2003.

[20] ——, "Characterization of high-power lithium-ion cells during constant current cycling: Part i. cycle performance and electrochemical diagnostics," *Journal of power sources*, vol. 122, no. 2, pp. 188–194, 2003.

[21] S. T. Hung, D. C. Hopkins, and C. R. Mosling, "Extension of battery life via charge equalization control," *IEEE Transactions on Industrial Electronics*, vol. 40, no. 1, pp. 96–104, 1993.

[22] J. Gallardo-Lozano, E. Romero-Cadaval, M. I. Milanes-Montero, and M. A. Guerrero-Martinez, "Battery equalization active methods," *Journal of Power Sources*, vol. 246, pp. 934–949, 2014.

[23] D. C. Hopkins, C. Mosling, and S. Hung, "The use of equalizing converters for serial charging of long battery strings," in *[Proceedings] APEC'91: Sixth*

Annual Applied Power Electronics Conference and Exhibition. IEEE, 1991, pp. 493–498.

[24] N. H. Kutkut and D. M. Divan, "Dynamic equalization techniques for series battery stacks," in *Proceedings of Intelec'96-International Telecommunications Energy Conference*. IEEE, 1996, pp. 514–521.

[25] J. Gallardo-Lozano, E. Romero-Cadaval, M. I. Milanes-Montero, and M. A. Guerrero-Martinez, "Battery equalization active methods," *Journal of Power Sources*, vol. 246, pp. 934–949, 2014.

[26] G. Landrum, T. A. Stuart, and Wei Zhu, "Fast equalization for large lithium ion batteries," in *OCEANS 2008*, Sep. 2008, pp. 1–6.

[27] A. Manenti, A. Abba, A. Merati, S. M. Savaresi, and A. Geraci, "A new bms architecture based on cell redundancy," *IEEE Transactions on Industrial Electronics*, vol. 58, no. 9, pp. 4314–4322, 2010.

[28] Y. Zheng, M. Ouyang, L. Lu, J. Li, X. Han, and L. Xu, "On-line equalization for lithium-ion battery packs based on charging cell voltages: Part 2. fuzzy logic equalization," *Journal of Power Sources*, vol. 247, pp. 460 – 466, 2014. [Online]. Available: http://www.sciencedirect.com/science/article/pii/S0378775313015036

[29] M. J. Isaacson, R. P. Hollandsworth, P. J. Giampaoli, F. A. Linkowsky, A. Salim, and V. L. Teofilo, "Advanced lithium ion battery charger," in *Fifteenth Annual Battery Conference on Applications and Advances (Cat. No.00TH8490)*, Jan 2000, pp. 193–198.

[30] M. Isaacson, R. Hollandsworth, P. Giampaoli, F. Linkowsky, A. Salim, and V. Teofilo, "Advanced lithium ion battery charger," in *Battery Conference on*

Applications and Advances, 2000. The Fifteenth Annual. IEEE, 2000, pp. 193–198.

[31] Y. Ye and K. W. E. Cheng, "An automatic switched-capacitor cell balancing circuit for series-connected battery strings," *Energies*, vol. 9, no. 3, 2016. [Online]. Available: http://www.mdpi.com/1996-1073/9/3/138

[32] Y. Yuanmao, K. Cheng, and Y. Yeung, "Zero-current switching switched-capacitor zero-voltage-gap automatic equalization system for series battery string," *IEEE transactions on power electronics*, vol. 27, no. 7, pp. 3234–3242, 2012.

[33] M. Daowd, M. Antoine, N. Omar, P. Van den Bossche, and J. Van Mierlo, "Single switched capacitor battery balancing system enhancements," *Energies*, vol. 6, no. 4, pp. 2149–2174, 2013. [Online]. Available: http://www.mdpi.com/1996-1073/6/4/2149

[34] Y. Wang, H. Yin, S. Han, A. Alsabbagh, and C. Ma, "A novel switched capacitor circuit for battery cell balancing speed improvement," in *2017 IEEE 26th International Symposium on Industrial Electronics (ISIE)*, June 2017, pp. 1977–1982.

[35] A. C. Baughman and M. Ferdowsi, "Double-tiered switched-capacitor battery charge equalization technique," *IEEE Transactions on Industrial Electronics*, vol. 55, no. 6, pp. 2277–2285, 2008.

[36] A. Baughman and M. Ferdowsi, "Double-tiered capacitive shuttling method for balancing series-connected batteries," in *2005 IEEE Vehicle Power and Propulsion Conference*, Sep. 2005, pp. 109–113.

[37] T. H. Phung, J.-C. Crebier, A. Chureau, A. Collet, and V. Nguyen, "Optimized structure for next-to-next balancing of series-connected lithium-ion cells," in

Applied Power Electronics Conference and Exposition (APEC), 2011 Twenty-Sixth Annual IEEE. IEEE, 2011, pp. 1374–1381.

[38] S. Yarlagadda, T. T. Hartley, and I. Husain, "A battery management system using an active charge equalization technique based on a dc/dc converter topology," *IEEE Transactions on Industry Applications*, vol. 49, no. 6, pp. 2720–2729, Nov 2013.

[39] S. Wang, L. Kang, X. Guo, Z. Wang, and M. Liu, "A novel layered bidirectional equalizer based on a buck-boost converter for series-connected battery strings," *Energies*, vol. 10, no. 7, p. 1011, 2017.

[40] W. Ji, F. Ran, Y. Ji, X. Lu, and A. Guo, "A low cost battery equalizing scheme with buck-boost and series lc converter using synchronous phase-shift controller," *IEICE Electronics Express*, vol. 14, no. 2, pp. 20 161 166–20 161 166, 2017.

[41] Y.-S. Lee and G.-T. Cheng, "Quasi-resonant zero-current-switching bidirectional converter for battery equalization applications," *IEEE Transactions on Power Electronics*, vol. 21, no. 5, pp. 1213–1224, 2006.

[42] Y. Lee, C. Tsai, Y. Ko, and M. Cheng, "Charge equalization using quasi-resonant converters in battery string for medical power operated vehicle application," in *The 2010 International Power Electronics Conference - ECCE ASIA -*, June 2010, pp. 2722–2728.

[43] C.-S. Lim, K.-J. Lee, N.-J. Ku, D.-S. Hyun, and R.-Y. Kim, "A modularized equalization method based on magnetizing energy for a series-connected lithium-ion battery string," *IEEE Transactions on power Electronics*, vol. 29, no. 4, pp. 1791–1799, 2014.

[44] Yuang-Shung Lee, Chun-Yi Duh, Guo-Tian Chen, and Shen-Ching Yang, "Battery equalization using bi-directional cuk converter in dcvm operation," in *2005 IEEE 36th Power Electronics Specialists Conference*, June 2005, pp. 765–771.

[45] Y.-S. Lee and M.-W. Cheng, "Intelligent control battery equalization for series connected lithium-ion battery strings," *IEEE Transactions on Industrial electronics*, vol. 52, no. 5, pp. 1297–1307, 2005.

[46] R. Ugle, Y. Li, and A. Dhingra, "Equalization integrated online monitoring of health map and worthiness of replacement for battery pack of electric vehicles," *Journal of Power Sources*, vol. 223, pp. 293–305, 2013.

[47] R. K. Vardhan, T. Selvathai, R. Reginald, P. Sivakumar, and S. Sundaresh, "Modeling of single inductor based battery balancing circuit for hybrid electric vehicles," in *IECON 2017 - 43rd Annual Conference of the IEEE Industrial Electronics Society*, Oct 2017, pp. 2293–2298.

[48] S. Park, Tae-Sung Kim, Jin-Sik Park, Gun-Woo Moon, and Myung-Joong Yoon, "A new battery equalizer based on buck-boost topology," in *2007 7th Internatonal Conference on Power Electronics*, Oct 2007, pp. 962–965.

[49] Y. Shang, C. Zhang, N. Cui, and J. M. Guerrero, "A cell-to-cell battery equalizer with zero-current switching and zero-voltage gap based on quasi-resonant lc converter and boost converter," *IEEE Transactions on Power Electronics*, vol. 30, no. 7, pp. 3731–3747, 2015.

[50] S. Park, T. Kim, J. Park, G. Moon, and M. Yoon, "A new buck-boost type battery equalizer," in *2009 Twenty-Fourth Annual IEEE Applied Power Electronics Conference and Exposition*, Feb 2009, pp. 1246–1250.

[51] S. W. Moore and P. J. Schneider, "A review of cell equalization methods for lithium ion and lithium polymer battery systems," SAE Technical Paper, Tech. Rep., 2001.

[52] M.-Y. Kim, C.-H. Kim, J.-H. Kim, and G.-W. Moon, "A modularized bms with an active cell balancing circuit for lithium-ion batteries in v2g system," in *Vehicle Power and Propulsion Conference (VPPC), 2012 IEEE*. IEEE, 2012, pp. 401–406.

[53] A. M. Imtiaz, F. H. Khan, and H. Kamath, "A low-cost time shared cell balancing technique for future lithium-ion battery storage system featuring regenerative energy distribution," in *2011 Twenty-Sixth Annual IEEE Applied Power Electronics Conference and Exposition (APEC)*, March 2011, pp. 792–799.

[54] K. Zhi-Guo, Z. Chun-Bo, L. Ren-Gui, and C. Shu-Kang, "Comparison and evaluation of charge equalization technique for series connected batteries," in *Power Electronics Specialists Conference, 2006. PESC'06. 37th IEEE*. IEEE, 2006, pp. 1–6.

[55] D. V. Cadar, D. M. Petreus, and T. M. Patarau, "An energy converter method for battery cell balancing," in *33rd International Spring Seminar on Electronics Technology, ISSE 2010*, May 2010, pp. 290–293.

[56] M. Einhorn, W. Roessler, and J. Fleig, "Improved performance of serially connected li-ion batteries with active cell balancing in electric vehicles," *IEEE Transactions on Vehicular Technology*, vol. 60, no. 6, pp. 2448–2457, July 2011.

[57] F. Mestrallet, L. Kerachev, J.-C. Crebier, and A. Collet, "Multiphase interleaved converter for lithium battery active balancing," *IEEE Transactions on Power Electronics*, vol. 29, no. 6, pp. 2874–2881, 2014.

[58] C. Moo, K. S. Ng, and Y. Hsieh, "Parallel operation of battery power modules," *IEEE Transactions on Energy Conversion*, vol. 23, no. 2, pp. 701–707, June 2008.

[59] C. S. Moo, Y.-C. Hsieh, and I. Tsai, "Charge equalization for series-connected batteries," *IEEE Transactions on Aerospace and Electronic Systems*, vol. 39, no. 2, pp. 704–710, 2003.

[60] W. Hong, K.-S. Ng, J.-H. Hu, and C.-S. Moo, "Charge equalization of battery power modules in series," in *Power Electronics Conference (IPEC), 2010 International*. IEEE, 2010, pp. 1568–1572.

[61] C. S. Moo, Y. C. Hsieh, and I. S. Tsai, "Charge equalization for series-connected batteries," *IEEE Transactions on Aerospace and Electronic Systems*, vol. 39, no. 2, pp. 704–710, April 2003.

[62] H.-S. Park, C.-E. Kim, C.-H. Kim, G.-W. Moon, and J.-H. Lee, "A modularized charge equalizer for an hev lithium-ion battery string," *IEEE Transactions on Industrial Electronics*, vol. 56, no. 5, pp. 1464–1476, 2009.

[63] J. Gallardo-Lozano, E. Romero-Cadaval, M. I. Milanes-Montero, and M. A. Guerrero-Martinez, "Battery equalization active methods," *Journal of Power Sources*, vol. 246, pp. 934–949, 2014.

[64] C.-H. Kim, H.-S. Park, and G.-W. Moon, "A modularized two-stage charge equalization converter for series connected lithium-ion battery strings in an hev," in *Power Electronics Specialists Conference, 2008. PESC 2008. IEEE*. IEEE, 2008, pp. 992–997.

[65] T. Gottwald, Z. Ye, and T. Stuart, "Equalization of ev and hev batteries with a ramp converter," *IEEE Transactions on Aerospace and Electronic Systems*, vol. 33, no. 1, pp. 307–312, 1997.

[66] S. Li, C. C. Mi, and M. Zhang, "A high-efficiency active battery-balancing circuit using multiwinding transformer," *IEEE Transactions on Industry Applications*, vol. 49, no. 1, pp. 198–207, 2013.

[67] M. Uno and K. Tanaka, "Single-switch cell voltage equalizer using multistacked buck-boost converters operating in discontinuous conduction mode for series-connected energy storage cells," *IEEE Transactions on Vehicular Technology*, vol. 60, no. 8, pp. 3635–3645, 2011.

[68] M. Evzelman, M. M. U. Rehman, K. Hathaway, R. Zane, D. Costinett, and D. Maksimovic, "Active balancing system for electric vehicles with incorporated low-voltage bus," *IEEE Transactions on Power Electronics*, vol. 31, no. 11, pp. 7887–7895, 2016.

[69] M. Caspar, T. Eiler, and S. Hohmann, "Systematic comparison of active balancing: A model-based quantitative analysis," *IEEE Transactions on Vehicular Technology*, 2016.

[70] A. Tavakoli, S. Khajehoodin, and J. Salmon, "Switching pattern of a modular voltage balancing circuit for battery cells," in *Energy Conversion Congress and Exposition (ECCE), 2016 IEEE*. IEEE, 2016, pp. 1–8.

[71] A. Tavakoli, I. Smith, S. Khajehoodin, and J. Salmon, "Performance comparison of two controllers for a modular voltage balancing circuit," in *Applied Power Electronics Conference and Exposition (APEC), 2017 IEEE*. IEEE, 2017, pp. 1667–1674.

[72] A. Tavakoli, S. A. Khajehoddin, and J. Salmon, "Control and analysis of a modular battery voltage balancing cell," *IEEE Transactions on Power Electronics*, 2018.

[73] Y. Yuanmao, K. Cheng, and Y. Yeung, “Zero-current switching switched-capacitor zero-voltage-gap automatic equalization system for series battery string,” *Power Electronics, IEEE Transactions on*, vol. 27, no. 7, pp. 3234–3242, 2012.

[74] G. Oriti, A. L. Julian, and P. Norgaard, “Battery management system with cell equalizer for multi-cell battery packs,” in *Energy Conversion Congress and Exposition (ECCE), 2014 IEEE*. IEEE, 2014, pp. 900–905.

[75] C.-H. Kim, M.-Y. Kim, H.-S. Park, and G.-W. Moon, “A modularized two-stage charge equalizer with cell selection switches for series-connected lithium-ion battery string in an hev,” *Power Electronics, IEEE Transactions on*, vol. 27, no. 8, pp. 3764–3774, 2012.

[76] P. Cassani, S. S. Williamson *et al.*, “Design, testing, and validation of a simplified control scheme for a novel plug-in hybrid electric vehicle battery cell equalizer,” *Industrial Electronics, IEEE Transactions on*, vol. 57, no. 12, pp. 3956–3962, 2010.

[77] Y. Li and Y. Han, “A module-integrated distributed battery energy storage and management system,” *IEEE Transactions on Power Electronics*, vol. 31, no. 12, pp. 8260–8270, 2016.

[78] M. Uno and A. Kukita, “Bidirectional pwm converter integrating cell voltage equalizer using series-resonant voltage multiplier for series-connected energy storage cells,” *IEEE Transactions on Power Electronics*, vol. 30, no. 6, pp. 3077–3090, 2015.

[79] F. Baronti, G. Fantechi, R. Roncella, and R. Saletti, “High-efficiency digitally controlled charge equalizer for series-connected cells based on switching converter and super-capacitor,” *IEEE Transactions on Industrial Informatics*, vol. 9, no. 2, pp. 1139–1147, 2013.

[80] J. Cao, N. Schofield, and A. Emadi, "Battery balancing methods: A comprehensive review," in *Vehicle Power and Propulsion Conference, 2008. VPPC'08. IEEE.* IEEE, 2008, pp. 1–6.

[81] W. G. Hurley and W. H. Wölfle, *Transformers and inductors for power electronics: Theory, design and applications.* John Wiley & Sons, 2013.